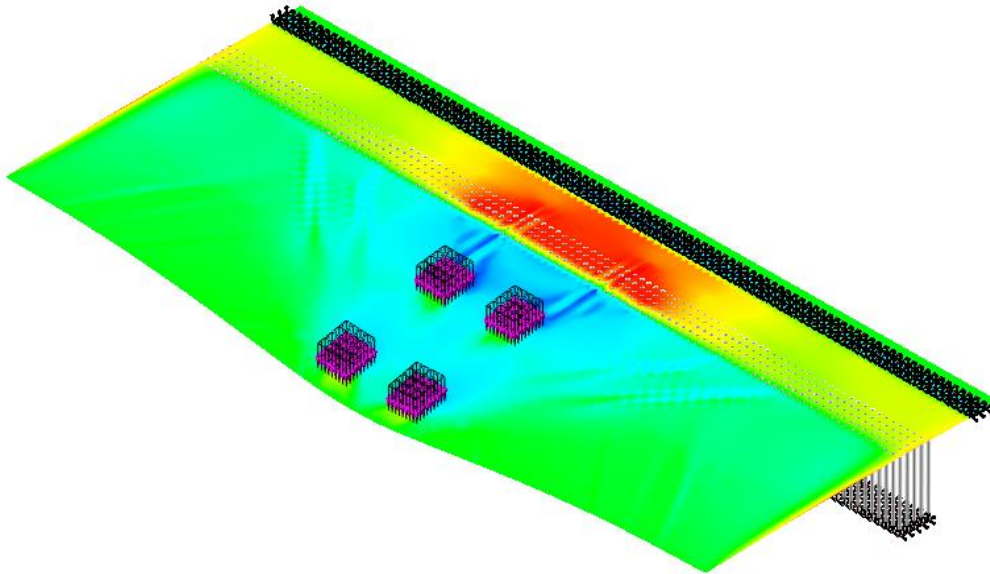# CHALMERS

Shear Distribution in Reinforced Concrete Bridge Deck Slabs

Non-linear Finite Element Analysis with Shell Elements

Master of Science Thesis in the Master's Programme Structural Engineering and Building Performance Design

ALICJA KUPRYCIUK
SUBI GEORGIEV

Department of Civil and Environmental Engineering
Division of Structural Engineering
Concrete Structures
CHALMERS UNIVERSITY OF TECHNOLOGY
Göteborg, Sweden 2013
Master's Thesis 2013:127

Shear Distribution in Reinforced Concrete Bridge Deck Slabs

Non-linear Finite Element Analysis with Shell Elements

Master of Science Thesis in the Master's Programme Structural Engineering and Building Performance Design

ALICJA KUPRYCIUK

SUBI GEORGIEV

Department of Civil and Environmental Engineering
Division of Structural Engineering
Concrete Structures
CHALMERS UNIVERSITY OF TECHNOLOGY
Göteborg, Sweden 2013

Shear Distribution in Reinforced Concrete Bridge Deck Slab

Non-linear Finite Element Analysis with Shell Elements

Master of Science Thesis in the Master's Programme Structural Engineering and Building Performance Design
ALICJA KUPRYCIUK
SUBI GEORGIEV

Department of Civil and Environmental Engineering
Division of Structural Engineering
Concrete Structures
Chalmers University of Technology
SE-412 96 Göteborg
Sweden
Telephone: + 46 (0)31-772 1000

Cover:
Shear distribution in the reinforced concrete slab under concentrated loads as a result of non-linear finite element analysis.

Shear Distribution in Reinforced Concrete Bridge Deck Slab

Non-linear Finite Element Analysis with Shell Elements

Master of Science Thesis in the Master's Programme Structural Engineering and Building Performance Design
ALICJA KUPRYCIUK
SUBI GEORGIEV
Department of Civil and Environmental Engineering
Division of Structural Engineering
Concrete Structures
Chalmers University of Technology

ABSTRACT

The aim is to provide more accurate predictions of the response and capacity of bridge deck slabs under shear loading. The objective is to form a basis for how shear forces determined through linear analysis can be distributed when assessing existing bridges. The shear force distribution, and how this change due to concrete cracking and reinforcement yielding is studied through finite element analyses of a bridge deck cantilever. Recommendations for non-linear analysis of reinforced concrete slabs with shell elements are established and verified.

This study shows that shear distribution can be captured with shell elements. However finding relatively accurate results requires selecting the appropriate modelling methods. Also it shows the importance of what Poisson's ratio is selected with respect to the acquired results. The evaluation of shear response for varied models is given. Results from non-linear analysis are verified by comparison with tests.

Key words: Reinforced concrete, shear force, punching shear, non-linear finite element analysis, distribution, bridge, slab, deck, fluctuation.

II

Contents

Preface

This thesis investigates the use of non-linear finite element analysis for the design and assessment of reinforced concrete bridge deck slabs subjected to shear loading. It was carried out at Concrete Structures, Division of Structural Engineering, Department of Civil and Environmental Engineering, Chalmers University of Technology, Sweden. The work on this thesis started March 2013 and ended June 2013.

The work in this study was based on an experimental tests carried out at the Ecole Polytechnique Fédérale de Lausanne in 2007. The experimental program consisted of tests on large scale reinforced concrete bridge cantilevers without shear reinforcement, subjected to different configurations of concentrated loads simulating traffic loads.

Notations

Roman upper case letters

A_{sl} area of fully anchored tensile reinforcement

D_b plane flexural rigidity

D_{max} aggregate size

D_s plane shear rigidity

E_s modulus of elasticity for steel

E_c modulus of elasticity for concrete

G_t shear module

M bending moment at critical section

V_{crit} shear force at which cracking starts

V_{Ed} design shear force value

V_R resisting punching shear force

$V_{Rd,c}$ shear capacity of concrete

Roman lower case letters

b cross-sectional width of the beam

b_w smallest width of the cross-section in the tensile area

$c_{RD,c}$ coefficient derived from tests

d effective depth of a slab; effective height of cross-section

u control perimeter

f_{cc} concrete compressive strength

f_{ck} characteristic concrete compressive strength

f_{ct} concrete tensile strength

f_y design yield stress

k coefficient dependent on the effective depth of the slab

k_{dg} parameter accounting for the aggregate size D_{max}

k_{xx} curvature in x-direction

k_{yy} curvature in y-direction

m_{xx} bending moment per meter length in x-direction

m_{yy} bending moment per meter length in y-direction

m_{xy} twisting moment per meter length

n_{xx}	membrane force in x-direction
n_{yy}	membrane force in y-direction
q_{xz}	shear force in xz-direction
q_{yz}	shear force in yz-direction
v_x	shear force per meter length in x-direction
v_y	shear force per meter length in y-direction
w	deflection
x	depth of compression zone

Greek letters

γ_c	partial safety factor for concrete
ε	normal strain in cross-section
η	shape factor for the parabolic variation over a rectangular cross section
θ	rotation of the slab
ν	Poisson ratio
ρ_l	longitudinal reinforcement ratio
ρ	geometric reinforcement ratio
σ_c	stress in concrete
τ_c	nominal shear strength of concrete
τ_R	shear strength
φ	rotation

1 Introduction

1.1 Background of the project task

Bridge deck slabs are one of the most exposed bridge parts and are often critical for the load carrying capacity. Nowadays, design procedures for concrete slabs regarding bending moment are well-known. However, there is still a lack of well-established recommendations for distribution of shear forces from concentrated loads. Consequently, it is important to examine the appropriateness of current analysis and design methods to describe the actions of shear. A common way to design reinforced concrete is by linear elastic FE analysis. Such analysis gives good results as long as the structure remains un-cracked. To describe the real behaviour of the slab non-linear analysis is needed due to stress redistribution to other regions after cracking. However, to avoid a demanding non-linear analysis the concentrated shear forces gained through a linear analysis can be distributed within larger parts of the structure to take into account the stress redistribution. Such redistribution needs more specified recommendations, especially when the influence of flexural cracking is to be taken into account. In 2012, a study of how to distribute shear force from linear FE analyses in bridge decks was performed by one of the master students - Poja Shams Hakimi. However, fluctuations of shear results occurred when increasing the load. Discovering the reason of this tendency, and how to avoid this kind of response became the basis case for this project, which in addition, is part of a PhD project at Chalmers University of Technology, financed by the Swedish Transport Administration.

1.2 Purpose and scope

The purpose of this master's thesis was to provide more accurate predictions of the response and capacity of bridge deck slabs under loading with respect to shear. The behaviour of shear and failures caused by shear in concrete slabs was investigated. The distribution and re-distribution of shear forces in concrete slabs with respect to bending cracks and yielding of the reinforcement was studied. In order to investigate it, non-linear analysis using FE software was required. Therefore, the purpose was also to establish a method for non-linear analysis of reinforced concrete slabs with shell elements. The scope was limited to the study of cantilever bridge deck slabs. One typical load and geometry configuration, previously tested, was chosen for the study.

1.3 Method

The project started with a literature study of Vaz Rodrigues' research in this field (Vaz Rodrigues 2007). Since this master's thesis is closely related to an on-going research project concerning load carrying capacity of existing bridge deck slabs, the literature study helped to get an overview of what experiments had been carried out before and

what thing may need further investigation. Finite element analyses of a bridge deck cantilever, both where cracking had occurred and had not occurred, were performed in order to identify common parameters for the cases. The results from different analyses are compared.

2 Shear in Concrete Slabs

Shear response in reinforced concrete members has been investigated from its early developments (Ritter 1899, Mörsch 1908) with theoretical and experimental works. However, there is no existing theory that is capable of fully describing the complex behaviour of reinforced concrete elements subjected to shear. Based on the validation of experimental tests, shear stresses can result in inclined cracks compared to the direction of the reinforcement in concrete member. Possible failure modes due to shear cracks have been studied during the years. In the following sections focus is put on failure modes and failure criteria. To compare and verify the results, tests on full scale specimens that previously have been loaded until failure is presented. Overview of the codes of practice in this field is also given.

2.1 Shear failure

Understanding the nature of failures in bridge deck slabs without shear reinforcement is very important in order to evaluate and improve existing designing process for such structures. The actual behaviour of slabs is very complex as there are many possible failure modes that interact. As the scope of this thesis is to investigate the shear behaviour of bridge deck slabs, different failure modes with respect to shear will be discussed, see *Figure* 1.
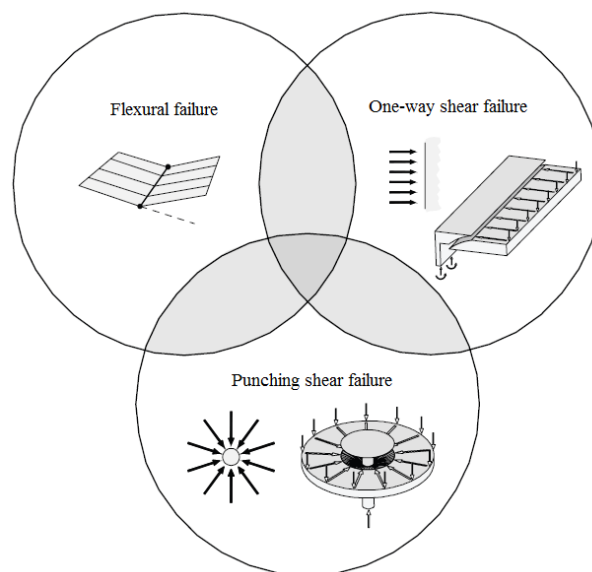

Figure 1.   *The main failure modes for reinforced concrete slabs. From Vaz Rodrigues (2007).*

- Punching shear failure: occurs in slabs under concentrated loads such as stored heavy machinery, heavy vehicle wheels in bridges, and where slabs are supported by columns. This failure mode is highly undesirable as it is brittle and results in complete loss of load carrying capacity of the slab.

- One-way shear failure: this failure mode is also undesirable since it exhibits brittle failure as well. It can occur in slabs loaded with line loads and near line supports.
- Failure due to the combined effect of shear forces and bending moments: Even though flexural failure has different mechanisms when combined with normal and shear stresses, neither of the maximum value for pure flexural or shear failure need to be reached in order for failure to occur.

Reinforced concrete bridge cantilever slabs not provided with shear reinforcement can fail in shear under high traffic loads. This is an undesirable failure mode, which can prevent the structure from deforming and reaching the ultimate load predicted by pure flexural analysis. Thus, it has to be proven whether the flexural reinforcement and concrete will provide sufficient resistance. Moreover, in bridge decks the flow of shear forces is different for punching shear and one-way shear. Shear failure may occur either before or after the yielding of flexural reinforcement, depending on the loading and the geometry of the structure. For these reasons, better understanding of the various failure types governing the behaviour of concrete bridge decks is necessary.

2.1.1 One-way shear

2.1.1.1 General overview

One-way shear takes place under line loads and along line supports. As shown in *Figure 2*, in the case of line load on a cantilever the shear flow is causing inclined cracks and a potential one-way shear failure.
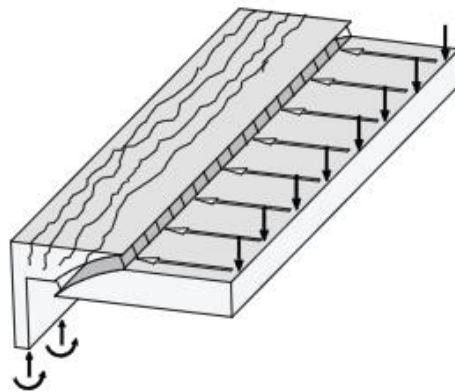

Figure 2. *One-way shear failure and corresponding flow of forces. From Vaz Rodrigues (2007).*

Using the strut and tie model, Vaz Rodrigues (Vaz Rodrigues 2007) gives an explanation on how the load carrying mechanism develops in a strip of a slab. The mechanism is determine by the location of the cracks and is accompanied by phenomena such as dowel action, aggregate interlock and cantilever action. Their effect varies with the magnitude of the applied load and crack pattern. *Figure 3* shows the evolution of the mechanism through different stages of cracking. Before cracking,

the theory of elasticity describes the behaviour accurately. The model implies that tension forces cannot be transferred across cracks, thus the dowel action of the flexural reinforcement at the bottom of the section deals with them. At *Figure 3c* one could see that a new stress field is provoked by the propagating cracks and that an inclined straight strut develops all the way from the applied load to the zero moment point, even though the strut is crossed by cracks. Muttoni suggests that when a strut is crossed by cracks only a limited amount of compression can be transmitted (Muttoni, Schwartz 1991). In order for the system to keep the equilibrium, the strut drives towards the edge but no longer in a straight manner, which leads to decompression of the region below it and tensile stresses will occur above the compressive strut. Complete failure is reached when the tensile strength of the concrete in that tie is reached. The example shows the most important factors dictating the shear strength of the sample:

- Concrete compressive and tensile strength
- Location of the crack opening in relation of the struts
- Coarse aggregate`s properties, since aggregate influence the amount of shear force transferred across the cracks.
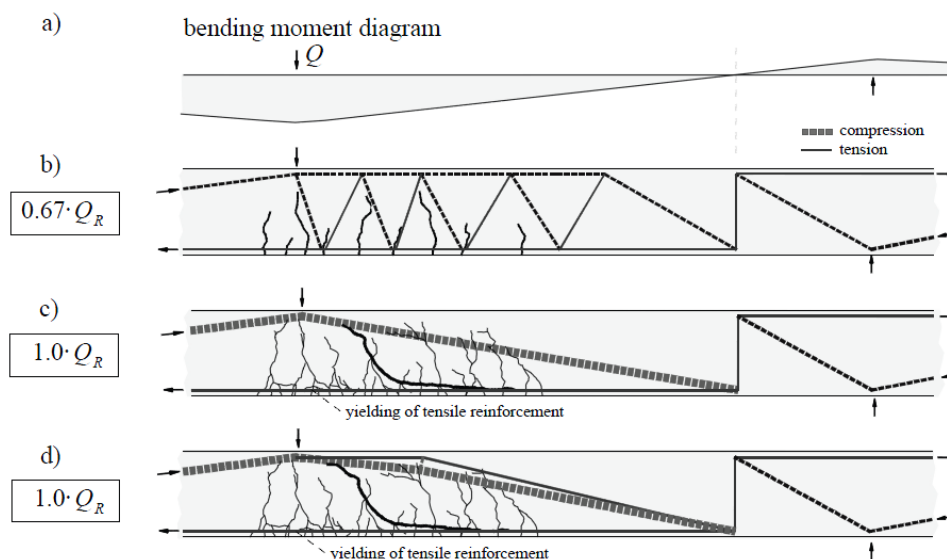

Figure 3.   *Development of load-carrying mechanism. From Vaz Rodrigues (2007).*

2.1.1.2   Failure Criteria

2.1.1.2.1   Muttoni's failure criterion

A model to determine one-way shear strength was proposed by Muttoni based on a rotational model for concrete slabs without shear reinforcement (Muttoni 2003). A prerequisite to this model is the crack's nominal opening in the critical region. It is also based on the following hypotheses:

- The critical zone is located at a cross section a distance of $0.5 \cdot d$ from the point of introduction of the load and at $0.6 \cdot d$ from the extreme compression fibre.
- The crack opening in the critical region is proportional to the product of the section's strains ε by the effective depth d.
- Plane sections remain plain.

Accordingly to these hypotheses, strains calculated according to the properties of the cross-section and the acting moment and axial force, can be expressed as:

$$\varepsilon = \frac{M}{d \cdot \rho \cdot E_s \cdot \left(d - \frac{x}{3}\right)} \cdot \frac{0.6 \cdot (d-x)}{d-x}, \quad x = d \cdot \rho \cdot \frac{E_s}{E_c} \cdot \left(\sqrt{1 + \frac{2 \cdot E_c}{\rho \cdot E_s}} - 1\right) \tag{2.1}$$

Where M – bending moment at critical section, d – effective depth of the slab, x – depth of compression zone, ρ – geometric reinforcement ratio, E_s – modulus of elasticity for steel, E_c – modulus of elasticity for concrete.

The shear strength directly depends on the strains calculated at the critical cross-section. The one-way shear strength of members without shear reinforcement is expressed by the following equation:

$$\tau_R = \frac{V_R}{b \cdot d} = \frac{\tau_c}{0.9 + 2.3 \cdot \varepsilon \cdot d \cdot k_{dg}} \tag{2.2}$$

Where V_R – resisting punching shear force, b – width of the beam, d – effective depth of the slab, τ_c – nominal shear strength of concrete, ε–section's strains, k_{dg} – parameter accounting for the aggregate size D_{max} [mm].

As shown in *Figure 4*, on the basis of the systematic analysis of 253 shear tests, *equation 2.2* predicts well the measured shear strength. The comparison shows an excellent agreement between theory and experiments, with a very small coefficient of variation. Such results are better than those obtained with some codes of practice. However, since *equation 2.2* is too complex for practical applications, a simplified version proposed by building codes is usually used, see *section 2.1.1.2.2*.
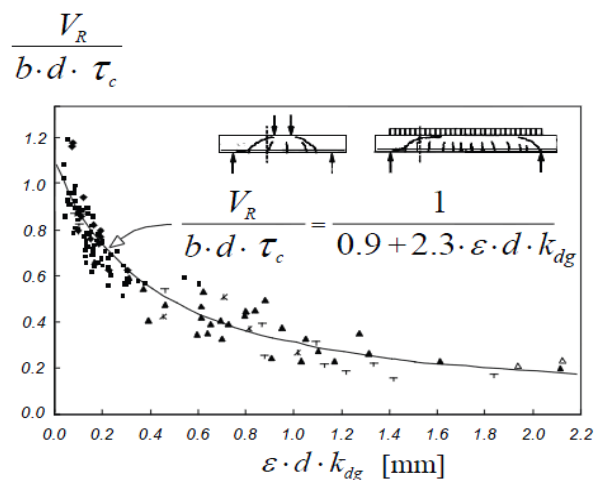

Figure 4.   *Test results from 253 shear tests without shear reinforcement and prediction of the suggested equation. From Muttoni (2003).*

2.1.1.2.2 Eurocode 2 failure criterion

In all codes of practice, during design process it is necessary to ensure that the concrete shear stress capacity without shear reinforcement is more than the applied shear force:

$$V_{Ed} \leq V_{Rd,c} \qquad (2.3)$$

The total shear strength should be divided with the control perimeter (u) to obtain the shear strength per unit of length. If the design shear force is larger than shear force capacity, shear reinforcement is necessary for the full design shear force.

To calculate the shear strength, Eurocode 2 (2001) proposes the following equation:

$$V_{Rd,c} = \left[c_{Rd,c} \cdot (100 \cdot \rho_1 \cdot f_{ck})^{\frac{1}{3}} + k_1 \cdot \sigma_{cp} \right] \cdot b_w \cdot d \qquad (2.4)$$

This empirical expression includes the effect of pre-stressing or other axial force, represented by compressive stress at the centroidal axis for fully developed pre-stress σ_{cp}. Without additional influences the equation can be expressed as:

$$V_{Rd,c} = \left[c_{Rd,c} \cdot k \cdot (100 \cdot \rho_1 \cdot f_{ck})^{\frac{1}{3}} \right] \cdot b_w \cdot d \qquad (2.5)$$

Where $c_{RD,c}$ − coefficient derived from tests,], k − coefficient dependent on the effective depth of the slab, ρ_l − longitudinal reinforcement ratio, f_{ck} − characteristic concrete compressive strength, b_w − smallest width of the cross-section in the tensile area, d − effective height of cross-section.

With a minimum of

$$V_{Rd,c} = V_{min} \cdot b_w \cdot d \qquad (2.6)$$

Where

$$c_{Rd,c} = \frac{0,18}{\gamma_C}, \qquad k = 1 + \sqrt{\frac{200}{d}} \leq 2.0, \qquad \rho_1 = \frac{A_{sl}}{b_w \cdot d} \leq 0,02 \qquad (2.7)$$

Where γ_C − partial safety factor for concrete, A_{sl} − area of fully anchored tensile reinforcement.

2.1.2 Punching shear

2.1.2.1 General overview

Most typically punching shear is observed with reinforced concrete flat slabs, where there are no beams to spread the load over greater area and the slabs are supported by columns (point supports).The load transfer between the slab and the column induces high stresses near the column that incites to cracking and even failure. The punching shear failure occurs in a brittle manner and the shape of the failure is a result of the interaction between the shear effects and flexure in a region close to the column as in *Figure 5*.
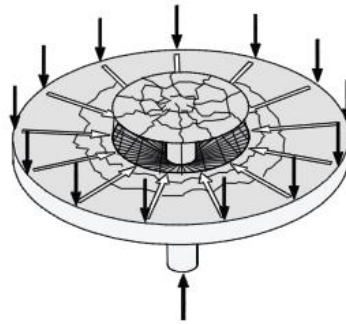
Figure 5.   *Punching shear failure and corresponding flow of forces. From Vaz*
             Rodrigues (2007).

According to Vaz Rodrigues (2007) the load bearing loss develops in three stages. The first flexural cracks develop at an early linear elastic phase. Once the radial cracking moment is reached in *Figure 6, V=V_{cr}*, redistribution starts and radial cracks initiates as shown in *Figure 6, $V_{cr} \leq V \leq 0,9V_R$*. Also additional tangential cracks opens at distance of the initial one. At certain load no more cracks occur and a truncated conical crack propagates all the way to the column with increasing width see *Figure 6, V=V_R*.
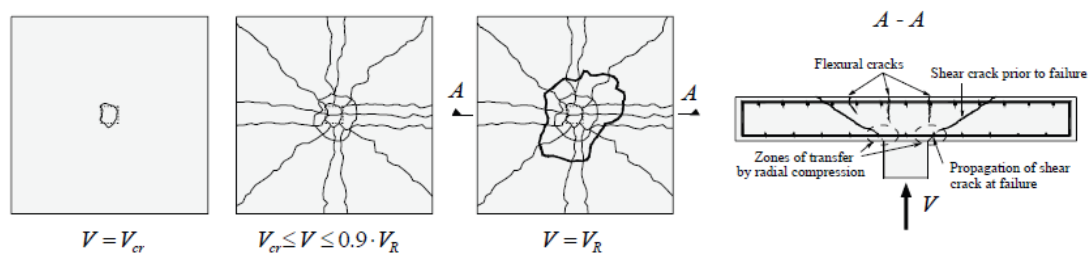
Figure 6.   *Crack pattern development on the top surface. From Guandalini*
             (2005).

In case of only flexural reinforcement the failure occurs in brittle manner with only small deformations. Even though top bar cannot contribute to suspending the slab from collapsing, due to the loss of interaction between the steel and concrete, sufficiency of bottom reinforcement could retain the fault slab and prevent further damage and loss of life.

A peculiar phenomena occurs when load exceed 80-90% of resisting punching shear force (V_R). The compressive strains on the bottom surface increase up to this limit and then the effect is reversed and they are reduced, in some case even tensile strains might take place.

In order to keep the truss model in equilibrium when the cracks initiates some of the ties are cut and the new truss looks differently, as can be seen in *Figure 7*. To keep the system in equilibrium, a tensile strut appears at the bottom surface.
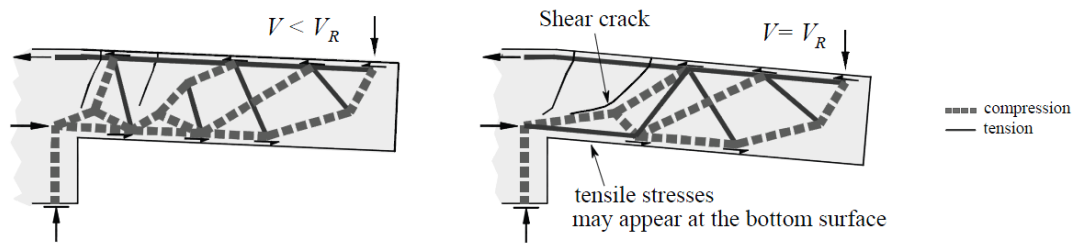
Figure 7. *Flow of inner forces prior to punching shear failure. From Muttoni, Schwartz (1991), and Guandalini (2005).*

2.1.2.2 Failure Criteria

2.1.2.2.1 Muttoni's failure criterion

Estimating punching shear strength was proposed by Muttoni (Muttoni 2003) based on rotational model for concrete slabs without shear reinforcement. In this model rotation θ of the slab is set as controlling parameter, since the deformations of the slab concentrate near the column edge. The author concluded that the width of the critical crack is significantly affected by $\theta \cdot d$ and the shear strength can be expressed as:

$$\tau_R = \frac{V_R}{u \cdot d} = \frac{\tau_c}{0.4 + 0.125 \cdot \theta \cdot d \cdot k_{dg}} \tag{2.8}$$

Where V_R – resisting punching shear force, u –control perimeter, d – effective depth of the slab, τ_c– nominal shear strength of concrete, θ –rotation of the slab , k_{dg} – parameter accounting for the aggregate size D_{max} [mm].

The control perimeter (u) is situated at a distance of $0.5 \cdot d$ of the edge of the loaded area as shown in *Figure 8*. The length of the control perimeter u should take into account the distribution of transverse shear forces.
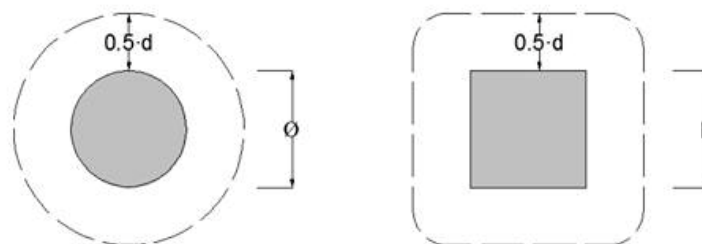

Figure 8. *Control perimeter for circular and square columns. Adapted from Swiss concrete code (SIA 262).*

Equation 2.8 can be compared with experimental results in *Figure 9*. It can be observed that there is lack of tests with large rotations. In order to show that even slabs with low reinforcement ratios will eventually fail in punching shear after yielding of the flexural reinforcement, high flexural reinforcement ratios were generally used. Such an assumption prevented the yielding of reinforcement in tension.
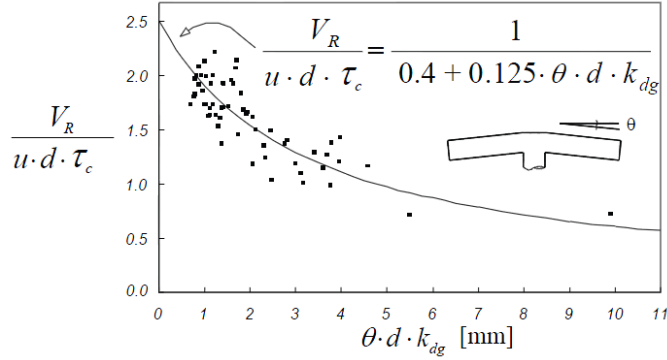
Figure 9.   *Comparison of equation 2.3 with punching shear tests. From Muttoni 2003.*

2.1.2.2.2 Eurocode 2 failure criterion

According to Eurocode 2 (2001) the design procedure for punching shear is based on checks at a series of control sections, which have a similar shape as the basic control section. Punching shear reinforcement is not necessary if:

$$V_{Rd,c} \geq V_{Ed} \tag{2.9}$$

The punching shear resistance per unit area ($V_{Rd,c}$) can be expressed as:

$$V_{Rd,c} = \frac{0.18}{\gamma_c} \cdot k \cdot (100 \cdot \rho_l \cdot f_{ck})^{1/3} - 0.1 \cdot \sigma_{cp} \nless 0.4 \cdot (f_{ctd} - 0.1 \cdot \sigma_{cp}) \tag{2.10}$$

Where ρ_l – anchorage length of tensile reinforcement, f_{ck} – characteristic concrete compressive strength [MPa], k – coefficient dependent on the effective depth of the slab, σ_{cp} – compressive stress at the centroidal axis, f_{ctd} – design value of axial tensile strength of concrete.

$$k = 1 + \sqrt{\frac{200}{d}} \leq 2.0, \qquad \rho_l = \sqrt{\rho_{lz} \cdot \rho_{ly}} \leq 0.02, \qquad \sigma_{cp} = \frac{(\sigma_{cy} + \sigma_{cz})}{2} \tag{2.11}$$

Where

ρ_{ly}, ρ_{lz} – relate to the tension steel in x- and y- directions respectively. The values ρ_{ly} and ρ_{lz} should be calculated as mean values taking into account a slab width equal to the column width plus $3d$ each side.

σ_{cy}, σ_{cz} – normal concrete stresses in the critical section in y- and z- directions (MPa, negative if compression):

$$\sigma_{c,y} = \frac{N_{Ed,y}}{A_{cy}} \text{ and } \sigma_{c,z} = \frac{N_{Ed,z}}{A_{cz}} \tag{2.12}$$

Where

$N_{Ed,y}$, $N_{Ed,z}$ – longitudinal forces across the full bay for internal columns and the longitudinal force across the control section for edge columns. The force may be from a load or prestressing action.

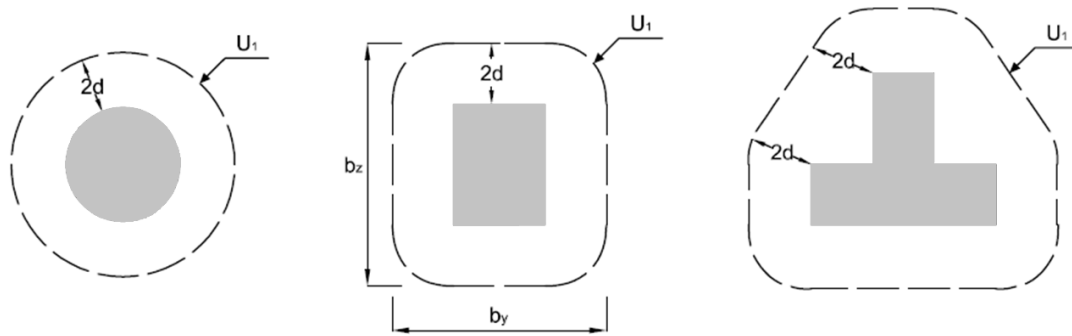A_c – area of concrete according to the definition of N_{Ed}

CHALMERS, *Civil and Environmental Engineering*, Master's Thesis 2013:127

Figure 10.   Basic control perimeters around loaded areas. Adapted from Eurocode EN 1992-1 (2001).

2.2   Vaz Rodrigues' tests

The behaviour of bridge deck slabs under concentrated loads simulating traffic loads is complex. Depending on the loading conditions and the geometry of the structure several load-carrying mechanisms can develop and coexist as stated in *section 2.1*. To investigate the structural behaviour and failure mode of bridge deck slabs, several tests were performed by Vaz Rodrigues (Vaz Rodrigues 2007).

2.2.1   Test set-up

The experimental work involved six tests on two specimens, in 3/4s of full scale, representing the cantilever deck slab of a bridge, without shear reinforcement in the slab. It was designed using the traffic loads prescribed by Eurocode 1 (2003) and the scale factor was applied to keep the same reinforcement ratios as in the full scale structure. The cantilever had dimensions corresponding to a large concrete box girder bridge, with a span of 2.78 m and a length of 10 m. The slab thickness varied from 0.38 m at the clamped edge to 0.19 m at the cantilever tip as shown in *Figure 11*. The main reinforcement of the top layer at the fixed end consisted of 16 mm diameter bars at 75 mm spacing. Only half of the main reinforcement continued to the free edge of the cantilever while the other half was cut-off 1380 mm from the clamped edge. The second reinforcement of the top layer consisted of 12 mm diameter bars at 150 mm spacing. The bottom reinforcement consisted of 12 mm diameter bars at 150 mm spacing in both directions. The concrete cover was 30 mm. The fixed end support was clamped by means of vertical pre-stressing, see *Figure 11*.
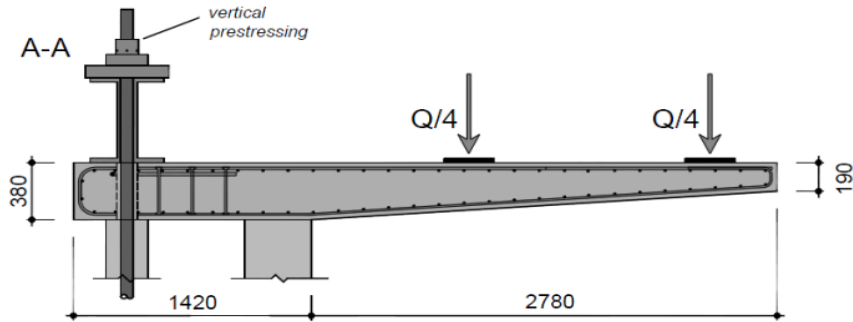
Figure 11. Slab dimensions, reinforcement layout, support arrangement and applied loads for the tests. From Vaz Rodrigues (2007).

The specimens were subjected to various configurations of concentrated forces simulating traffic loads, see *Figure 12*. Each slab was tested three times varying the position and the number of applied loads.
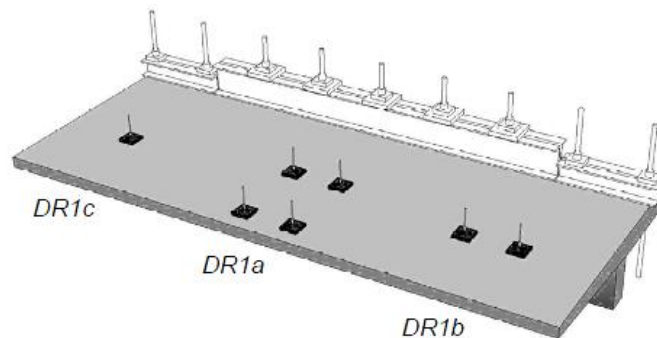

Figure 12. Schematic layout of tests. From Vaz Rodrigues (2007).

The load was introduced by a hollow hydraulic jack connected to a hand pump, see *Figure 13*. The jack was anchored to the laboratory strong floor by a 75 mm diameter bar, where spherical nuts and washers were used to accommodate rotation. The concentrated loads were applied on the top of the slab using steel plates with dimensions 300 x 300 x 30 mm.
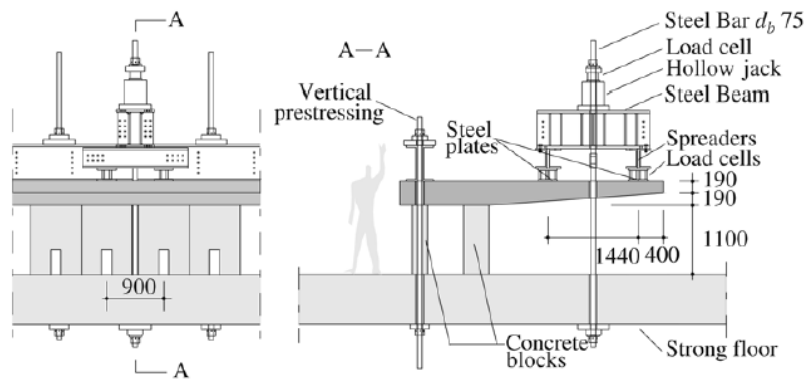
Figure 13. Test set-up for test DR1a. From Vaz Rodrigues (2007).

2.2.2 Failure mode

All tests failed by development of a shear failure around the concentrated loads in a brittle manner. First, flexural cracks developed on the top surface at the clamped edge. At the bottom surface, cracks developed below the applied loads following the transverse direction. For test DR1a significant yielding in the top and in the bottom reinforcement occurred. For this test, the failure surface developed around the two concentrated loads near the tip of the cantilever and another large shear crack in the region between the clamped edge and the applied loads was observed, see *Figure 14*. Important flexural and shear cracks occurred near the fixed end of the cantilever. However, the failure mode was a brittle shear failure at the two loads near the edge. This suggests possible redistributions of the internal shear flow, with the progressive formation of shear cracks until equilibrium is no longer possible.
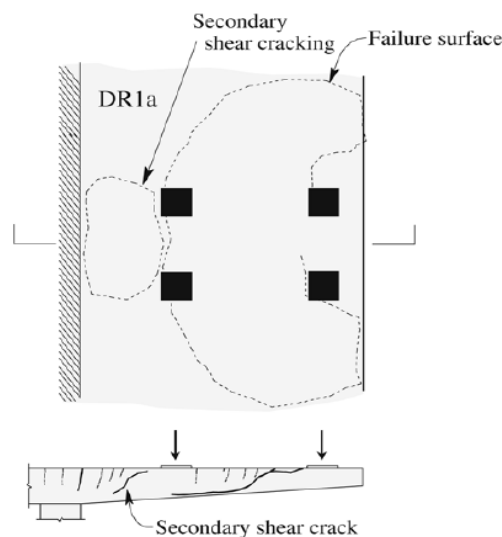
Figure 14.   Failure surface of test DR1a. From Vaz Rodrigues (2007).

The flexural ultimate load was never reached in any of the three tests. The design of bridge slab cantilevers with respect to bending is usually made using either elastic calculations or yield-line theory, based on the upper bound theory of limit analysis. For each test, the flexural ultimate load was estimated based on the yield-line method, see *Figure 15*, which included the effect of variable depth, orthotropic reinforcement and discontinuity of the main reinforcement in the top layer.
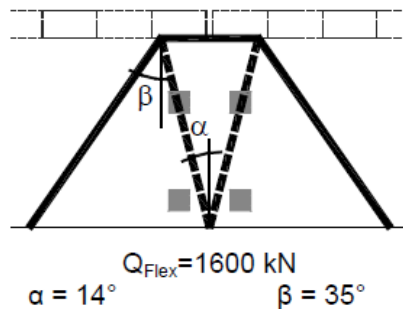
Figure 15.   Yield-line mechanism and yield-line failure load. From Vaz Rodrigues (2007).

In test DR1a the failure load was closest to the calculated capacity. Plastic strains were present both in the top transversal reinforcement at the fixed end and in the bottom longitudinal reinforcement underneath the edge loads.

The deflection measured at the tip of the cantilever was also larger for test DR1a compared to the other tests, but mostly due to the load configuration with two loads close to the edge of the cantilever, see *Figure 16*. The load-deflection curve shows that for all the tests that the yield-line pattern was not fully developed and a plastic plateau was not attained.
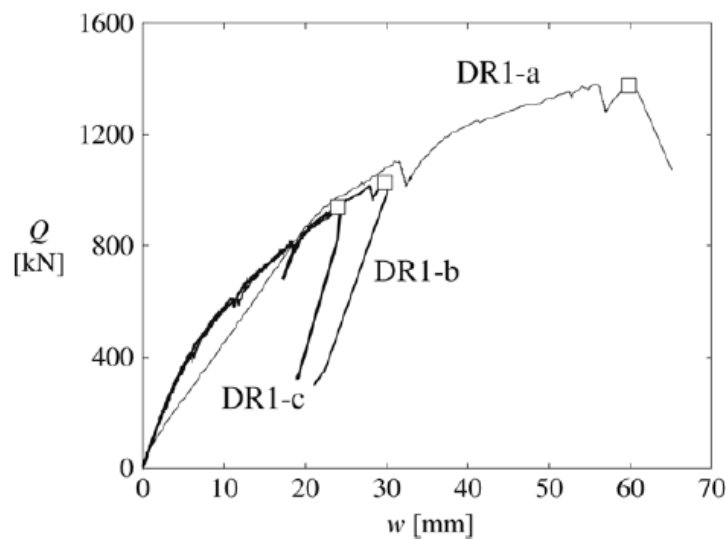
Figure 16.   Load-deflection curve for three tests. From Vaz Rodrigues (2007).

3 FE Analysis

FE analysis in the engineering community provides the possibility of finding relatively accurate results for complex structures in an easy way. In the past years the usage of such analyses has significantly increased, leaving more traditional design tools behind (Broo H., Lundgren K., Plos M., 2008). In order to perform it some important choices are required. There are many ways to build a FE model; thus it is important to know what kind of response is expected from the structure that is of interest. Moreover, during modelling, certain idealizations of the structure are necessary to make. The first major set-up is the theoretical background as different theories exist to describe the same type of structural members. Before modelling one must know the prerequisites and assumptions of the theory behind the elements that are to be used. Also the choices during modelling, such as geometry, boundary conditions and mesh density, affect the possibility to obtain a realistic behaviour of the modelled structure. Furthermore, in order to set up an appropriate model, element types and materials models must also be wisely chosen.

3.1 Thick Plates Theory

The finite elements used in this study are based on the Mindlin-Reissner Theory, TNO Diana User's Manual v. 9.4.4 (2012). Contrary to the Thin Plates Theory where no shear deformations are considered, in the Mindlin-Reissner Theory (also known as "Thick Plates Theory") these deformations are taken into account. Thus the moments and shear forces are derived as follows:

$$
\left|
\begin{aligned}
m_{xx} &= D_b\left(k_{xx} + \nu k_{yy}\right) = D_b\left(\frac{\partial \varphi_x}{\partial x} + \nu \frac{\partial \varphi_y}{\partial y}\right) \\
m_{yy} &= D_b\left(k_{yy} + \nu k_{xx}\right) = D_b\left(\frac{\partial \varphi_y}{\partial y} + \nu \frac{\partial \varphi_x}{\partial x}\right) \\
m_{xy} &= D_b(1-\nu)k_{xy} = \tfrac{1}{2}D_b(1-\nu)\left(\frac{\partial \varphi_x}{\partial y} - \frac{\partial \varphi_y}{\partial x}\right) \\
v_x &= D_s\gamma_x \\
v_y &= D_s\gamma_y
\end{aligned}
\right.
$$

Where

$D_b = \frac{Et^3}{12(1-\nu^2)}$ – plane flexural rigidity,

$D_s = \frac{G_t}{\eta}$ – plane shear rigidity,

G_t – shear module,

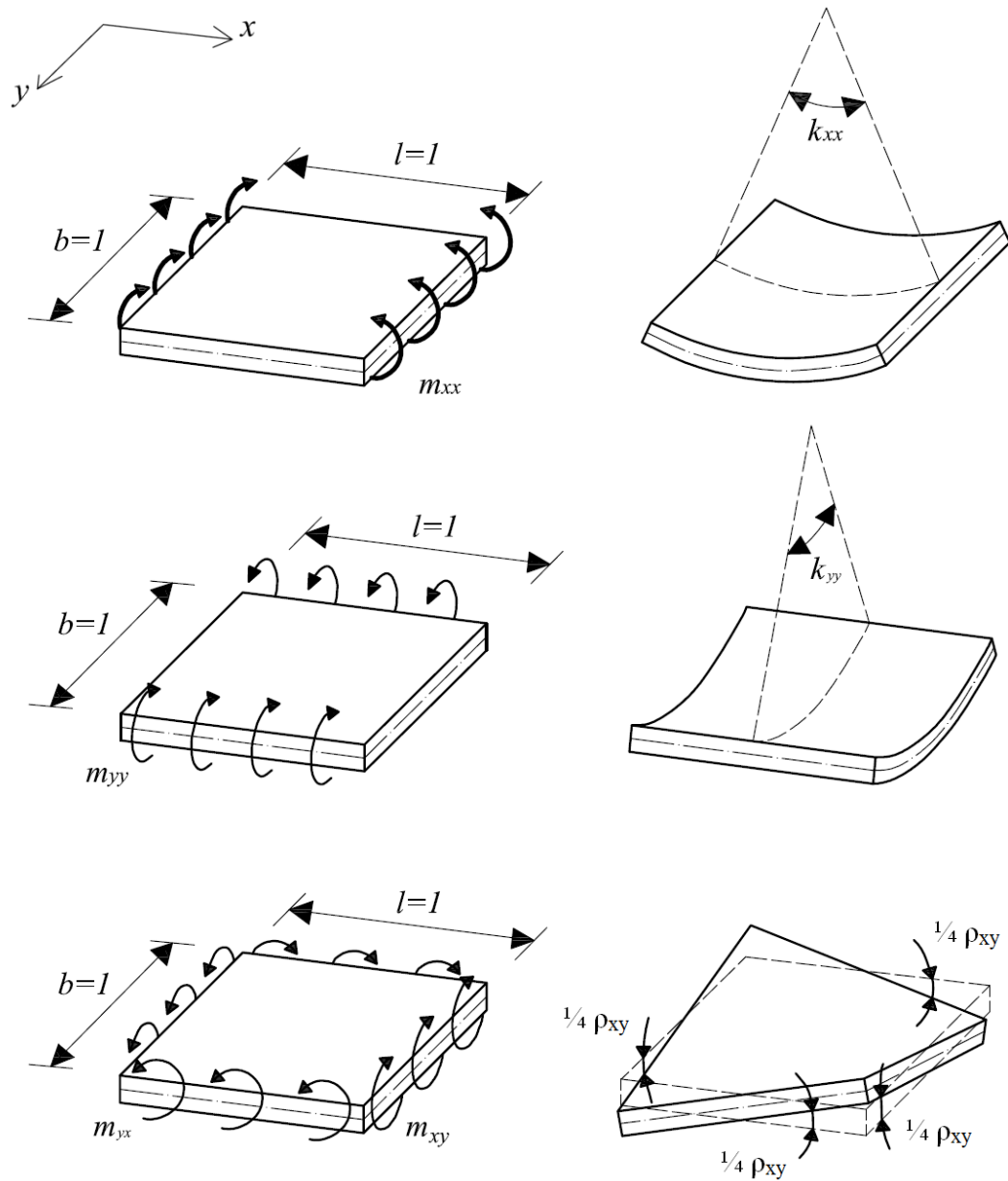$\eta = \frac{6}{5}$ – shape factor for the parabolic variation over a rectangular cross section.

Figure 17.   Moments and curvatures definitions for the Thick Plates Theory. Adapted from Blaauwendraad (2010).

CHALMERS, *Civil and Environmental Engineering*, Master's Thesis 2013:127

3.2 FE modelling

3.2.1 Types of elements

When carrying out FE analysis, selection of a particular type of element is necessary to make. As the main scope of the thesis is to investigate the appropriateness of shell elements for the task, curved shell elements were used. They are based on Mindlin-Reissner Thick Plates Theory. Such elements are generally triangular or quadrilateral as the nodes are positioned in the mid-thickness of each layer of the element, see *Figure 18*. Different order elements exist as 4, 8, and 12 nodes elements are supported by TNO Diana v. 9.4.4 (2013).
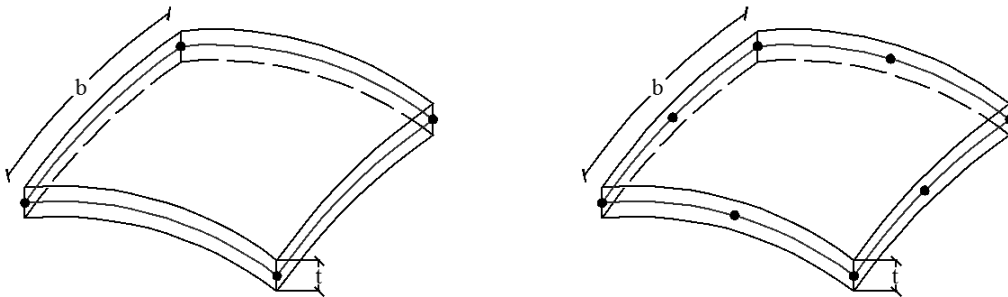
Figure 18.   *Curved shell element with 4 and 8 nodes in one layer. Adapted from Diana User's Manual (v. 9.4.4)(2012).*

The element geometry is described by the nodal point coordinates. Five degrees of freedom (DOF) are defined in every element node: three translations and two rotations see *Figure 19*. The translational DOF are in the global coordinate system. The rotations are about two orthogonal axes on the shell surface defined at each node. The rotational boundary condition restraints and applied moments also refer to this nodal rotational system.
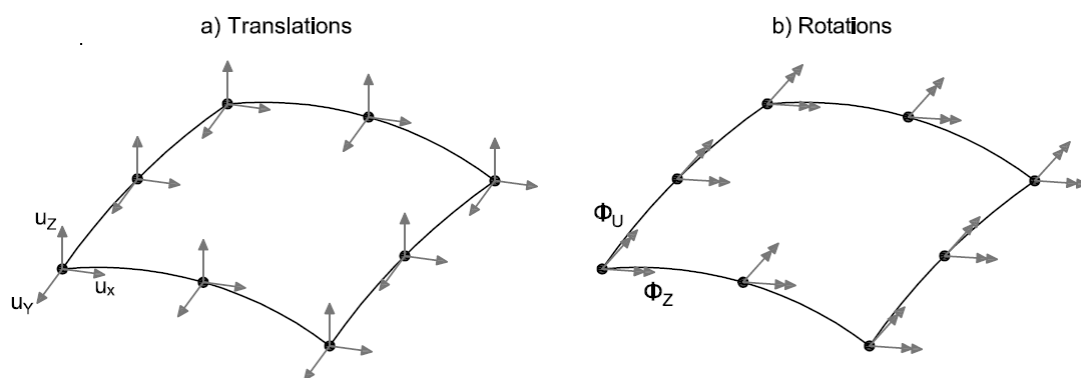

Figure 19.   *Degrees of freedom. Adapted from Diana User's Manual (v. 9.4.4) (2012).*

The generalized element is defined by means of a parametric coordinate system − ξ, η and ζ, see *Figure 20*.
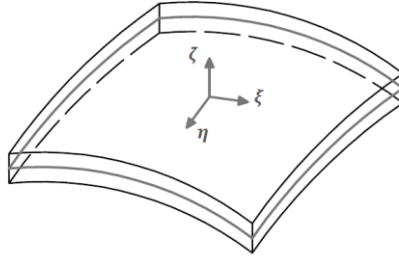
Figure 20.   Element with parametric coordinate system.

A minimum number of integration points is required by the numerical integration method and depends on the order of the interpolation polynomial. The polynomials for the translations *u* and the rotations *φ* for a 4 nodes element can be expressed as:

$$u_i(\xi, \eta) = a_0 + a_1\xi + a_2\eta + a_3\xi\eta \tag{2.9}$$

$$\varphi_i(\xi, \eta) = b_0 + b_1\xi + b_2\eta + b_3\xi\eta \tag{2.10}$$

and for a 8 nodes element as:

$$u_i(\xi, \eta) = a_0 + a_1\xi + a_2\eta + a_3\xi\eta + a_4\xi^2 + a_5\eta^2 + a_6\xi^2\eta + a_7\xi\eta^2 \tag{2.11}$$

$$\varphi_i(\xi, \eta) = b_0 + b_1\xi + b_2\eta + b_3\xi\eta + b_4\xi^2 + b_5\eta^2 + b_6\xi^2\eta + b_7\xi\eta^2 \tag{2.12}$$

Typically, for a rectangular element, these polynomials yield approximately the following strain and stress distribution along the element area in a ζ lamina. The strain ε_{xx}, the curvature k_{xx}, the moment m_{xx}, the membrane force n_{xx}, and the shear force q_{xz} are constant in *x* direction and vary linearly in *y* direction. The strain ε_{yy}, the curvature k_{yy}, the moment m_{yy}, the membrane force n_{yy}, and the shear force q_{yz} are constant in *y* direction and vary linearly in *x* direction, Diana User's Manual (v. 9.4.4) (2012).

Cook, Malkus, Plesha, Witt (2004) alongside other FE modelling guides suggest that for non-linear analyses higher order elements have to be used. Due to the fact that the previous work was carried out with first order elements this thesis considered both 4 nodes and 8 nodes elements.

3.2.2   Types of material

For bridge structures different types of materials are used such as concrete, steel, pre-stressing tendons, etc. The materials' properties that are used for a linear analysis are modulus of elasticity, Poisson's ration and the mass density. However, FE software always offers a wide variety of material models which can be applied in the various analysis types. The purpose of the material model is to describe the link between the deformations of the finite elements and the forces transmitted by them. Due to that, the material model should be selected based on a material's deformation under external loads. In order to model adequate behaviour of the material, the failure mechanisms which can occur in the structure must be known. For instance, in

reinforced concrete structures the behaviour is mainly influenced by cracking and crushing of the concrete and yielding of the reinforcement.

Different material properties must be assigned to the concrete elements than to the steel reinforcements. The material model of concrete should account for cracking failure under tensile stresses and crushing failure at compressive and shear stresses. It is important to take non-linear material response into account and using proper non-linear material models in finite element analysis is one way of doing this. Regarding steel properties, this material can be modelled with Von Mises plasticity model with a yield criterion.

An important parameter that is generally considered as granted is the Poisson ratio. For un-cracked concrete normally it is $v=0.2$ but in case of fully-cracked concrete members it tends to $v=0$. That is why both values are considered in the process of modelling.

3.2.2.1 Stress-strain relationship of concrete

For linear structural analysis the simple isotropic elasticity model can be chosen. Such an analysis is based on linear constitutive stress-strain equation. Some materials behave in this way only if the deformation is small. With the increase in deformation the uni-axial stress-strain relationship becomes non-linear. Cracking of concrete is the main source of material nonlinearity so concrete has to be treated as a material with distinct properties. Since it has different properties in tension and compression adequate idealizations of models must be used for both cases, see *Figure 21*. The softening curves are based on fracture energy and by the definition of the crack bandwidth.
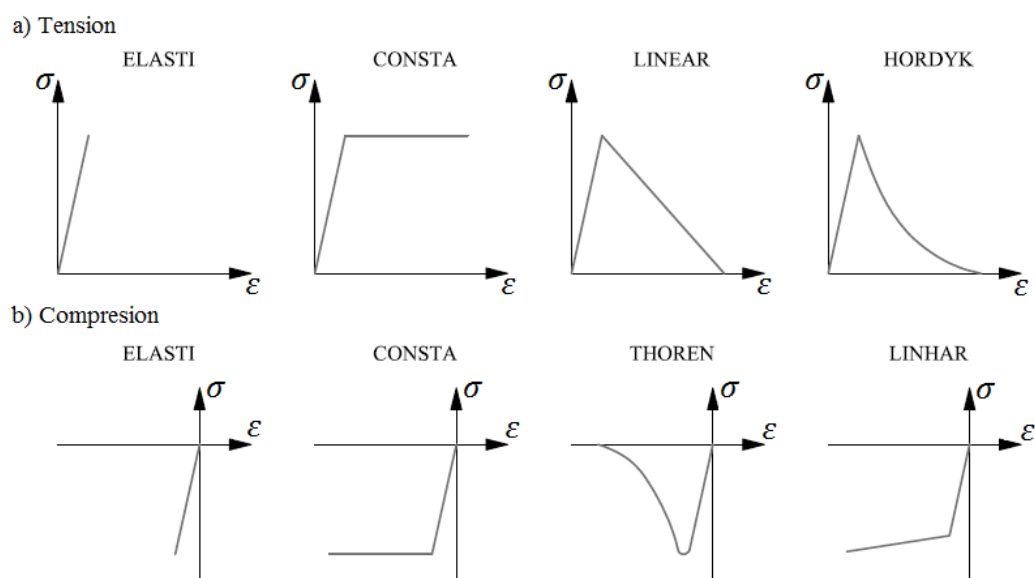

Figure 21.   *Examples of stress-strain relations for concrete, a) Concrete in tension, b) Concrete in compression. Adapted from Diana User's Manual (v. 9.4.4) (2012).*

3.2.2.2 Crack approaches

In order to model concrete cracking in FE software an appropriate material model has to be used. The description of concrete cracking and failure within finite element has led to three fundamentally different approaches - discrete, smeared and embedded one. In discrete crack approach, cracks are described as discontinuities and separate elements are placed where cracks are expected. This is the main problem of this approach since the crack positions and directions must be predicted. With smeared crack approach, cracks are smeared out over the continuum elements and no predefinition of crack positions is needed. However, one of the disadvantages is that the crack band width of the cracked region needs to be defined in the software in advance. It is assumed that a crack will localize within this width and the crack opening will be smeared over this width. In addition, the cracks can be described with fixed or rotating directions after crack initiation or with plasticity models, however for reinforced concrete structures rotating crack model is often most suitable. In this model the crack direction is always perpendicular to the principal stress direction and no shear stress along the crack occurs. Although the rotating crack approach does not explicitly treat shear slip and shear stress transfer along a crack, it does simplify the calculations and is reasonably accurate under monotonic load where principal stress rotates a little, Maekawa (2003). The last approach, the embedded crack approach, is the most advanced method of simulating cracks. It has the advantages from both approaches, though it is not available in commercial FE software.

The smeared crack approach with rotating crack model was developed specially for cracking concrete under tensile load. However, the behaviour and size of concrete cracking cannot be defined with strains alone. Due to cracking the stress-strain diagram for different length of specimen is not the same. Some tensile stress can be transferred after micro-cracking has started, so tensile stress depends on the crack opening rather than on the strain. In order to compensate for that, the response should be submitted as stress versus crack opening diagram representing the deformations that occur in addition to the overall strains within the fracture zone. This results in modelling of the concrete response in tension with two different curves, one stress-strain relation for the un-cracked concrete and one stress versus crack opening relation for the cracked concrete, see *Figure 22*. The most important parameters that affect the fracture behaviour are the tensile strength, the shape of the descending part of the graph and the fracture energy, which refers to the area under the descending part.
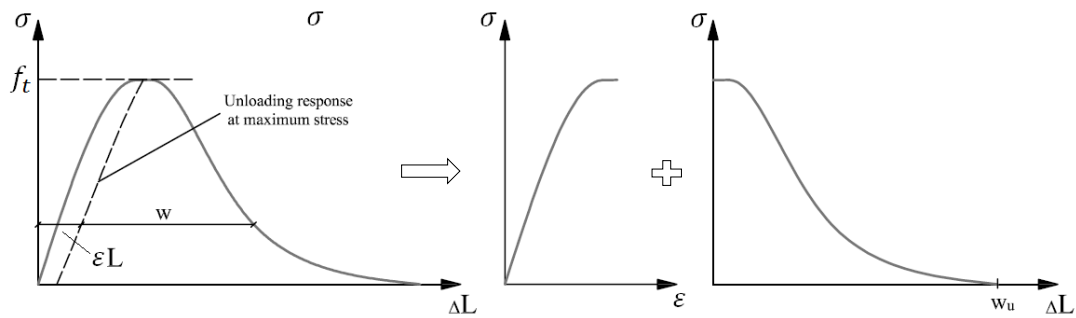
Figure 22. *Tensile behaviour of concrete specimen represented by two different curves – a stress-strain relation for the un-cracked concrete and a stress-crack opening relation for the crack. Adapted from Plos, M. (2000).*

3.2.3 Types of reinforcement

Selecting the proper way of modelling reinforcement has an important role in the structural analysis. Large reinforced concrete members can be modelled with so called embedded reinforcement, which adds stiffness to the model. This type of modelling embeds reinforcement in structural elements, so-called mother elements, which means that concrete elements are strengthened in the reinforcement direction. Reinforcements do not have degrees of freedom of their own. The elements and the reinforcements can be defined independently from each other, each with reference to their own geometry and material definition. FE software can have two types of embedded reinforcements, bars and grids. When the steel reinforcement is composed of a number of bars which are located at a fixed intermediate distance from each other, it is better to use reinforcement grids, which can be embedded in all curved shell elements. In solid elements embedded reinforcement with bond-slip included is also available. In this case the reinforcement bar is internally modelled as a truss or beam elements, which are connected to the mother elements by line-solid interface elements.

3.2.4 Boundary conditions

Selecting the proper boundary conditions has an important role in the structural analysis. For a static analysis, simple assumptions of supports are used, such as fixed, pinned or roller. However, in most cases more factors have to be taken into account, for instance stiffness having a critical influence on the analysis result. Modelling of supports in FE software requires a careful consideration of each translational and rotational component of displacement in order to imitate reality as much as possible. The boundary conditions basically define the restrictions on the degrees of freedom in the nodes. A supported degree of freedom is defined by a node number, type and direction.

3.2.5 Meshing

In FE software the quality and accuracy of results depend crucially on the mesh size. Various methods of generating mesh exist and most of them are based on prescribed mesh density values. During the mesh generation process, elements are described in terms of nodes and the connection between the geometry and mesh is established. Since meshing plays a significant role in the precision and stability of the numerical computation, checking its quality is always essential. Usually control tools are available to provide information about elements and their desired shape. For improving the quality, the mesh at certain areas of the geometry may need to be refined.

3.3 Types of Analysis

3.3.1 Linear Analysis

Performing linear analysis is the fastest and easiest way to acquire the resultant forces and stresses on a structure subjected to a certain loading. It treats the material as elastic and isotropic which requires substantial simplifications and assumptions. Due to the complexity of the reinforced concrete as material the results from this analysis are not valid in all the cases. Peak moments and forces occur around supports and concentrated loads. However in reality these high values are never reached as the concrete cracks at very early stage in the loading and allows redistribution of the stresses along the structure. Also the reinforcing steel will yield in the cracked tensile zones and let plastic deformations take place with even greater redistribution that is violation of the elastic assumption. Therefore choosing a linear method can lead to incorrect results due to the strong non-linear material behaviour caused by cracking.

3.3.2 Non-linear Analysis

A non-linear analysis is a simulation of the response of the structure subjected to increased loading. The main purpose is to estimate the maximum load that the structure can carry before it collapses. The maximum load is calculated by simply performing an incremental analysis using non-linear formulations. The analysis is sub-divided in increments and equilibrium is found for each increment using iteration methods. Consequently the results are more accurate providing real material and structural response. A non-linear analysis can be helpful in understanding the behaviour of a structure, since the stress redistribution, and failure mode can be studied. However, it is important to be aware of the limitations of the model and it is advisable to validate the modelling method with test results.

3.3.2.1 Integration methods

An integration scheme for shell elements must be chosen carefully. Among various numerical integration schemes, Gauss and Simpson integration methods are mostly used in view of the accuracy and the efficiency of calculations. Quadrilateral elements may be integrated in-plane only with a Gauss scheme and in thickness direction either by the Gauss or Simpson rule.

As previously mentioned in *section 3.2.1* for the purposes of this thesis, elements of the same type but different order were used. With increasing the order of the elements, normally a higher order of integration scheme comes. Four nodes elements use 2x2 Gauss rule and 8 nodes elements use 3x3 Gauss rule in the plane. Also the Simpson rule creates, as in this case, 9 layers in the elements thickness which means that in total 2x2x9=36 or 3x3x9=81 integration points exist in the element. However for elements based on Mindlin-Reissner Theory a reduced integration is required in order to prevent phenomenon as shear locking. Thus 2x2 integration points have to be used for 8 nodes elements, but a model with 3x3 points in the plane was created in order to investigate the effects on the results.

3.3.2.2 Load stepping

What distinguish non-linear analysis from linear is that the non-linear solution is not calculated straight forward. Load is applied gradually in order for the exact behaviour to be captured. This process requires assumptions of force and searches for corresponding displacement or vice versa as for each predictor the equilibrium is solved by iterations. As the FEM is merely an approximation, the solution requires a limit of accuracy. A convergence criterion is to be introduced, which sets a limit between two consecutive iterations to determine when the equilibrium could be assumed as reached.

Various load stepping methods exist that approach the problem differently. They are load-controlled, displacement-control, and arc-length method. The problem in hands dictates which method is to be used. The load-controlled method applies the load in portions and looks for the corresponding displacement field. The type of loading does not affect the response; it works as good for point loads as for distributed loads. On the other hand the displacement-controlled prescribes displacement as boundary conditions on selected nodes and searches the stress fields; this method is easy to use for concentrated loads but troublesome for distributed loading. A reasonable question arises why one would need to use displacement control as in reality only in very few situations displacements cause forces, but not the other way round. Also sometimes prescribing displacement would take more efforts to build the model. The answer to that question is in the kind of response that is expected. The so called "snap-through" response is possible, see *Figure 23*, which is typical for non-linear analysis.
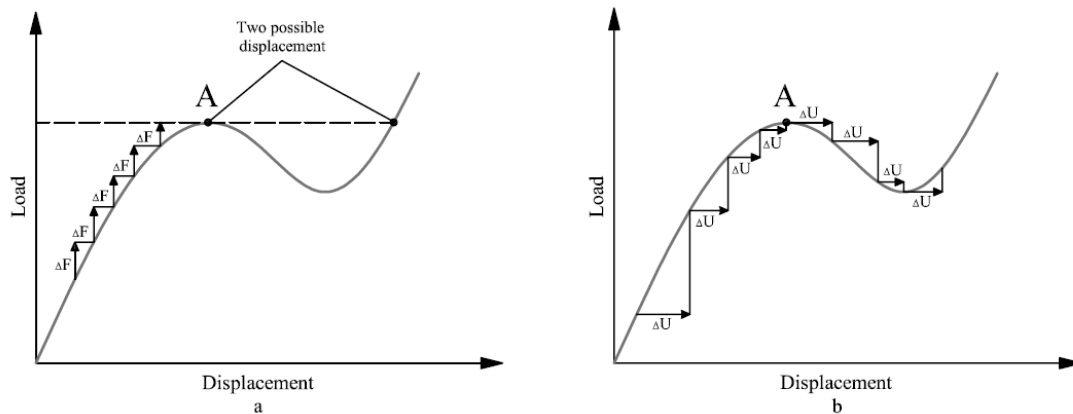
Figure 23. *The difference between the load-controlled (left) and displacement-controlled (right) methods for a snap-through response.*

This occurs frequently for concrete structures where the material starts cracking at very early stage. By increasing the force the solution will reach a point where multiple displacements are possible. Due to inability to evaluate the solution the software will terminate further increments. As a result only behaviour up to failure could be observed, which leads to the following issues, Crisfield (1994):

- 'A' may only be the local maximum, see *Figure 24a*
- The 'structure' being analysed may be only a component. It may later be desirable to incorporate the load/deflection response of this component within a further analysis of a complete structure.
- In the above and other situations, it may be important to know not just the collapse load but whether or not this collapse is of a 'brittle', *Figure 24a*, or 'ductile' form, *Figure 24b*.
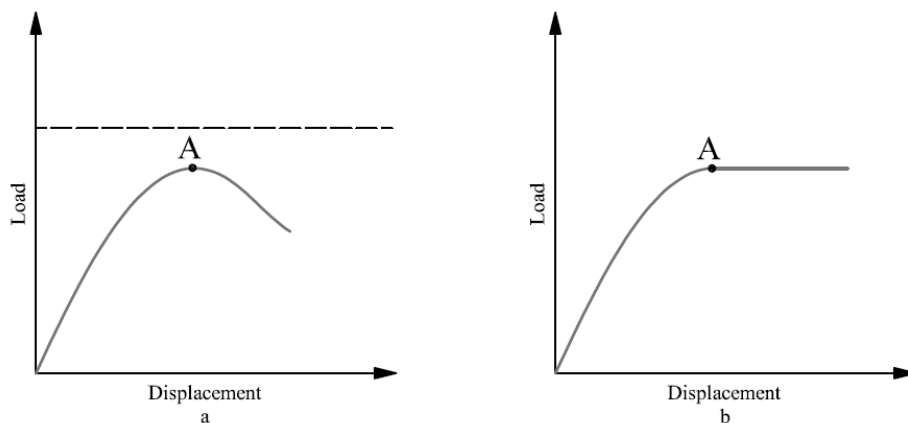
Figure 24. *Difference between brittle type failure (a) and ductile type failure (b).*

By applying displacement control, the structure's behaviour is properly described, see *Figure 23b*. However it is important to remind that the "snap-back" phenomenon exists as well, see *Figure 25*. It is typically associated with loss of stability of shell structures that are not discussed by this thesis.
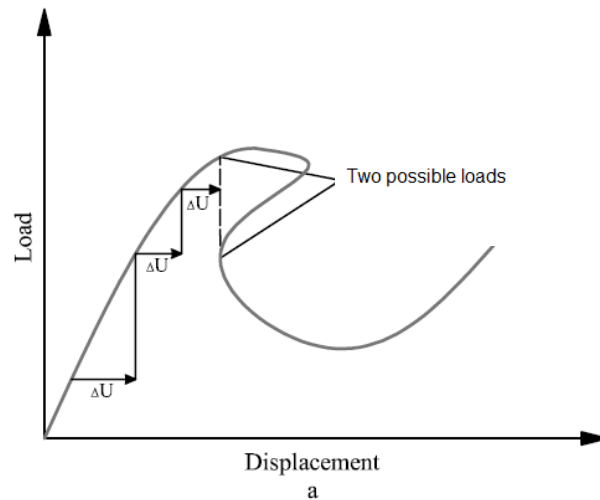
Figure 25.   Bifurcation problem for the displacement-controlled method in combination with a snap-back response.

The arc-length methods are intended to enable solution algorithms to pass limit points Crisfield (1994). Originally introduced by Risk and later modified by multiple researchers the concept is based on the idea that the algorithm is searching for the intersection between the equilibrium path and a pre-defined arc. In this manner the problematic points of maximum or minimum load are overcome and "snap-through" and "snap-back" effects are properly described. However this approach is unsuitable in the case of non-linear analysis of reinforced concrete structures due to the sudden changing stiffness of the structure.

3.3.2.3   Iteration

The choice of the iteration method is important since it determines computer power used and the speed at which the results from the analyses are calculated. In the case of complex models, where time needed for one analysis is substantial, one could save time and resources by selecting an appropriate iteration method. Some common options that could have been chosen are Newton`s, modified Newton`s, and BFGS methods.

Newton`s method requires most computation capacity but least number of iterations. The reason is that the system matrix, which is the tangent stiffness, is updated for each iteration. Due to this fact, a better estimation is achieved and fewer repetitions required. The rate of convergence of this method is quadratic, Larsson (2010). On the other hand the modified Newton`s method uses the same stiffness matrix during every iteration as it is changed for every step. Consequently the convergence rate is linear, less accurate, and requires more iteration, but it needs less computer power. In the case of sophisticated models with many degrees of freedom the BFGS method is suggested. It is based on Newton`s method, but also does not update the stiffness matrix after every iteration as the modified Newton`s method. The last converged step

is used to obtain the stiffness matrix and approximate. BFGS` advantage is the convergence rate which is between linear and quadratic.

3.3.3 Post-processing

The post-processing phase of the FE analysis involves investigation of the results. It begins with a thorough check for problems, such as warnings or errors that may have occurred during solution process. It is also important to check how well-behaved the numerical procedures were during solution. Once the solution is verified, the whole response of the structure can be studied - from initial loading and cracking to failure. Different results should be examined and compared with the test results or hand-calculations based on codes. For the ultimate limit state, both the load-carrying capacity and the failure mode are important. For the serviceability limit state, deformation, crack width or concrete stress/strains can be of interest. Moreover, many display options are available in every software. The results for critical sections can be presented with tables and graphs. Dynamic view and animation capabilities are also available to help acquire better understanding of the behaviour of the structure.

4 Bridge Deck Model and Analysis

The studied bridge deck model represents an actual large scale test of one of several bridge cantilevers in Switzerland, Vaz Rodrigues (2007).The full scale tests on the bridge deck cantilevers showed that the governing failure mode was shear failure and the theoretical flexural failure load was not reached. The main objective of this analysis was to predict the distribution of shear force and how shear was influenced by the flexural cracking and yielding of the flexural reinforcement. The redistribution of shear flow was simulated for a tested reinforced concrete bridge cantilever without shear reinforcement, subjected to the action of four concentrated loads representing vehicle wheels, see *Figure 26*. Similar tests were performed by Vaz Rodrigues, see *section 2.2*, using one and two concentrated load as well, however only the configuration of four concentrated forces provided yielding in reinforcement. This test was chosen for modelling since the non-linear flexural response was expected to have a significant influence on the shear force distribution for this case.
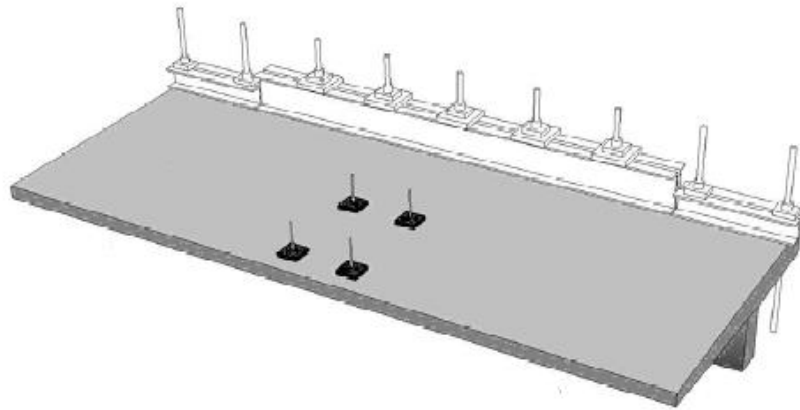
Figure 26.   Schematic layout. From Vaz Rodrigues (2007).

4.1 Finite element software

The main part of this project was to create a model and perform analyses of the tested reinforced concrete bridge deck using the Finite Elements Method (FEM). Such a method using iteration methods to observe non-linear behaviour of materials gives faster and more precise results then hand-calculations. The software used to perform the analysis is Midas FX+ v.3.1.0 for pre-processing and TNO Diana v.9.4.4 for computation and post-processing.

4.2 General overview

A 3D model of the bridge deck slab was developed in TNO Diana in order to analyse its behaviour under shear loading. The cantilever part had to be modelled as 14 separate longitudinal segments, each having constant thickness and the top and bottom reinforcement parallel to the system line, see *Figure 27*. The reason for this

simplification is that FE software produced incorrect results of shear forces when continuously varying shell thickness was used, Shams Hakimi (2012). Also, using reinforcement that was inclined in relation to the system line of the concrete, led to unreasonable results.
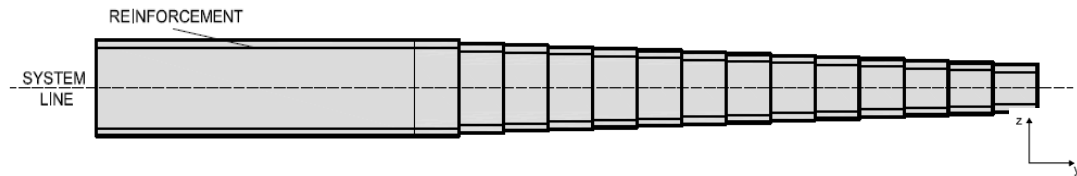
Figure 27.   Division of the slab.

The reinforcement layout, that had to be modelled, consisted of 12 mm bars with spacing of 150 mm, in both directions on the bottom, and in longitudinal direction on the top. The reinforcement of the top layer in transversal direction consisted of 16 mm bars at 75 mm spacing, where every second bar was curtailed, see *Figure 29* and *Figure 29*. All the reinforcement was modelled as embedded with planes of reinforcement grids, each representing reinforcement in both x- and y-directions. The concrete cover was 30 mm.
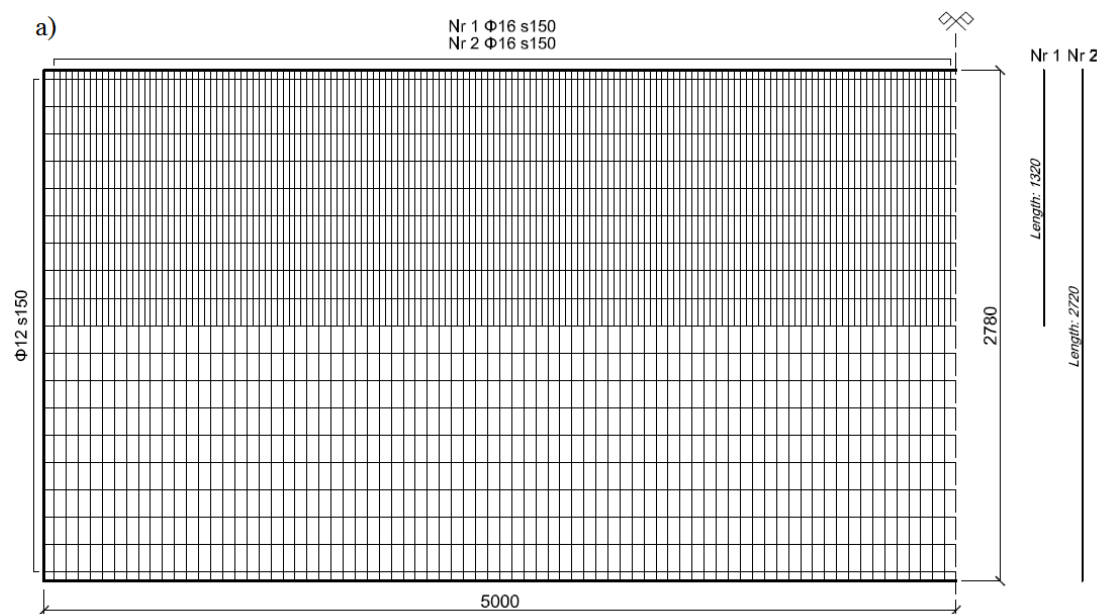
Figure 28.   Top reinforcement layout.

b)
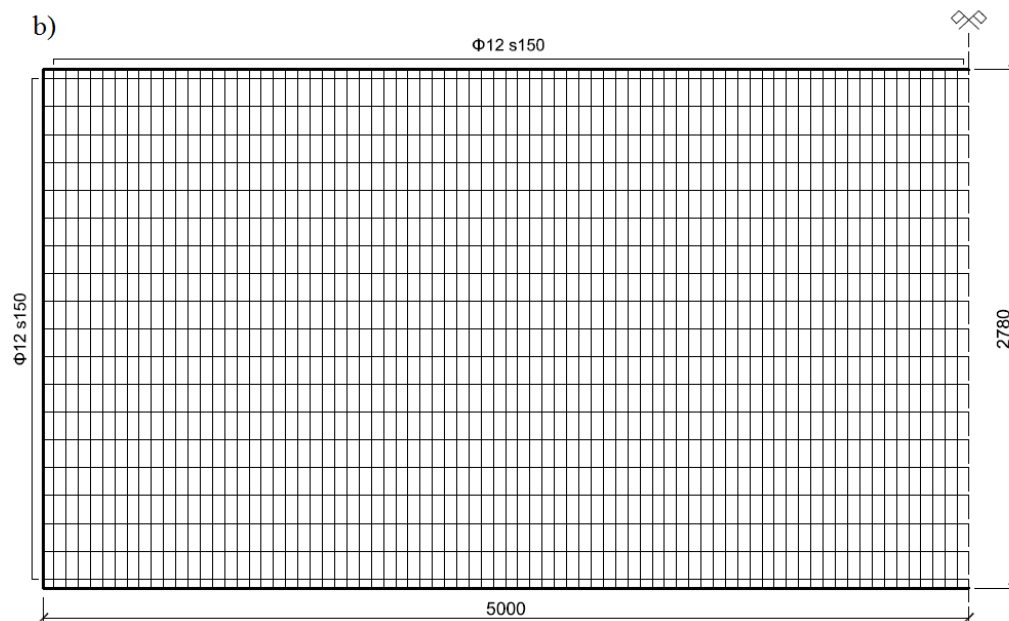
Figure 29.   *Bottom reinforcement layout.*

4.3 Geometry

The bridge deck was modelled to have a significant size with a thickness similar to that of actual cantilever deck slabs of bridges, see *Figure 30*. The cantilever had a length of 2,78m, from the support edge to the free end, and a length of 10,0m along the support. The thickness varied between 190 mm at the tip and 380 mm at the support edge. This allowed to correctly account for the size effect in shear (decreasing nominal shear strength with increasing size of the member) and thus to investigate whether failure developed in shear or bending, Vaz Rodrigues (2007).
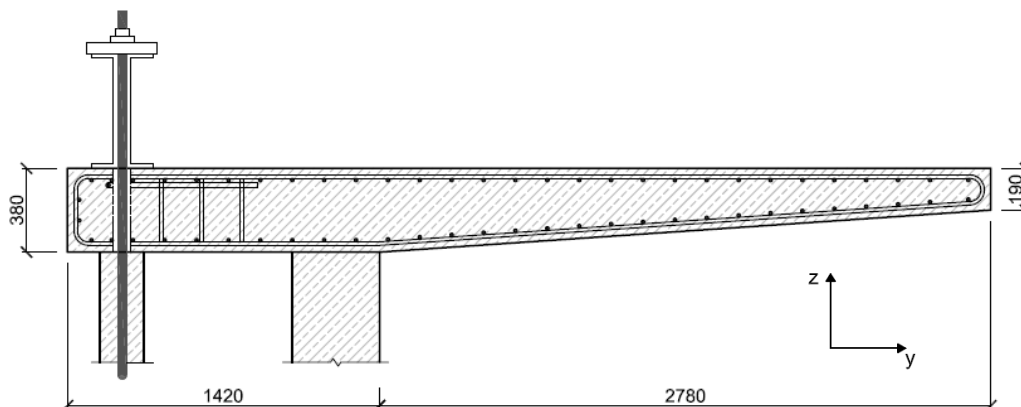
Figure 30.   *The dimensions of the bridge deck model.*

4.4 Materials

4.4.1 Concrete

The material properties were chosen to match the concrete in the tested cantilever, see *section 2.2.1*. The compressive strength and modulus of elasticity were given as result of concrete laboratory testing. To match the compressive strength, the tensile strength was chosen as for a C40/50 concrete, based on Eurocode 2 (2001). For the given concrete strength and the maximum size of aggregate used (16 mm), the fracture energy was set to 90 Nm/m^2 according to Model code 90 (1993). The properties of the concrete modelled in the FE analysis are presented in Table 1. In *Figure 31*, the stress-strain relations used are presented. Response in tension was chosen according to Hordijk (1991) and the response in compression was chosen according to Thorenfeldt (1987). The rotating crack approach was adopted. The crack bandwidth was set as 0,088m.
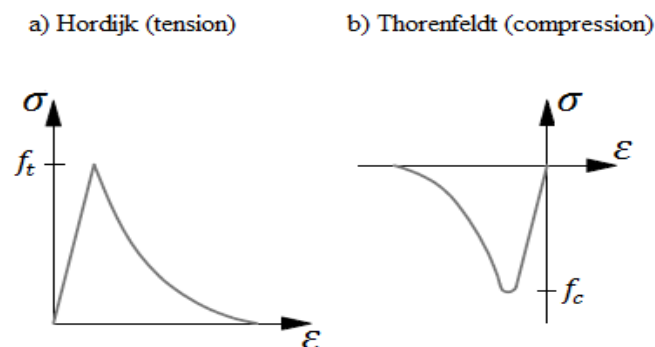
Figure 31.   *Stress-strain relationship of concrete.*

4.4.2 Steel

The reinforcement steel used in the transversal direction at the top layer was hot rolled deformed bars, with the yield strength of 515 MPa, Young's modulus of 200 GPa and an elastic-ideally plastic uni-axial response. The three-dimensional yield criterion is chosen according to von Mises. The properties of the steel modelled in the FE analysis are presented in Table 1.

CONCRETE						STEEL		
f_{cc}	f_{ct}	E_c	v	ρ	E_f	f_y	E_s	v
MPa	MPa	GPa	-	kg/m^3	Nm/m^2	MPa	GPa	-
40	3	36	0,2(0)	2500	90	515	200	0,3

Table 1.   *Material properties.*

4.5   Boundary Conditions

A correct modelling of the supports is important to reproduce the actual structural behaviour. The bridge deck has two different support conditions, see *Figure 32*. The region where the pre-stressing bars were used to fix the rear end of the support region was modelled by prescribing translations in x-, y- and z-directions, see *section 2.2.1*. The supporting concrete blocks at the front end of the support region were modelled using non-linear springs, representing the stiffness of the concrete in compression and having very low stiffness in tension to allow uplifting where it may occur. The ends of the springs were restrained for translation in all directions. This way of modelling the support gave more realistic flexibility and the axial stiffness of the support was equally distributed among the nodes inside the region of the support.
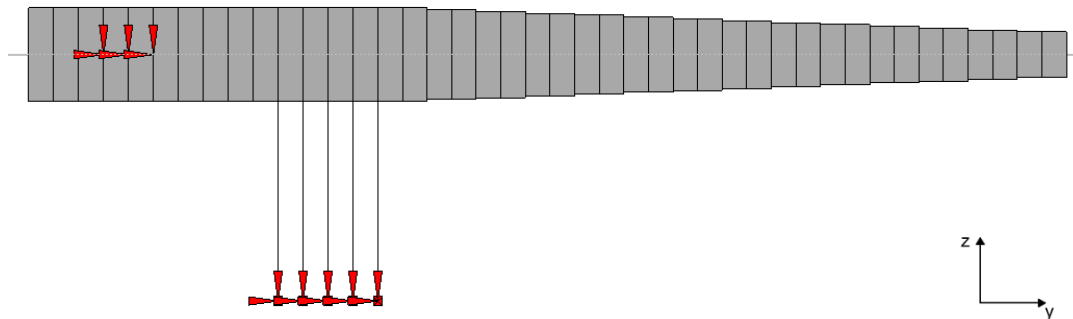
Figure 32.   Illustration of modelled supports.

4.6   Loads

4.6.1   Self-weight

The self-weight was modelled as gravity to properly account for the variation of thickness. This load was determined based on the acceleration of 9.81 m/s^2 and the density of 2500 kg/m^3 for concrete, including the weight of reinforcement.

4.6.2   Concentrated loads

The concentrated loads, simulating vehicle wheels, were applied on the top of the slab on areas of 0.4 x 0.4 m each. The distance between the loads in the transverse direction was 1400 mm and 1000 mm in the longitudinal direction. The concentrated loads were modelled using prescribed displacement so the analysis could be carried out with deformation control instead of load control. The reason for this type of loading was that deformation control analysis was more stable and had easier to reach convergence, see s*ection 3.3.2.2*. To model the distribution of the wheel loads it was necessary to create a loading sub-structure for each wheel in order to displace several nodes at once with equal load on each node. The sub-structure was modelled with very stiff steel beams (cross-sectional area 1x1 m^2). The stiff beams were connected

with tying elements, which were only prescribed for translation in z-directions at each node. All the ties were assigned to correct nodes on the concrete deck. This procedure ensured that the concrete nodes and each corresponding tie node got an equal displacement. The boundary conditions were defined as prescribed translation in y-direction and rotation around the y- and z-axes for all nodes. For one end-node on each beam element the boundary conditions are defined as prescribed translation in x-direction, see *Figure 33*.
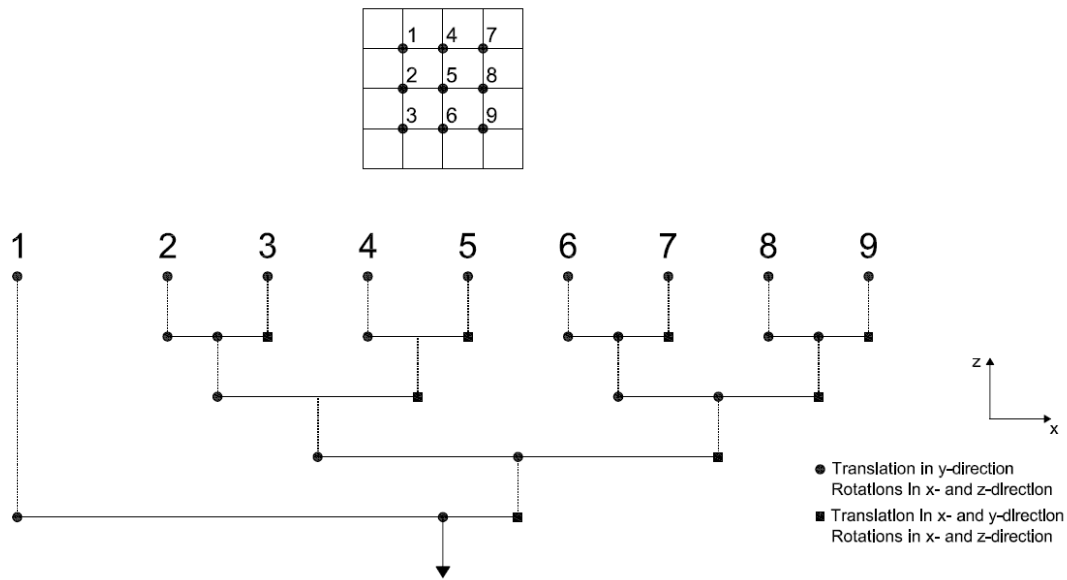
Figure 33.   *Loading sub-structure for displacement of nodes.*

Afterwards, the loading sub-structures for each wheel load were connected to create a loading structure for the group of wheel loads, see *Figure 34*.
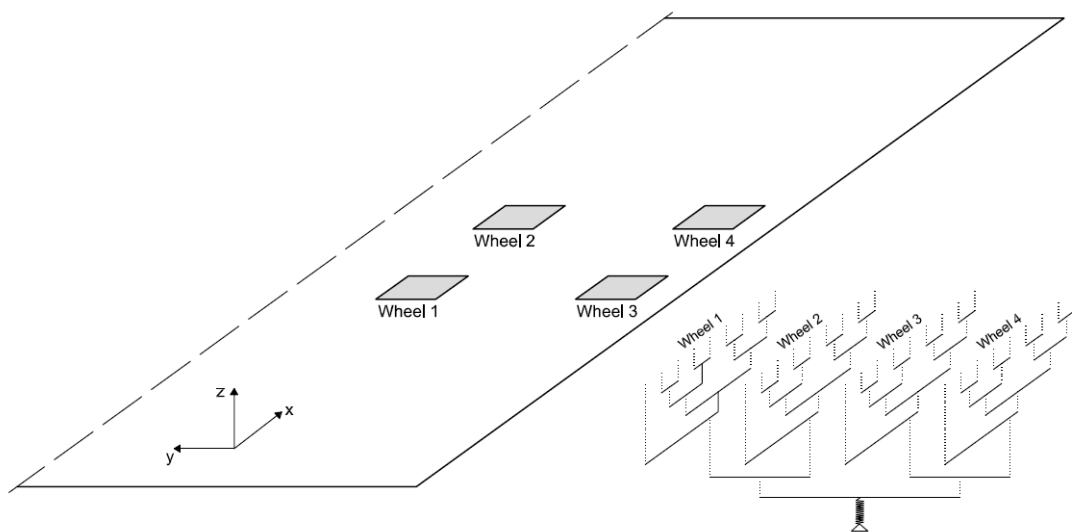
Figure 34.   *Loading structure for all wheel loads.*

     CHALMERS, *Civil and Environmental Engineering*, Master's Thesis 2013:127

To combine the distributed loading for the self-weight with the displacement-controlled wheel load a spring was used with insignificant stiffness in compression (1000 N/m) and a very high stiffness in tension (10^{10} N/m). Due to the spring the slab is able to move downwards when applying self-weight. The other reason for creating the spring is that FE software requires the node, which is displaced, to be modelled as support.

4.7 FE Mesh

The bridge deck slab was meshed with quadrilateral curved shell elements of size 0.1 x 0.1, creating 100 elements in the longitudinal and 28 elements in the transversal direction, see *Figure 35*.
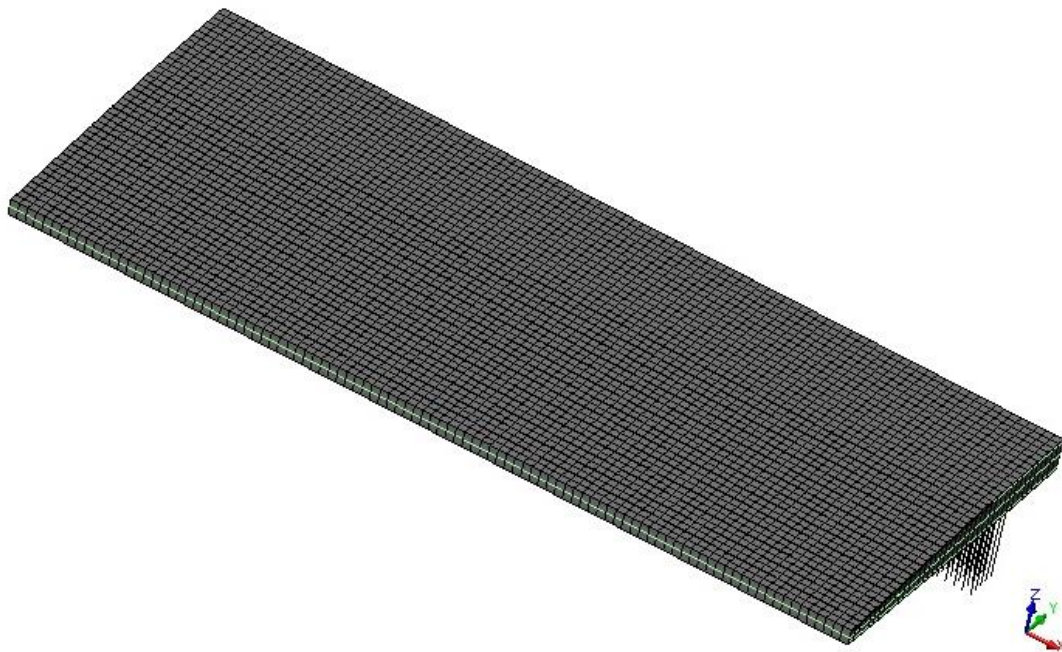
Figure 35.   *Mesh density.*

4.8 Processing

The best option for processing was to choose the BFGS "secant" iteration method, see section 3.2.2.3, with the option of starting with the tangential stiffness in the beginning of each step. Two convergence criteria were chosen, using displacement and force norm. To gain convergence both criteria must be fulfilled. The tolerance was set to 0.001 for both criteria.

The solutions from numerical non-linear calculations in TNO Diana were based on a two phase analysis. The first phase included the self-weight which was applied as a body load in 10 steps. When the complete self-weight had been applied, the spring was compressed by a certain amount. From step 11, a deformation of 0.25mm

(10 x 0.025) was applied in order to displace the spring to its original, un-stressed length quickly. After this step, the spring remained compressed but its length remained very close to the un-stressed one. During the next 40 steps, very small increments of prescribed displacement were applied to the "loading node" to avoid convergence difficulties that appeared when the step was too large at the transition of spring from compression to tension. After this, the rest of the load was applied with a factor of 5 (5 x 0.025) per step. The maximum number of iterations per increment was increased to 300.

5 Results

In this chapter, the results from non-linear analysis will be presented. First, the shear force distribution in the slab and along the support from a model based on the preceding master thesis by Shams Hakimi (2012) will be shown. Afterwards the results for different analyses approaches will be presented and compared. Crack pattern and yielding of reinforcement will be presented for a model with accurate shear distribution. At the end the validation and evaluation of the reasonability of the selected model is featured.

5.1 Previous work

In 2012, Shams Hakimi developed his master's thesis also based on Vaz Rodrigues' tests, see s*ection 1.1*. The main layout of the FE model was established with that work. For that model, 4 nodes elements were used, see *section 3.2.1*, with integration scheme 2x2 points in the plane of the element using Gauss rule and 9 integration points in thickness direction using Simpson's approach, see s*ection 3.3.2.1*. Other important feature of that model was that the Poisson coefficient was assumed to be *v=0.2,* see s*ection 3.2.2*. However, the level of complexity of the model failed to describe the shear distribution properly. Very peculiar phenomena occurred: instead of a smooth distribution of shear forces, they fluctuated with tremendous amplitude.

The current master's thesis uses the knowledge gained by the previous one and therefore, in this work, the same model's layout was adopted. In order to study the nature of the phenomena, the same model was re-built in the current work, with the very same parameters. The shear plots through different steps could be followed further on in the following sections.

5.1.1 Transversal shear force distribution in the slab

The results of the reproduced model regarding the distribution of the shear force component in transversal direction are presented for different load levels, see *Figure 36* to *Figure 49*. The *Q* value corresponds to the sum of the four applied loads.
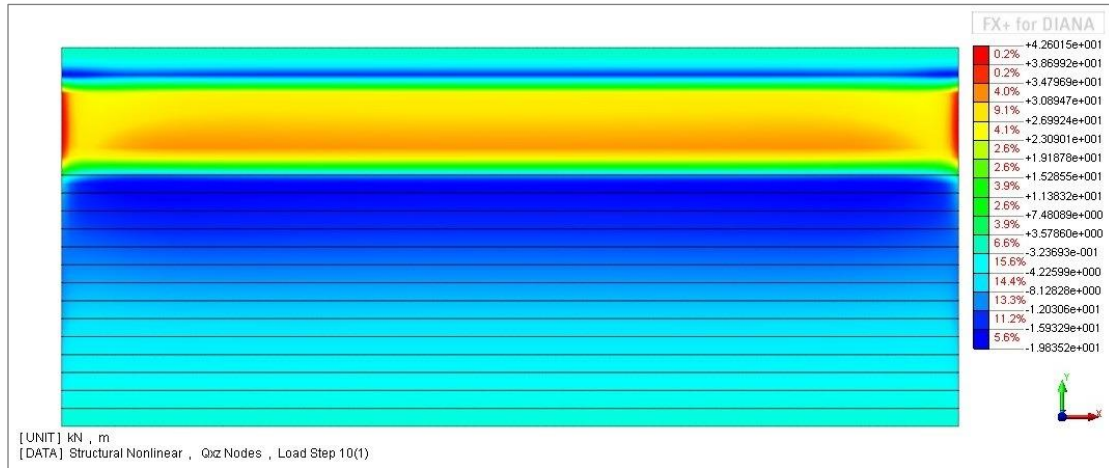
Figure 36.   Shear force per unit width [kN/m] in y-direction for self-weight
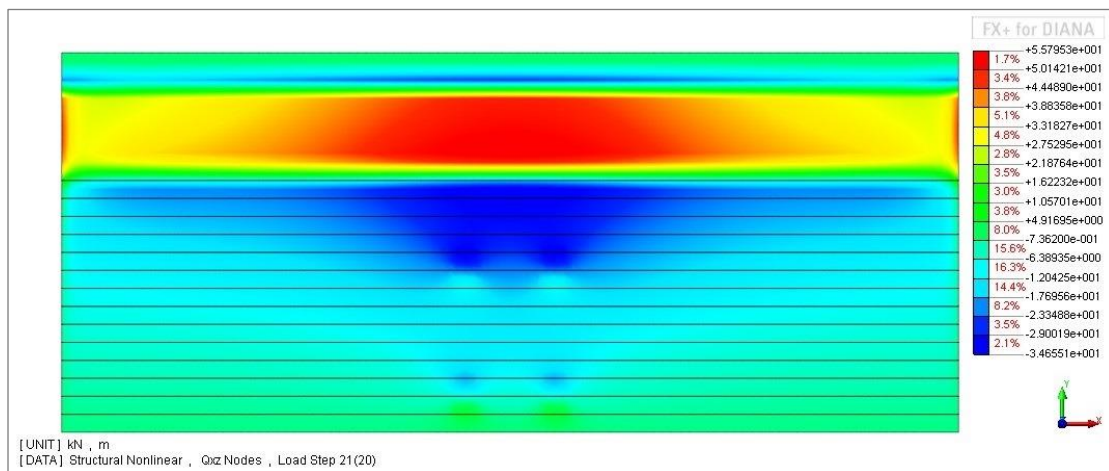
Figure 37.   Shear force per unit width [kN/m] in y-direction for Q = 50 kN
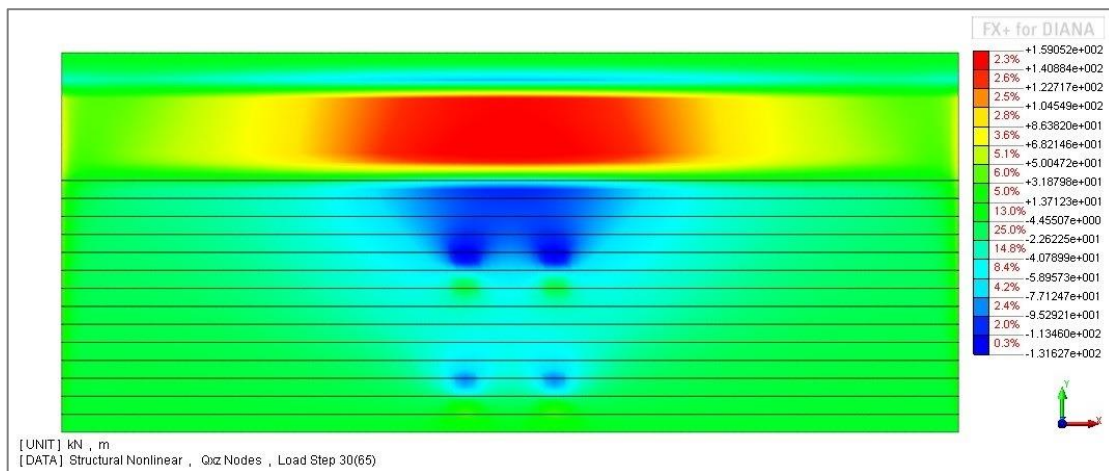
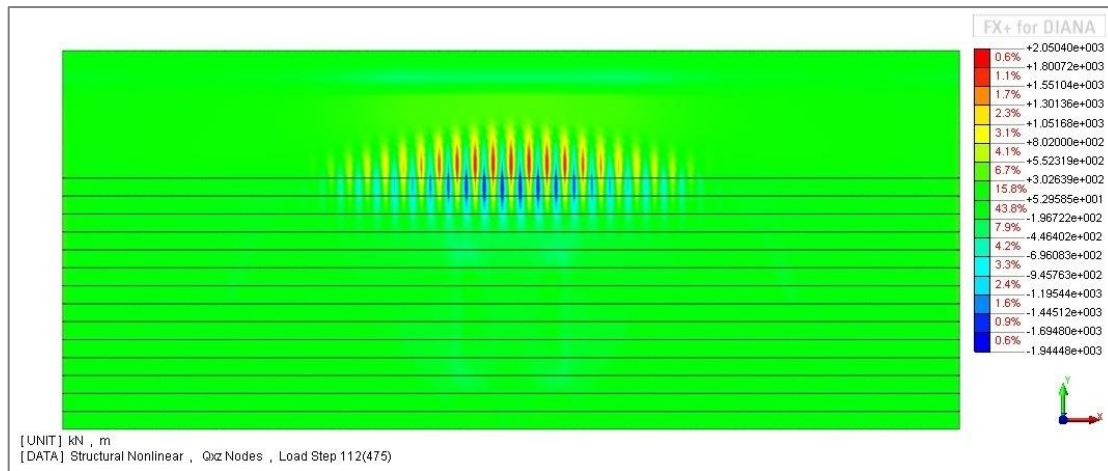*Figure 38.   Shear force per unit width [kN/m] in y-direction for Q = 300 kN*
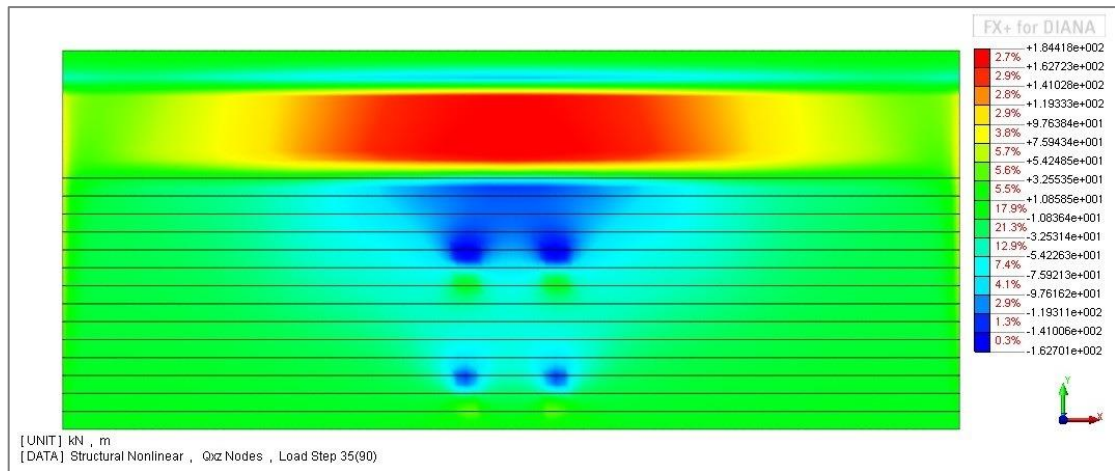
Figure 39.   Shear force per unit width [kN/m] in y-direction for Q = 400 kN
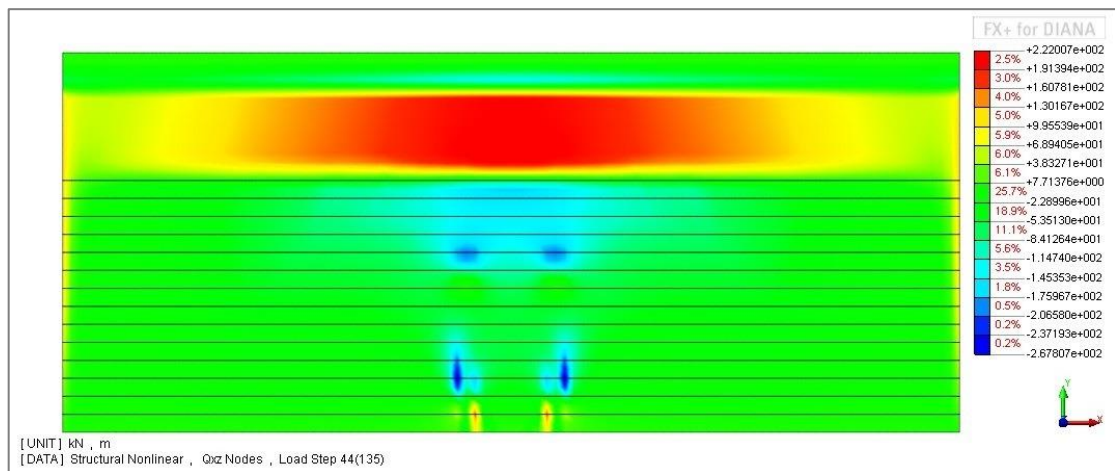
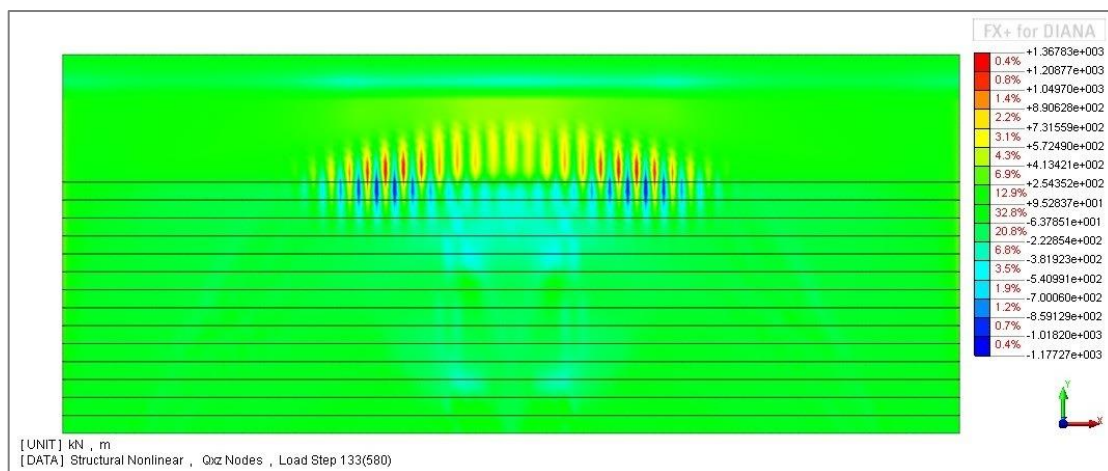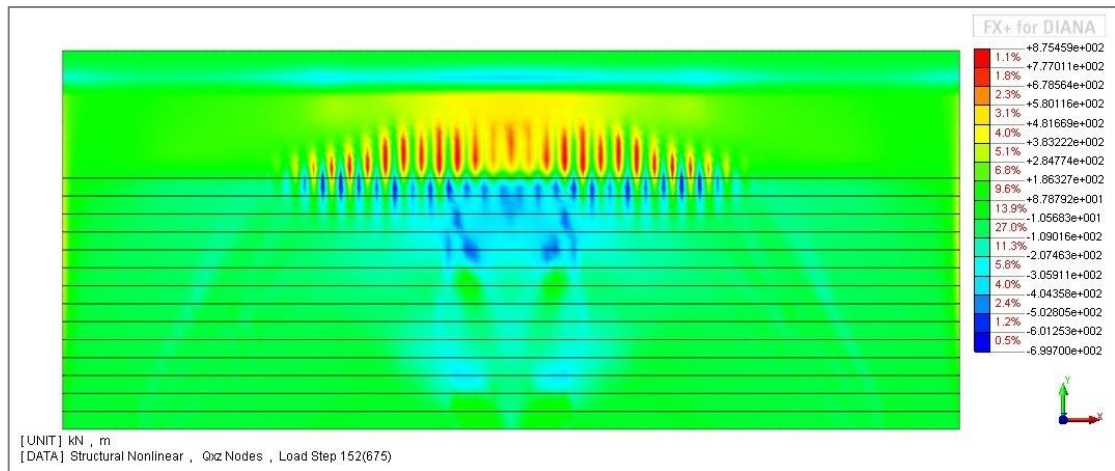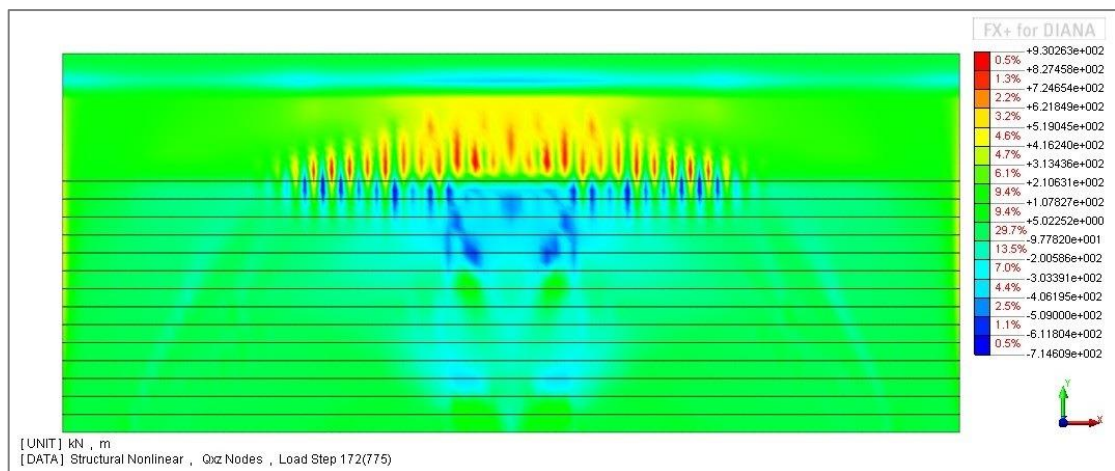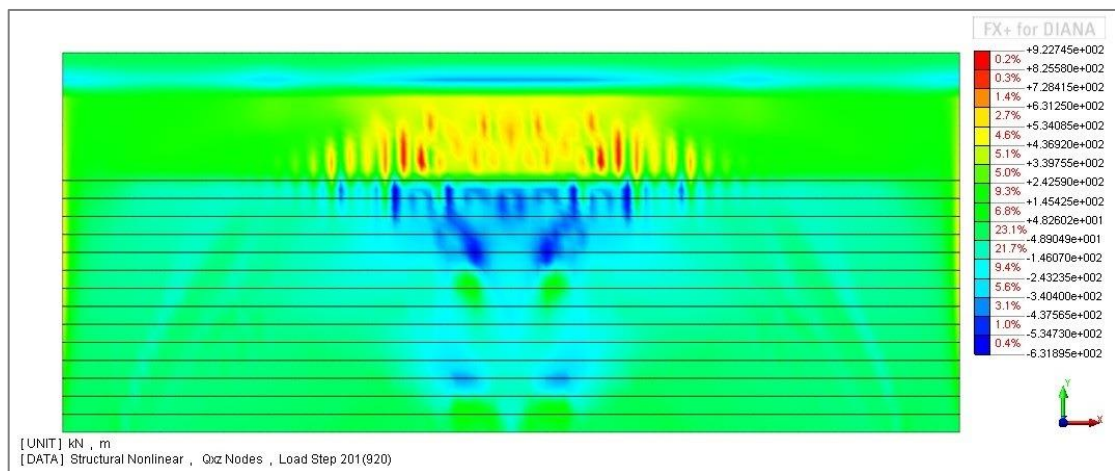*Figure 40.   Shear force per unit width [kN/m] in y-direction for Q = 500 kN*

The distribution and the re-distribution seem reasonable until load Q = 500 kN, see *Figure 40*, and then suddenly the shear becomes fluctuating with high magnitudes in areas with opposite signs, see *Figure 41*.
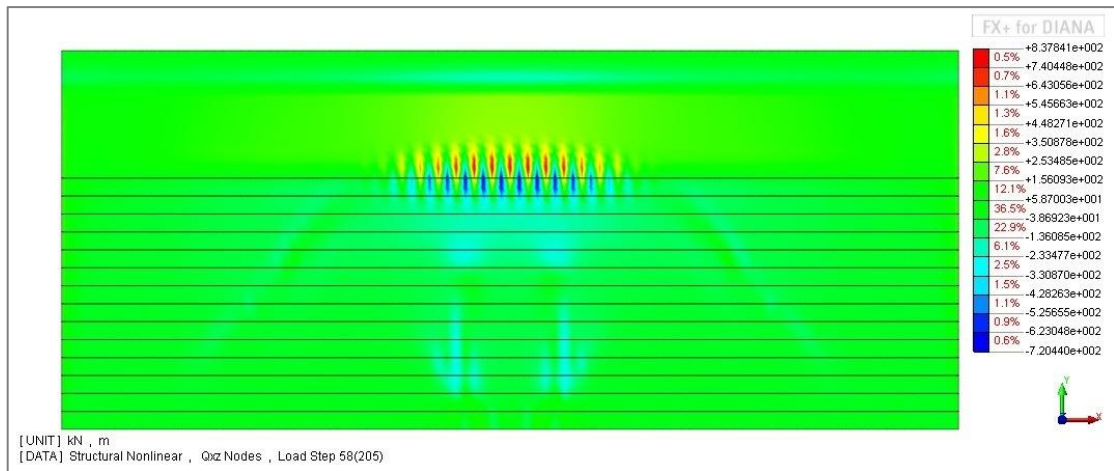
Figure 41. *Shear force per unit width [kN/m] in y-direction for Q = 600 kN*
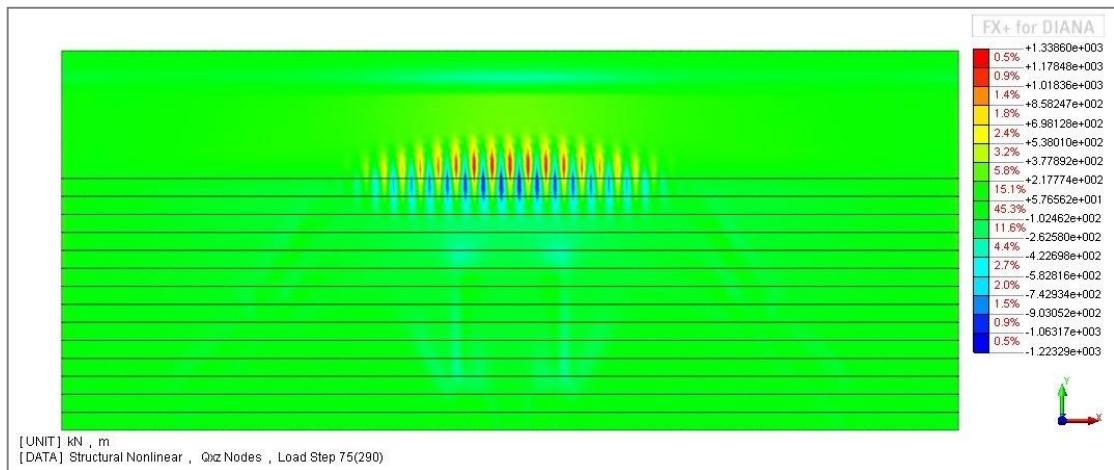
Figure 42. *Shear force per unit width [kN/m] in y-direction for Q = 700 kN*
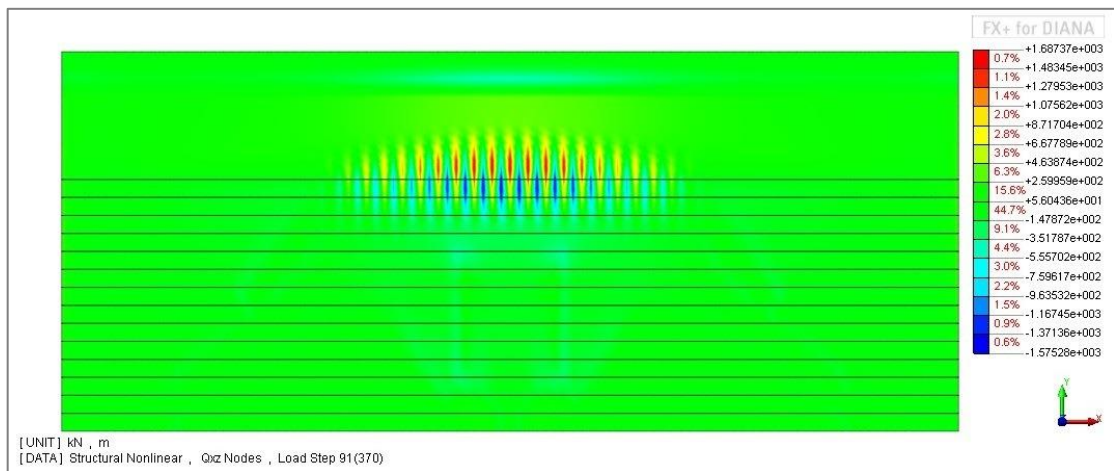
Figure 43. *Shear force per unit width [kN/m] in y-direction for Q = 800 kN*

Figure 44.   Shear force per unit width [kN/m] in y-direction for Q = 900 kN

Figure 45.   Shear force per unit width [kN/m] in y-direction for Q = 1000 kN

In *Figure 45*, after load Q = 1000 kN, the maximum magnitudes of the fluctuating shear force started to move apart from each other, and the maximum shear was not transferred in the middle of the support.

Figure 46.   Shear force per unit width [kN/m] in y-direction for Q = 1100 kN

Figure 47.   Shear force per unit width [kN/m] in y-direction for Q = 1200 kN

Figure 48.   Shear force per unit width [kN/m] in y-direction for Q = 1300 kN

CHALMERS, *Civil and Environmental Engineering, Master's Thesis 2013:127*

In *Figure 47*, it can be seen that the shear started to spread to larger parts of the support. Moreover, the maximum fluctuating shear forces becomes reduced. This can be connected with yielding in the top transversal reinforcement, which occurred at Q = 1120 kN.
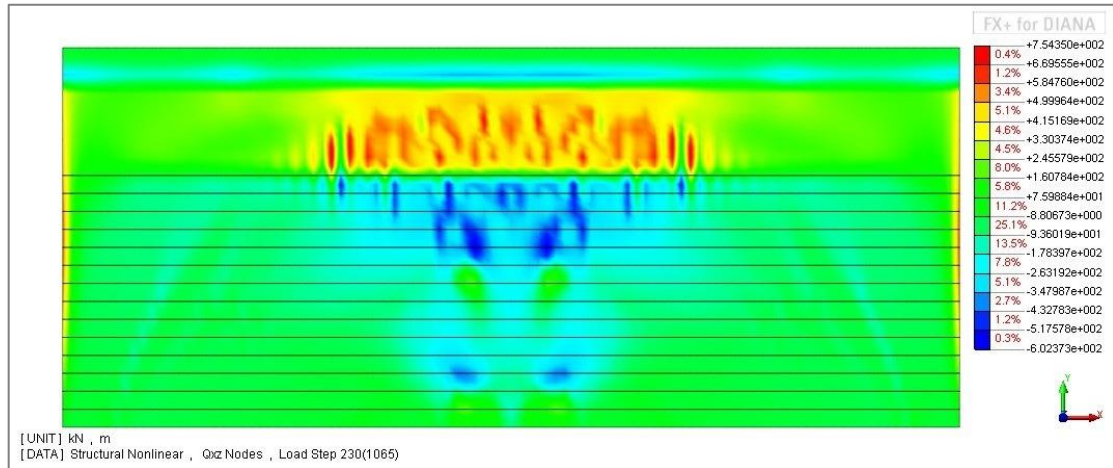
Figure 49.   *Shear force per unit width [kN/m] in y-direction for Q = 1380 kN*

For further steps after the failure load, Q = 1380 kN, was reached, small changes in the shear distribution appeared.

5.1.2   Transversal shear force distribution along the support.

The distribution of shear force in transversal direction was studied along a line parallel to the support in the cantilever slab at a distance 50 mm from the support edge. The diagram in *Figure 50* shows the shear force variation for each load level showed in *section* 5.1.1.
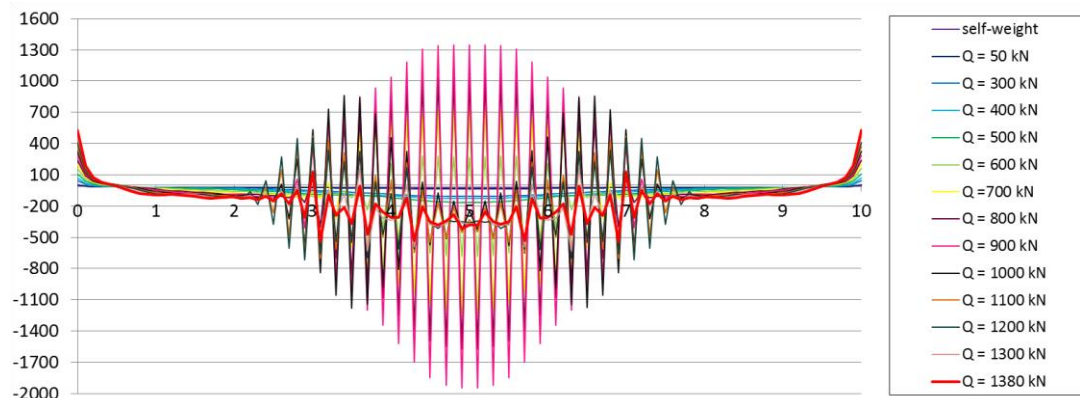
Figure 50.   *Shear force in y-direction for various loads.*

Since the fluctuation started suddenly, between step 48 (Q = 533 kN) and step 49 (Q = 540 kN), the contour plots for these steps are presented below, see *Figure 51*. The shear force diagram for the line perpendicular to the support is also shown for these steps. In addition, it has been investigated whether this phenomenon is connected with any expected behaviour of concrete slab.
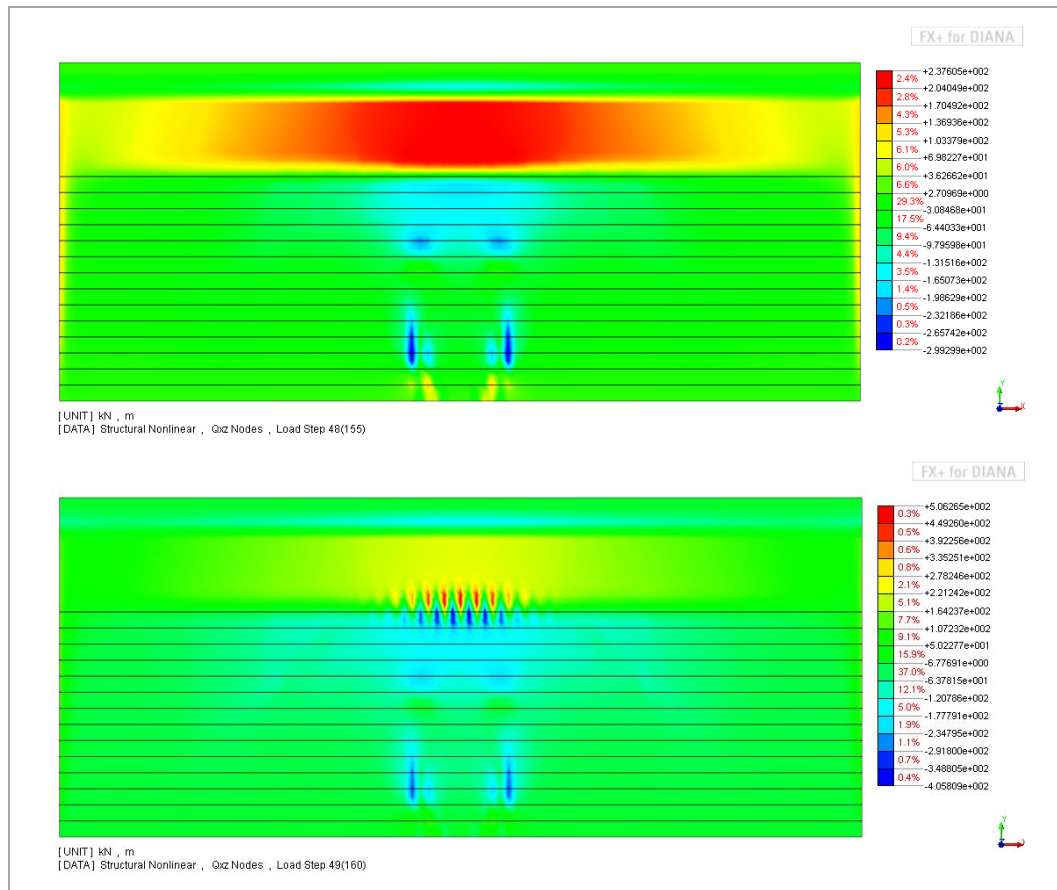
Figure 51.   *Shear force per unit width [kN/m] in y-direction for step 48 and step 49.*

It was observed that in the beginning of the analysis, no shear force fluctuation occurred at all, before step 48. In the diagram, see *Figure 52* this phenomenon is seen more clearly. In Shams Hakimi (2012), it was assumed that the shear force fluctuation can be due to alternation between different crack statues within neighbouring elements or integration points, available in the software. It was assumed that these fluctuations are only local effects and do not affect the global behaviour of the structure. Consequently, in Shams Hakimi (2012), the shear force fluctuations were averaged to see trend lines for the shear force variation along the support.
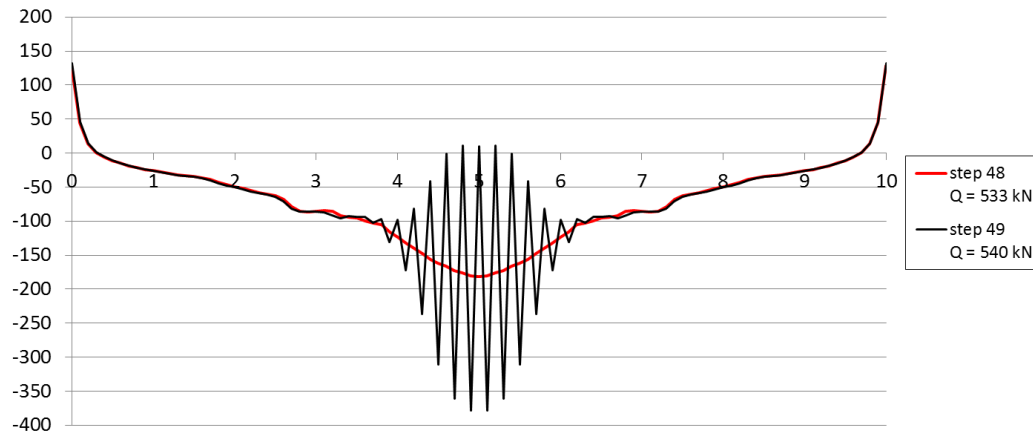
Figure 52.   Shear force in y-direction for step 48 and step 49.

5.1.3   Load – displacement curve

The relation between the occurrence of the fluctuation and the major events in the structural response of the slabs was tried to be found. However, as the load-displacement curve shows, see *Figure 53*, the moment when the problem starts does not coincide with any crack initiation in the concrete or yielding of the reinforcement.

First crack (top surface) — First crack (bottom surface)
Fluctuation — Yeilding of top reinforcement (transversal)
Yeilding of bottom reinforcement (longitudinal) — Failure load (Vaz Rodrigues)
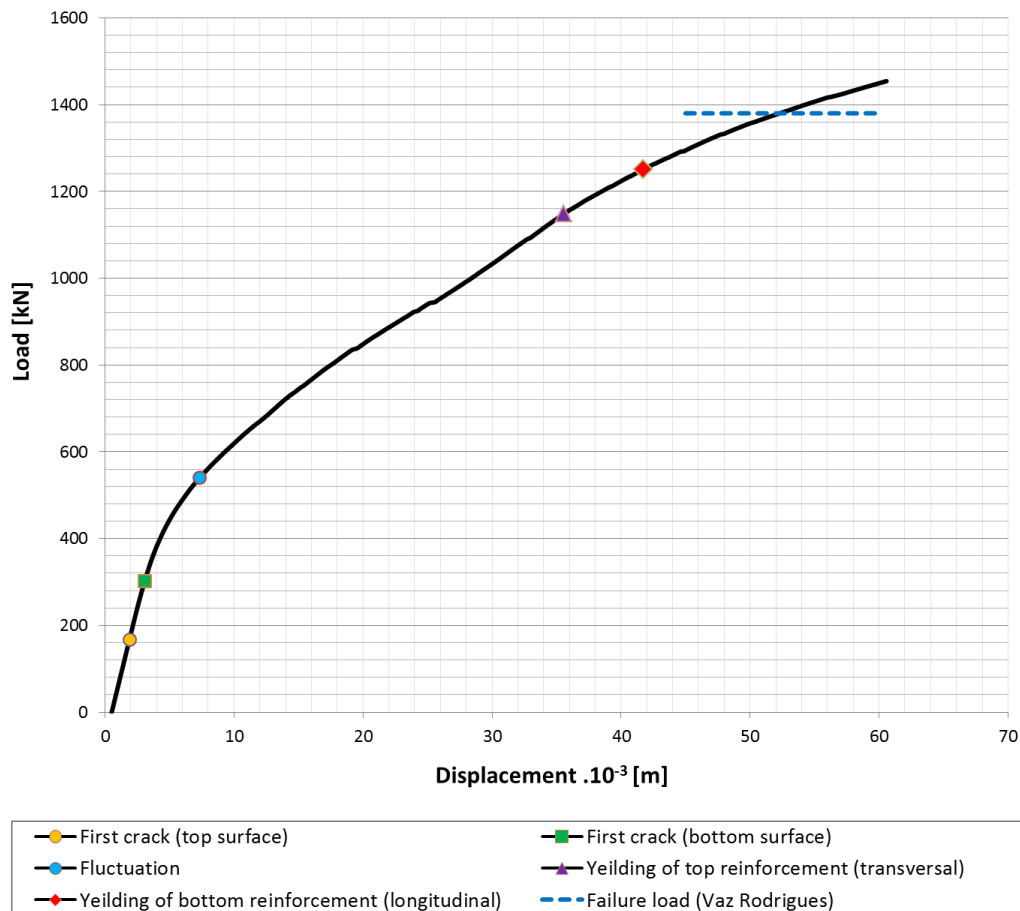
Figure 53.   Load-displacement curve.

The first crack on the top surface, close to the supporting springs, occurred at a total load of Q = 196 kN. The first crack on the bottom surface, under the applied point loads, occurred at a total load of Q = 300 kN. The next major event was yielding in the top transversal reinforcement in the same place where the first cracks occurred. The total load at this point reached 1120 kN. The bottom longitudinal reinforcement started to yield at a load of Q = 1281 kN. The fluctuation could be observed at a load of Q = 540 kN.

5.2 Choice of analyses

In order to understand better the reasons for the appearance of the fluctuation in the shear force, see *section 5.1*, as previously explain in *section 3.2.1, section 3.3.2.1*, and *section 3.2.2*, different modelling approaches were applied in order to improve the obtained results, which lead to the creation of 5 new models with different element orders, reflected by the number of nodes and integration points in the element plane, and different Poisson's ratios. All alternatives had the same number of integration points in the thickness direction. The six models studied were:

- **4 nodes, 2x2x9, *v = 0.2***
  4 nodes elements, 2 x 2 in-plane and 9 in-thickness integration points, Poisson ratio v = 0.2
- **4 nodes, 2x2x9, *v= 0***
  4 nodes elements, 2 x 2 in-plane and 9 in-thickness integration points, Poisson ratio v = 0
- **8 nodes, 2x2x9, *v= 0.2***
  4 nodes elements, 2 x 2 in-plane and 9 in-thickness integration points, Poisson ratio v = 0.2
- **8 nodes, 2x2x9, *v= 0***
  8 nodes elements, 2 x 2 in-plane and 9 in-thickness integration points, Poisson ratio v = 0
- **8 nodes, 3x3x9, *v=0,2***
  8 nodes elements, 3 x 3 in-plane and 9 in-thickness integration points, Poisson ratio v = 0.2
- **8 nodes, 3x3x9, *v= 0***
  8 nodes elements, 3 x 3 in-plane and 9 in-thickness integration points, Poisson ratio v = 0

5.2.1 Comparison of transversal shear force distribution in the slab for different analyses

In this section a direct comparison between the responses in all the models with respect to shear can be followed. First, transversal shear force distribution in the slab is shown for each analysis at the same value of load. Afterwards, the distribution of the shear force along a line at 50 mm distance from the support is shown for the same steps. At the end, the attention is put on the influence of Poisson's ration on the shear force distribution for the failure load (Q = 1380 kN) for each model.

5.2.1.1 Transversal shear force distribution in the slab

The contour plots of shear force in the slab are presented for all analyses for a number of chosen load levels with increasing load. Due to the very large differences in the values, a normalized colour scale was not a suitable option. Each plot represents its own range of values and maximum and minimum shear forces are stated.

It can be observed that at the beginning the behaviour for all models was similar. At a load of Q = 600 kN, see *Figure 59*, models with $\nu = 0.2$ demonstrated fluctuation over and in front of the support. The difference between maximum and minimum shear force can be also seen. For the models with $\nu = 0.2$, within the next few steps, the area with fluctuating shear force start to spread along the support, while models with $\nu = 0$ are still stable. At a load of Q = 1200 kN, see *Figure 65*, it can be observed that only one model is capable of describing the shear distribution over the support without fluctuating shear force, i.e. the model with 8 nodes elements, 2 x 2 in-plane integration points and Poisson ratio $\nu = 0.2$. However, at failure load unexpected small peaks occurred, see *Figure 67*.

Self-weight			
4 nodes, 2x2x9, ν = 0,2		**4 nodes, 2x2x9, ν = 0**	
Max shear force	**Min shear force**	**Max shear force**	**Min shear force**
43 [kN/m]	-20 [kN/m]	32 [kN/m]	-18 [kN/m]
8 nodes, 2x2x9, ν = 0,2		**8 nodes, 2x2x9, ν = 0**	
Max shear force	**Min shear force**	**Max shear force**	**Min shear force**
43 [kN/m]	-20 [kN/m]	32 [kN/m]	-18 [kN/m]
8 nodes, 3x3x9, ν = 0,2		**8 nodes, 3x3x9, ν = 0**	
Max shear force	**Min shear force**	**Max shear force**	**Min shear force**
43 [kN/m]	-20 [kN/m]	32 [kN/m]	-18 [kN/m]

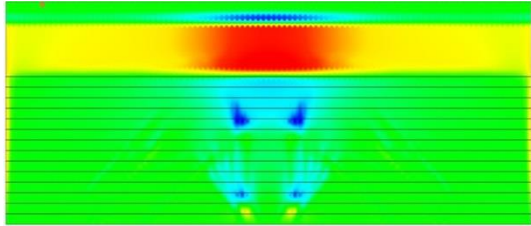*Figure 54.   Shear force per unit width [kN/m] in y-direction for six different analysis at self-weight.*

Q = 50 kN			
4 nodes, 2x2x9, v = 0,2		**4 nodes, 2x2x9, v = 0**	
Max shear force	**Min shear force**	**Max shear force**	**Min shear force**
56 [kN/m]	-35 [kN/m]	55 [kN/m]	-34 [kN/m]
8 nodes, 2x2x9, v = 0,2		**8 nodes, 2x2x9, v = 0**	
Max shear force	**Min shear force**	**Max shear force**	**Min shear force**
56 [kN/m]	-35 [kN/m]	55 [kN/m]	-35 [kN/m]
8 nodes, 3x3x9, v = 0,2		**8 nodes, 3x3x9, v = 0**	
Max shear force	**Min shear force**	**Max shear force**	**Min shear force**
56 [kN/m]	-35 [kN/m]	55 [kN/m]	-35 [kN/m]

Figure 55.   Shear force per unit width [kN/m] in y-direction for six different analysis at Q = 50 kN.

Q = 300 kN			
4 nodes, 2x2x9, ν = 0,2		**4 nodes, 2x2x9, ν = 0**	
Max shear force	**Min shear force**	**Max shear force**	**Min shear force**
159 [kN/m]	-132 [kN/m]	158 [kN/m]	-132 [kN/m]
8 nodes, 2x2x9, ν = 0,2		**8 nodes, 2x2x9, ν = 0**	
Max shear force	**Min shear force**	**Max shear force**	**Min shear force**
159 [kN/m]	-132 [kN/m]	157 [kN/m]	-145 [kN/m]
8 nodes, 3x3x9, ν = 0,2		**8 nodes, 3x3x9, ν = 0**	
Max shear force	**Min shear force**	**Max shear force**	**Min shear force**
158 [kN/m]	-142 [kN/m]	157 [kN/m]	-146 [kN/m]

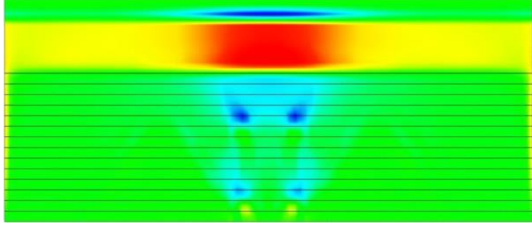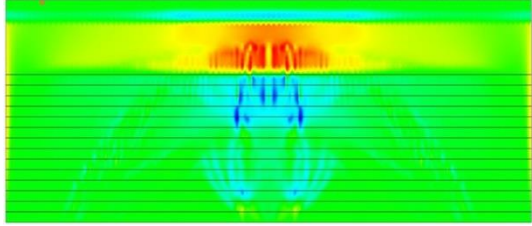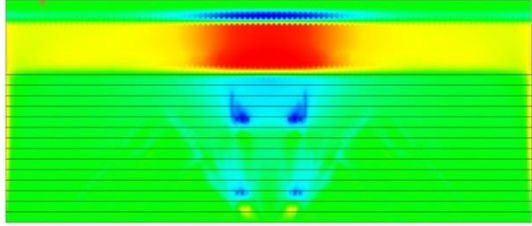*Figure 56.   Shear force per unit width [kN/m] in y-direction for six different analysis at Q = 300 kN.*

Q = 400 kN			
4 nodes, 2x2x9, ν = 0,2		**4 nodes, 2x2x9, ν = 0**	
Max shear force	**Min shear force**	**Max shear force**	**Min shear force**
184 [kN/m]	-162 [kN/m]	184 [kN/m]	-163 [kN/m]
8 nodes, 2x2x9, ν = 0,2		**8 nodes, 2x2x9, ν = 0**	
Max shear force	**Min shear force**	**Max shear force**	**Min shear force**
184 [kN/m]	-162 [kN/m]	183 [kN/m]	-183 [kN/m]
8 nodes, 3x3x9, ν = 0,2		**8 nodes, 3x3x9, ν = 0**	
Max shear force	**Min shear force**	**Max shear force**	**Min shear force**
183 [kN/m]	-162 [kN/m]	183 [kN/m]	-183 [kN/m]

Figure 57. *Shear force per unit width [kN/m] in y-direction for six different analysis at Q = 400 kN.*

Q = 500 kN			
4 nodes, 2x2x9, ν = 0,2		**4 nodes, 2x2x9, ν = 0**	
Max shear force	Min shear force	Max shear force	Min shear force
222 [kN/m]	-268 [kN/m]	210 [kN/m]	-200 [kN/m]
8 nodes, 2x2x9, ν = 0,2		**8 nodes, 2x2x9, ν = 0**	
Max shear force	Min shear force	Max shear force	Min shear force
222 [kN/m]	-268 [kN/m]	209 [kN/m]	-255 [kN/m]
8 nodes, 3x3x9, ν = 0,2		**8 nodes, 3x3x9, ν = 0**	
Max shear force	Min shear force	Max shear force	Min shear force
222 [kN/m]	-268 [kN/m]	209 [kN/m]	-220 [kN/m]

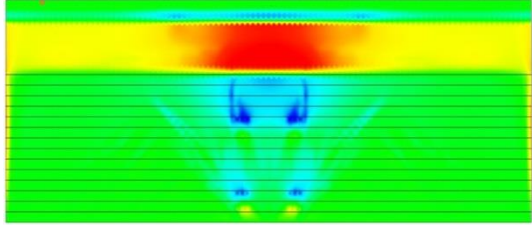*Figure 58.   Shear force per unit width [kN/m] in y-direction for six different analysis at Q = 500 kN.*

Q = 600 kN			
4 nodes, 2x2x9, v = 0,2		**4 nodes, 2x2x9, v = 0**	
Max shear force	**Min shear force**	**Max shear force**	**Min shear force**
837 [kN/m]	-720 [kN/m]	250 [kN/m]	-297 [kN/m]
8 nodes, 2x2x9, v = 0,2		**8 nodes, 2x2x9, v = 0**	
Max shear force	**Min shear force**	**Max shear force**	**Min shear force**
834 [kN/m]	-720 [kN/m]	249 [kN/m]	-294 [kN/m]
8 nodes, 3x3x9, v = 0,2		**8 nodes, 3x3x9, v = 0**	
Max shear force	**Min shear force**	**Max shear force**	**Min shear force**
468 [kN/m]	-358 [kN/m]	252 [kN/m]	-305 [kN/m]

Figure 59.   *Shear force per unit width [kN/m] in y-direction for six different analysis at Q =600 kN.*

Q = 700 kN			
4 nodes, 2x2x9, v = 0,2		**4 nodes, 2x2x9, v = 0**	
Max shear force	**Min shear force**	**Max shear force**	**Min shear force**
1339 [kN/m]	-1223 [kN/m]	314 [kN/m]	-344 [kN/m]
8 nodes, 2x2x9, v = 0,2		**8 nodes, 2x2x9, v = 0**	
Max shear force	**Min shear force**	**Max shear force**	**Min shear force**
1338 [kN/m]	-1223 [kN/m]	309 [kN/m]	-370 [kN/m]
8 nodes, 3x3x9, v = 0,2		**8 nodes, 3x3x9, v = 0**	
Max shear force	**Min shear force**	**Max shear force**	**Min shear force**
681 [kN/m]	-524 [kN/m]	311 [kN/m]	-400 [kN/m]

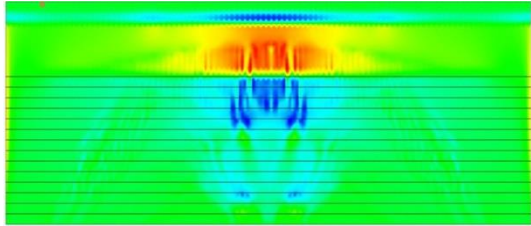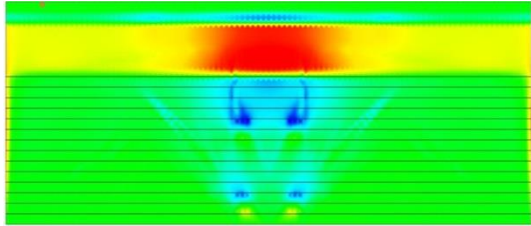*Figure 60.   Shear force per unit width [kN/m] in y-direction for six different analysis at Q = 700 kN.*
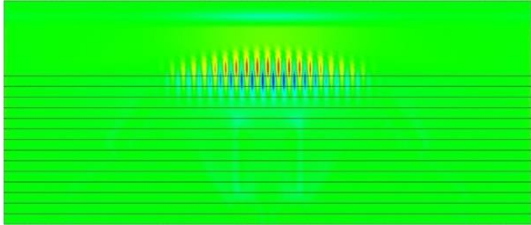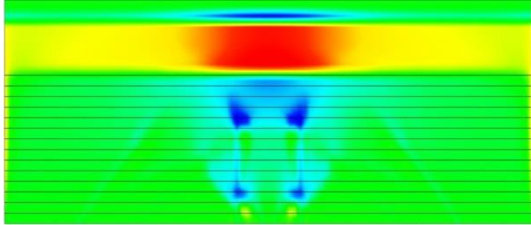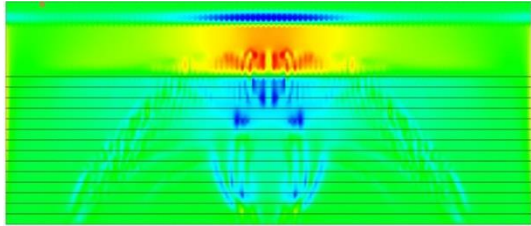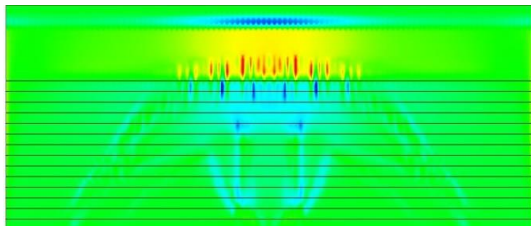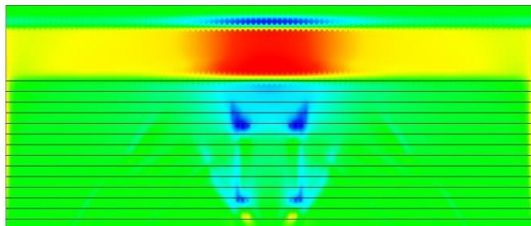
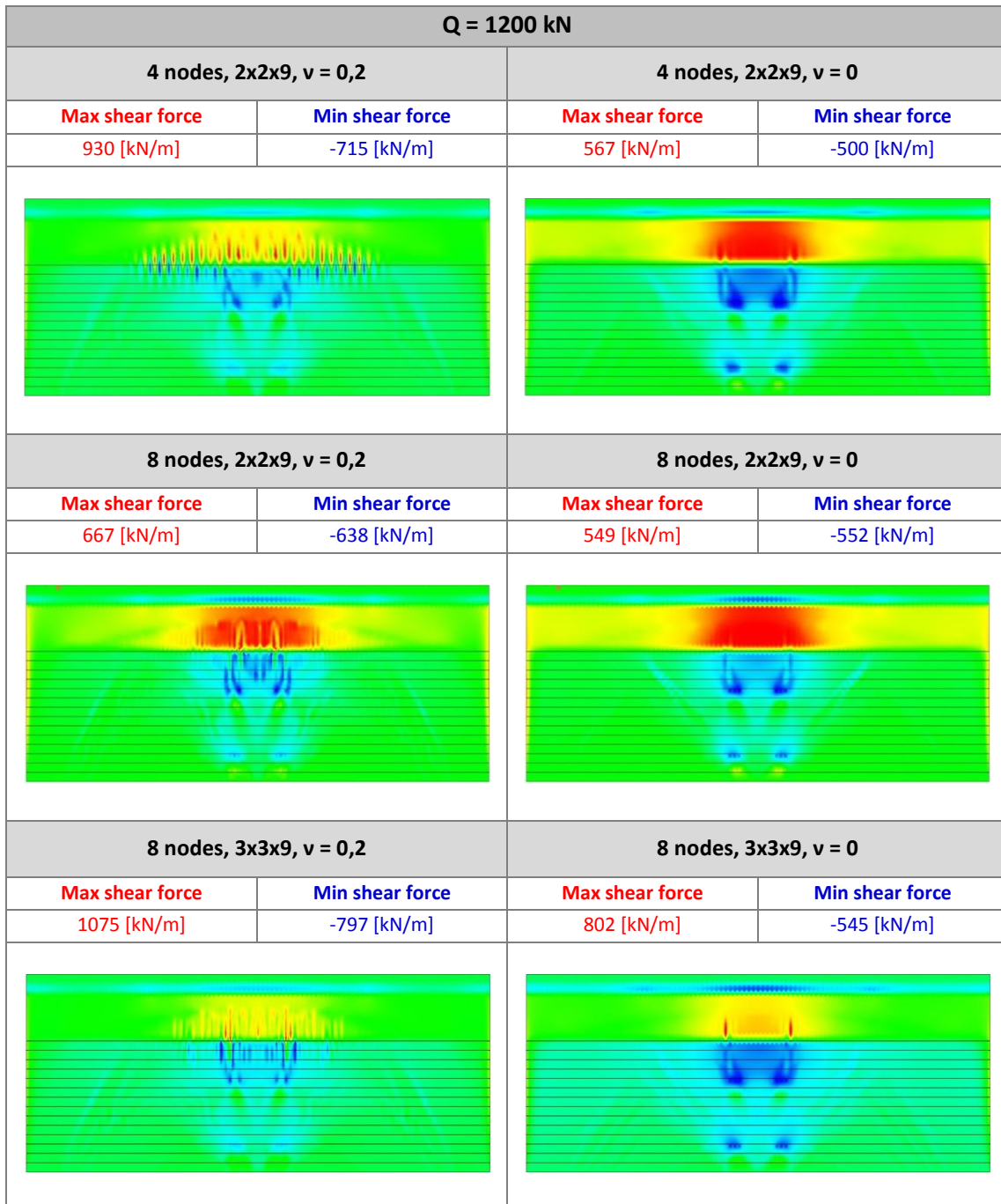| Q = 800 kN			
4 nodes, 2x2x9, v = 0,2		**4 nodes, 2x2x9, v = 0**	
Max shear force	Min shear force	Max shear force	Min shear force
1687 [kN/m]	-1575 [kN/m]	366 [kN/m]	-358 [kN/m]
8 nodes, 2x2x9, v = 0,2		**8 nodes, 2x2x9, v = 0**	
Max shear force	Min shear force	Max shear force	Min shear force
540 [kN/m]	-444 [kN/m]	365 [kN/m]	-400 [kN/m]
8 nodes, 3x3x9, v = 0,2		**8 nodes, 3x3x9, v = 0**	
Max shear force	Min shear force	Max shear force	Min shear force
717 [kN/m]	-604 [kN/m]	369 [kN/m]	-390 [kN/m]

Figure 61. *Shear force per unit width [kN/m] in y-direction for six different analysis at Q = 700 kN.*
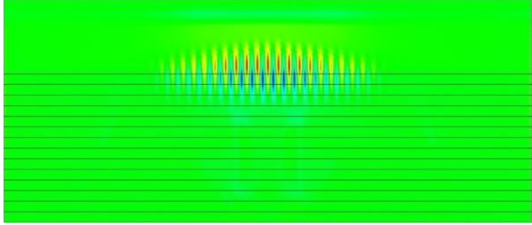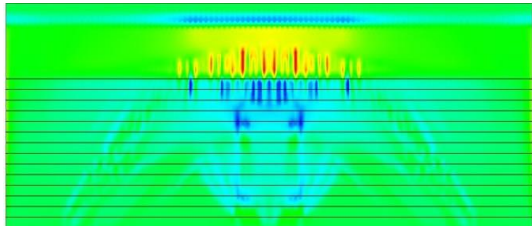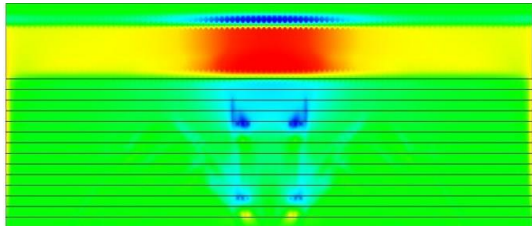
Q = 900 kN			
4 nodes, 2x2x9, v = 0,2		**4 nodes, 2x2x9, v = 0**	
Max shear force	**Min shear force**	**Max shear force**	**Min shear force**
2050 [kN/m]	-1944 [kN/m]	431 [kN/m]	-464 [kN/m]
8 nodes, 2x2x9, v = 0,2		**8 nodes, 2x2x9, v = 0**	
Max shear force	**Min shear force**	**Max shear force**	**Min shear force**
554 [kN/m]	-545 [kN/m]	422 [kN/m]	-445 [kN/m]
8 nodes, 3x3x9, v = 0,2		**8 nodes, 3x3x9, v = 0**	
Max shear force	**Min shear force**	**Max shear force**	**Min shear force**
765 [kN/m]	-549[kN/m]	424 [kN/m]	-458 [kN/m]

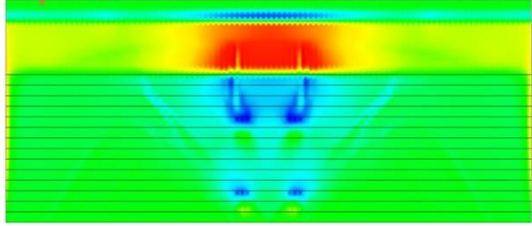*Figure 62.   Shear force per unit width [kN/m] in y-direction for six different analysis at Q = 900 kN.*
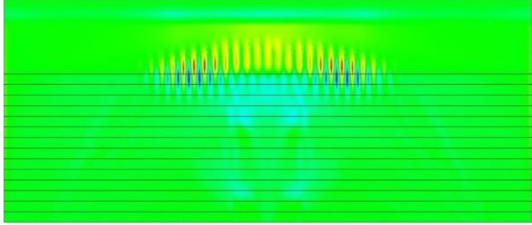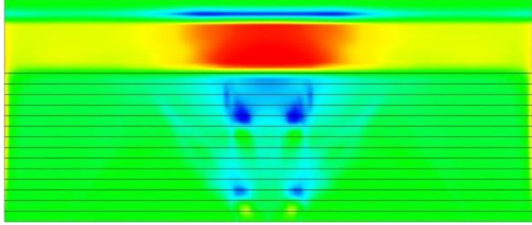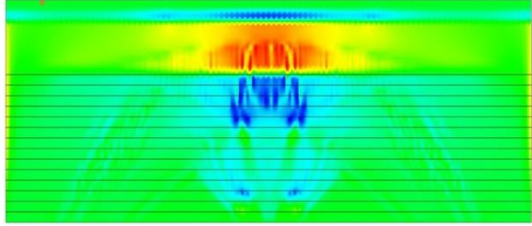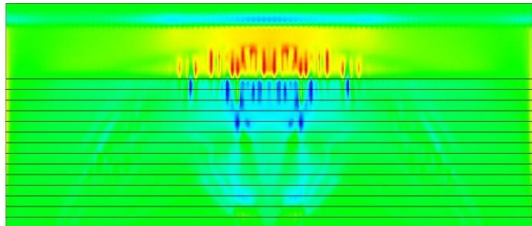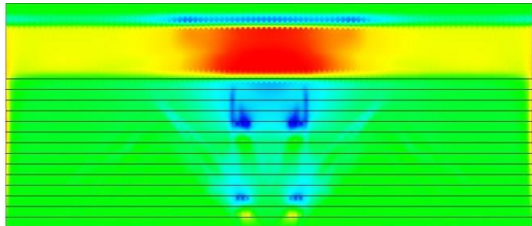
Q = 1000 kN			
4 nodes, 2x2x9, ν = 0,2		**4 nodes, 2x2x9, ν = 0**	
Max shear force	Min shear force	Max shear force	Min shear force
1367 [kN/m]	-117 [kN/m]	461 [kN/m]	-444 [kN/m]
8 nodes, 2x2x9, ν = 0,2		**8 nodes, 2x2x9, ν = 0**	
Max shear force	Min shear force	Max shear force	Min shear force
606 [kN/m]	-492 [kN/m]	441 [kN/m]	-467 [kN/m]
8 nodes, 3x3x9, ν = 0,2		**8 nodes, 3x3x9, ν = 0**	
Max shear force	Min shear force	Max shear force	Min shear force
726 [kN/m]	-630 [kN/m]	448 [kN/m]	-462 [kN/m]

Figure 63.   *Shear force per unit width [kN/m] in y-direction for six different analysis at Q = 1000 kN.*
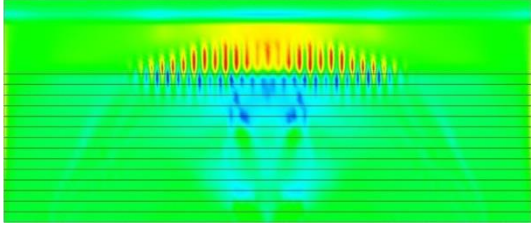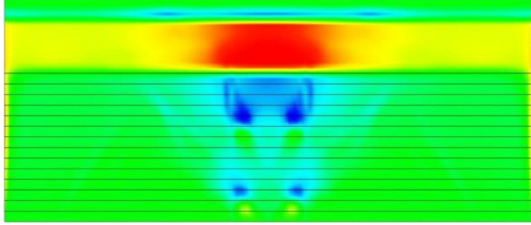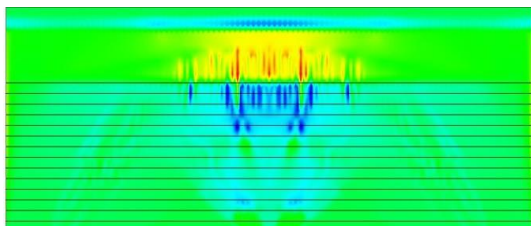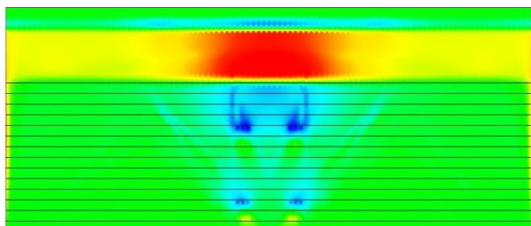
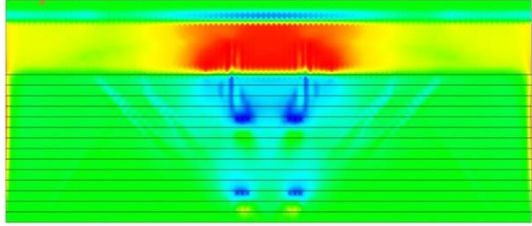| Q = 1100 kN			
4 nodes, 2x2x9, ν = 0,2		**4 nodes, 2x2x9, ν = 0**	
Max shear force	**Min shear force**	**Max shear force**	**Min shear force**
875 [kN/m]	-700 [kN/m]	487 [kN/m]	-470 [kN/m]
8 nodes, 2x2x9, ν = 0,2		**8 nodes, 2x2x9, ν = 0**	
Max shear force	**Min shear force**	**Max shear force**	**Min shear force**
686 [kN/m]	-561 [kN/m]	499 [kN/m]	-517 [kN/m]
8 nodes, 3x3x9, ν = 0,2		**8 nodes, 3x3x9, ν = 0**	
Max shear force	**Min shear force**	**Max shear force**	**Min shear force**
894 [kN/m]	-651 [kN/m]	491 [kN/m]	-510 [kN/m]

Figure 64. *Shear force per unit width [kN/m] in y-direction for six different analysis at Q = 1100 kN.*

Q = 1200 kN			
4 nodes, 2x2x9, v = 0,2		**4 nodes, 2x2x9, v = 0**	
Max shear force	**Min shear force**	**Max shear force**	**Min shear force**
930 [kN/m]	-715 [kN/m]	567 [kN/m]	-500 [kN/m]
8 nodes, 2x2x9, v = 0,2		**8 nodes, 2x2x9, v = 0**	
Max shear force	**Min shear force**	**Max shear force**	**Min shear force**
667 [kN/m]	-638 [kN/m]	549 [kN/m]	-552 [kN/m]
8 nodes, 3x3x9, v = 0,2		**8 nodes, 3x3x9, v = 0**	
Max shear force	**Min shear force**	**Max shear force**	**Min shear force**
1075 [kN/m]	-797 [kN/m]	802 [kN/m]	-545 [kN/m]

Figure 65.   Shear force per unit width [kN/m] in y-direction for six different analysis at Q = 1200 kN.
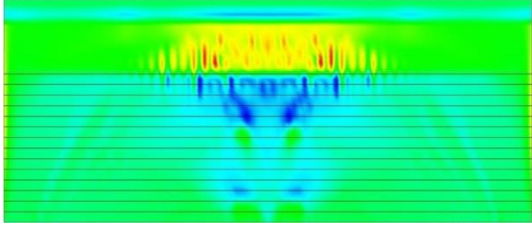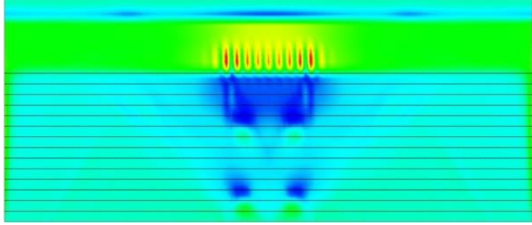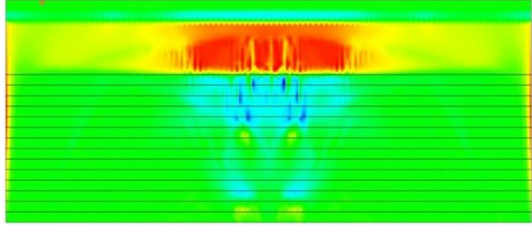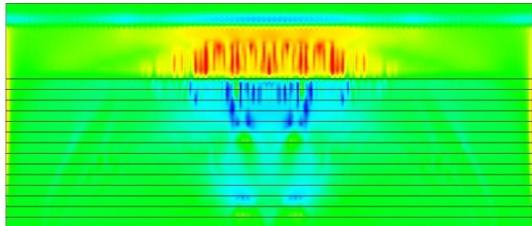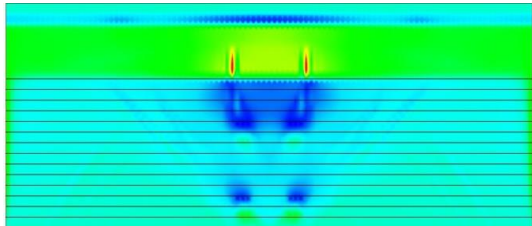
Q = 1300 kN			
4 nodes, 2x2x9, v = 0,2		**4 nodes, 2x2x9, v = 0**	
Max shear force	**Min shear force**	**Max shear force**	**Min shear force**
922 [kN/m]	-632 [kN/m]	1000 [kN/m]	-521 [kN/m]
8 nodes, 2x2x9, v = 0,2		**8 nodes, 2x2x9, v = 0**	
Max shear force	**Min shear force**	**Max shear force**	**Min shear force**
643 [kN/m]	-724 [kN/m]	630 [kN/m]	-575 [kN/m]
8 nodes, 3x3x9, v = 0,2		**8 nodes, 3x3x9, v = 0**	
Max shear force	**Min shear force**	**Max shear force**	**Min shear force**
759 [kN/m]	-661 [kN/m]	1154 [kN/m]	-572 [kN/m]

Figure 66.   Shear force per unit width [kN/m] in y-direction for six different analysis at Q = 1300 kN.
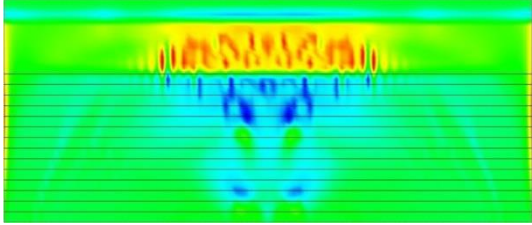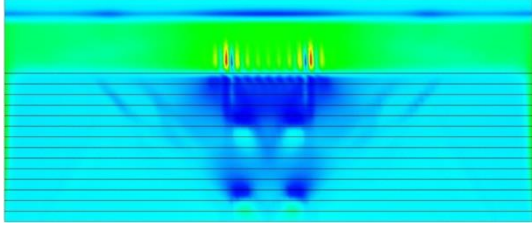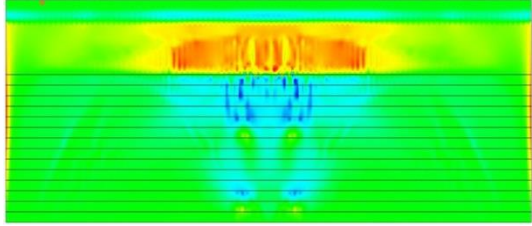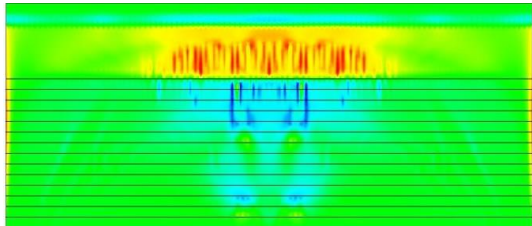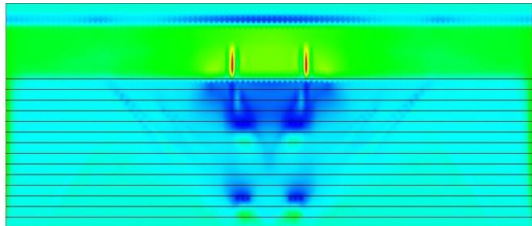
Q = 1380 kN			
4 nodes, 2x2x9, v = 0,2		**4 nodes, 2x2x9, v = 0**	
Max shear force	**Min shear force**	**Max shear force**	**Min shear force**
754 [kN/m]	-602 [kN/m]	1436 [kN/m]	-527 [kN/m]
8 nodes, 2x2x9, v = 0,2		**8 nodes, 2x2x9, v = 0**	
Max shear force	**Min shear force**	**Max shear force**	**Min shear force**
721 [kN/m]	-681 [kN/m]	591 [kN/m]	-579 [kN/m]
8 nodes, 3x3x9, v = 0,2		**8 nodes, 3x3x9, v = 0**	
Max shear force	**Min shear force**	**Max shear force**	**Min shear force**
763 [kN/m]	-708 [kN/m]	1238 [kN/m]	-578 [kN/m]

Figure 67.   Shear force per unit width [kN/m] in y-direction for six different analysis at Q = 1380 kN.

5.2.1.2 Transversal shear force distribution along the support.

The distribution of shear force in transversal direction was studied along a line parallel to the support at a distance of 50 mm from it. The diagrams were made for the same steps during loading.
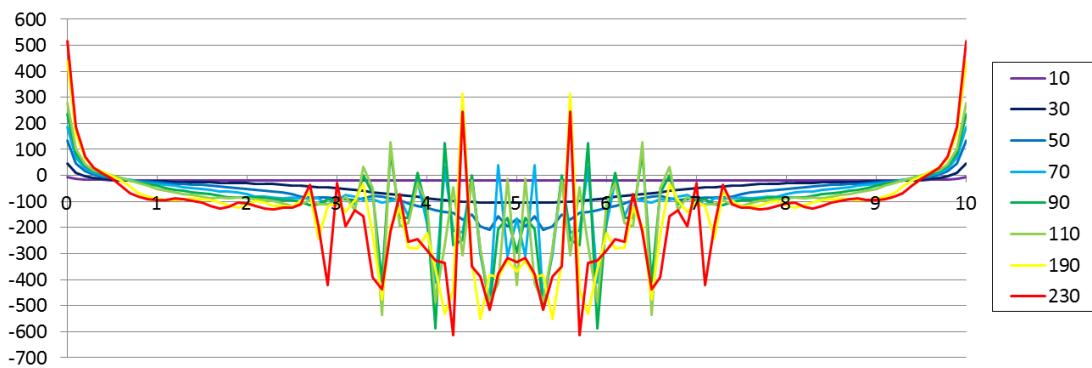
a) 4 nodes, 2x2x9, ν = 0.2
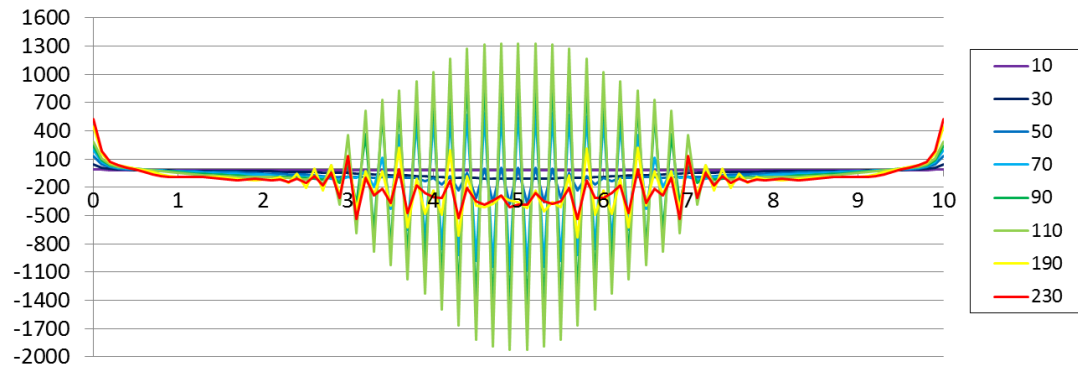
Figure 68.   Shear force in y-direction for analysis 4 nodes, 2x2x9, ν = 0.2.
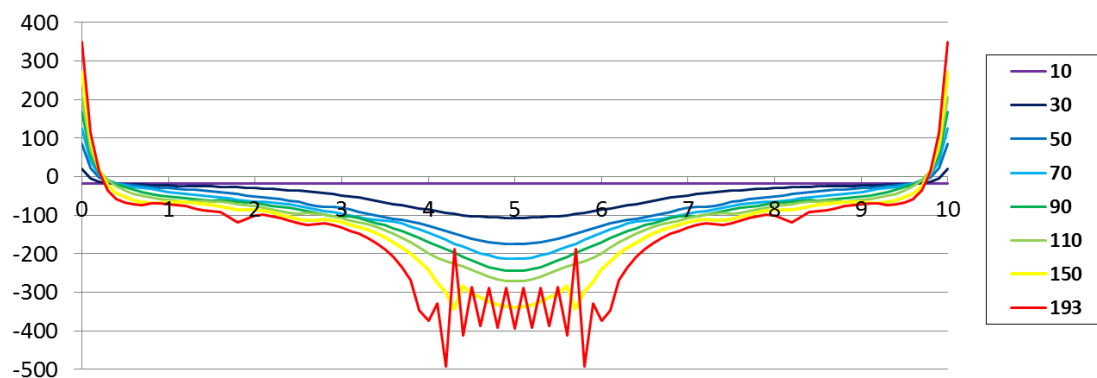
b) 4 nodes, 2x2x9, ν = 0

Figure 69.   Shear force in y-direction for analysis 4 nodes, 2x2x9, ν = 0.
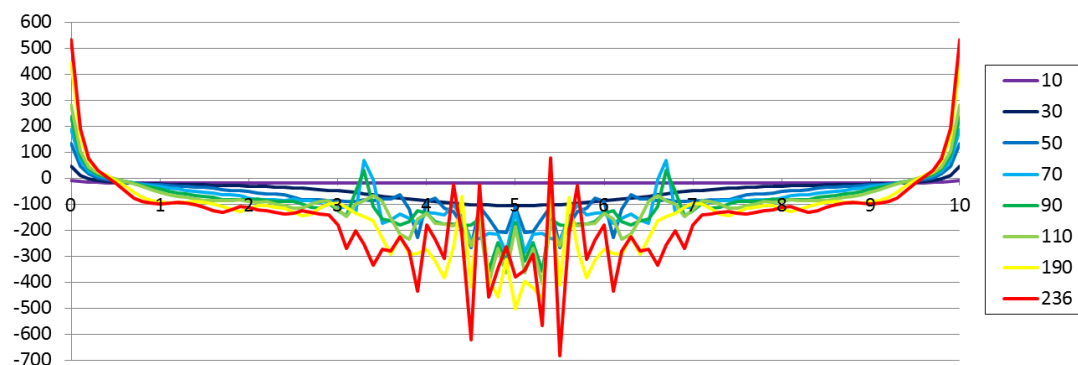
c) 8 nodes, 2x2x9, ν = 0.2

Figure 70.   Shear force in y-direction for analysis 8 nodes, 2x2x9, ν = 0.2.
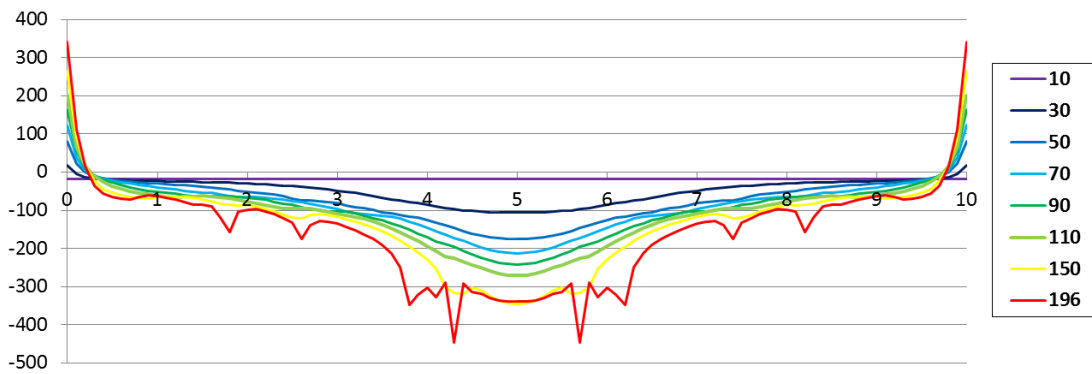
d) 8 nodes, 2x2x9, ν = 0

Figure 71.   Shear force in y-direction for analysis 8 nodes, 2x2x9, v = 0.

e) 8 nodes, 3x3x9, ν = 0.2

Figure 72.   Shear force in y-direction for analysis 8 nodes, 3x3x9, v = 0.2.
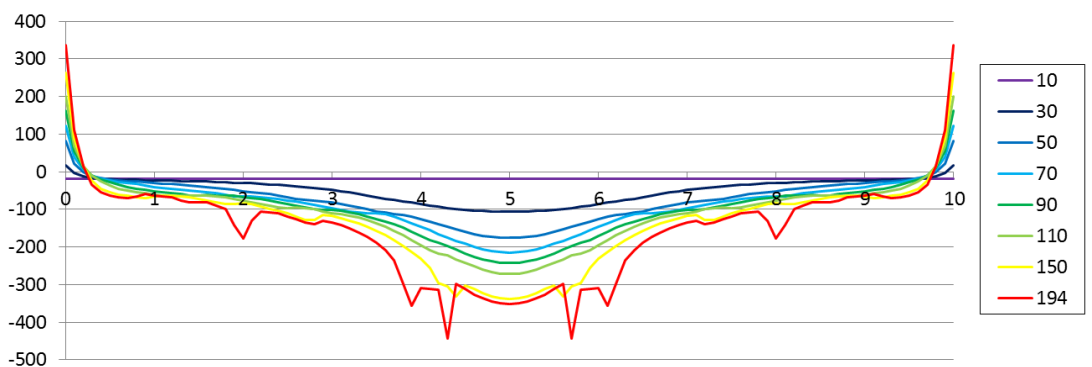
f) 8 nodes, 3x3x9, ν = 0

Figure 73.   Shear force in y-direction for analysis 8 nodes, 3x3x9, v = 0.

Clearly, the models with Poisson's ratio ν =0.2 show large fluctuations in shear force. Those with reduced Poisson's ratio (ν =0) seems to have a more realistic distribution along the support. However, for high load levels, both the model with 4 node elements

(*4 nodes, 2x2x9, v = 0*), see *Figure 69*, and with 8 nodes and 3x3 in-plane integration points (*8 nodes, 3x3x9, v = 0),* see *Figure 73*, have some extreme peaks over the support.

5.2.1.3 Transversal shear force distribution along the support for the failure load.

The distribution of shear force in transversal direction was studied along a line parallel to the support at a distance of 50 mm from it. The diagrams were made for the failure load only, see *Figure 74* to *Figure 76*. The main focus is put on comparison between analyses made with the same model except regarding Poisson's ratio. Trend lines were used to represent the average values along the parts of the control line, where the fluctuation occurred, in order to determine the overall shear distribution. These trend lines are 6th-order-polynomial functions that approximate the scattered shear force values into smooth-line functions.
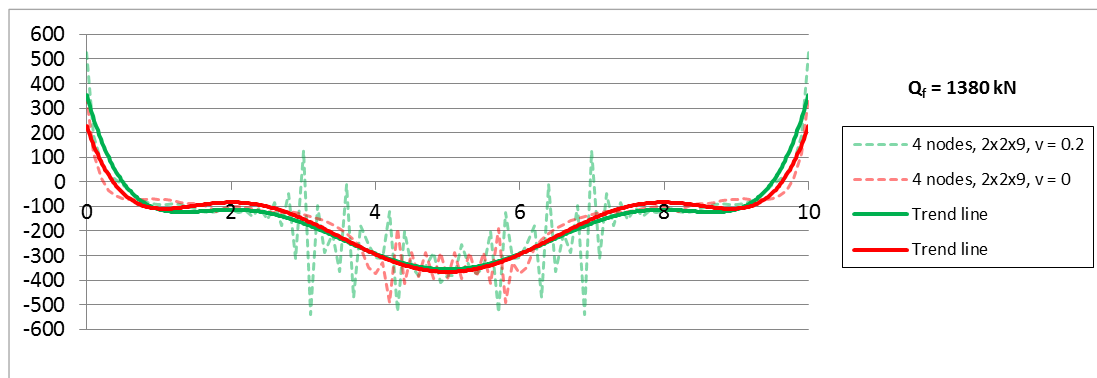
Figure 74.   *Shear force in y-direction and trend lines for model 4 nodes, 2x2x9, v = 0.2 and model 4 nodes, 2x2x9, v = 0 at failure load.*
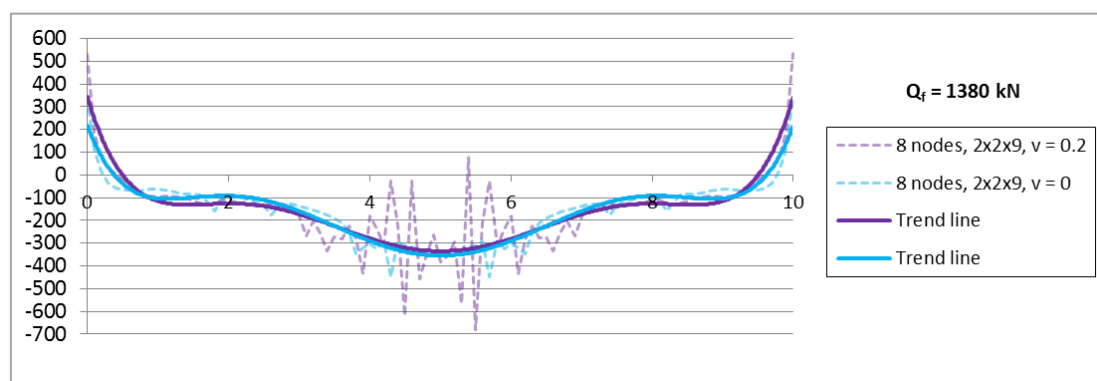
Figure 75.   *Shear force in y-direction and trend lines for model8 nodes, 2x2x9, v = 0.2 and model 8 nodes, 2x2x9, v = 0 at failure load.*
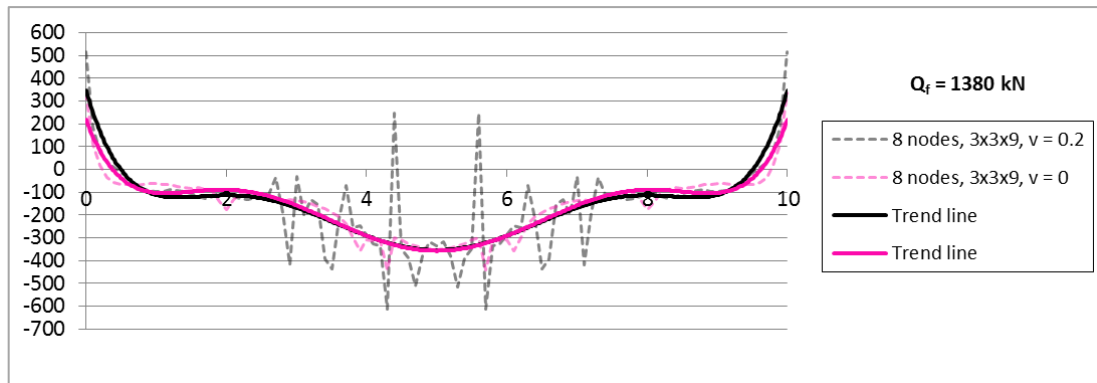
CHALMERS, *Civil and Environmental Engineering*, Master's Thesis 2013:127

Figure 76.   Shear force in y-direction and trend lines for model8 nodes, 3x3x9,
v = 0.2 and model 8 nodes, 3x3x9, v = 0 at failure load.

The differences between the trend lines for the compared analyses are rather small.
Those with reduced Poisson ratio (*v* =0) always have slightly higher shear force in the
middle of the support. The amount of shear flow over the support is the same and not
affected by any of the parameters that were changed.

5.3   Evaluation of results

With respect to the distribution of the shear forces, all models with unreduced
Poisson's ratio (*v*=0.2) were not able to describe it properly. Only one model, with 8
node shell elements with reduced integration, i.e. 2x2 integration points in the element
plane *(8 nodes, 2x2x9, v=0)* showed adequate results, with no fluctuation in the shear
force. However, it has been observed that models with reduced Poisson ratio (*v*=0)
had stiffer behaviour and reached the failure load with less steps. In *Figure 77*, the
load-displacement curve presents the difference between the two models with 8 node
elements and reduced integration (*8 nodes, 2x2x9, v=0* and *8 nodes, 2x2x9, v=0.2*).
Smaller deflection at the ultimate force can be seen for the models with reduced
Poisson's ratio (*v*=0). *Figure 77* also presents the load-displacement curve of the full-
scale test conducted and described by Vaz Rodrigues (2007), see s*ection 2.2.2*. For
lower load levels both analyses show a higher stiffness than the test results. This may
due to that bending cracking occurs for a lower load in the test due to microcracks
caused by shrinkage and other factors. After formation of bending cracks, the stiffness
of the analysis with *v*=0 corresponds rather well with that of the test, approximately
from Q = 850 kN to 1100 kN. For higher loads the stiffness of the test becomes lower,
a possible reason for that could be the appearance of the first shear crack which is
impossible to be detected with shell elements. The analysis with *v*=0.2 corresponds
better to the test results up to shear failure in the test, which is unexpected and
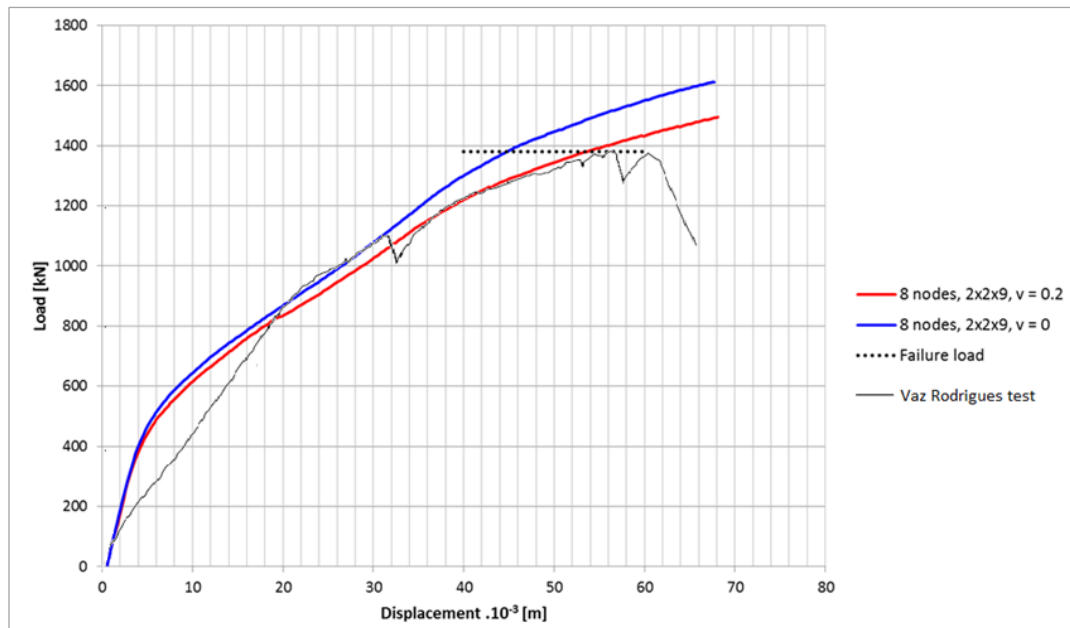misleading again because of the possible shear crack initiation.

Figure 77. *Comparison of load-displacement curve between model 8 nodes, 2x2x9, v=0 and model 8 nodes, 2x2x9, v=0.2 and Vaz Rodrigues' test (2007).*

5.3.1 Observation of shear distribution

When it comes to the reliability of the results regarding shear distribution of concrete slabs only, the model with eight node elements, reduced integration and Poisson's ratio v =0 (*8 nodes, 2x2x9, v=0)* presents the most accurate results. In *Figure 78*, the diagram illustrates the distribution of shear force in transversal direction along the control line for different loads, together with the contour plot of the transversal shear distribution for the failure load. It can be observed that several peaks in the shear distribution occurred at failure load (Q = 1380 kN).

CHALMERS, *Civil and Environmental Engineering*, Master's Thesis 2013:127
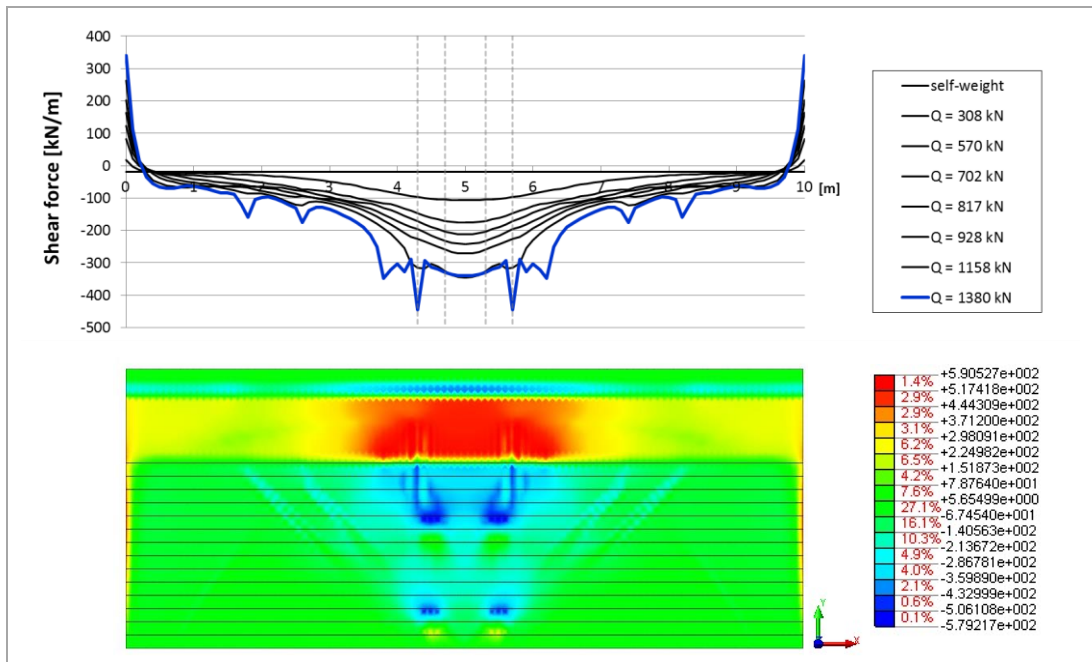
Figure 78. *Shear force diagram on controlled line compared to shear force contour plot for model 8 nodes, 2x2x9, v=0*

5.3.2 Principal tensile strains

The development of the principal tensile strains for the model with eight node elements, reduced integration and Poisson's ratio $v = 0$ (*8 nodes, 2x2x9, v=0*) is presented. The scale used was normalized to present un-cracked and cracked regions. The minimum principal tensile strain was set to $8,3 \cdot 10^{-5}$, and the maximum to $1,751 \cdot 10^{-3}$. Due to this choice the following contour plot for different loads present cracked region more clearly, as the dark blue colour applies to un-cracked regions and red to fully cracked regions where the concrete cannot transfer tensile stresses any more.

5.3.2.1 Top surface

From *Figure 79* to *Figure 87*, concentrations of strains can be seen at the middle part of the support line, indicating cracking. After increasing the load, regions with strain concentrations continued to spread at an angle of about 45° towards the free cantilever edge. At step 90, see *Figure 82*, a second line of strain concentration parallel to the support can be observed where half of the top reinforcement was curtailed. However, the cracks near the support were much larger, which corresponds well with the yielding of the top transversal reinforcement in this region.
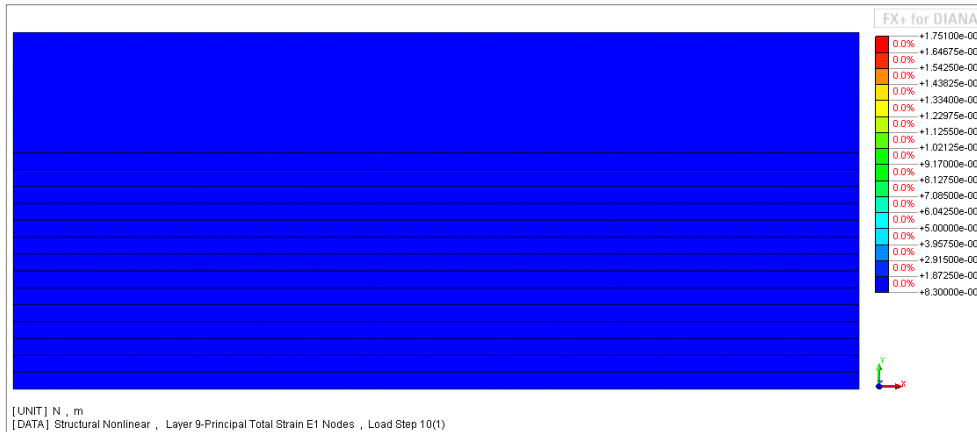
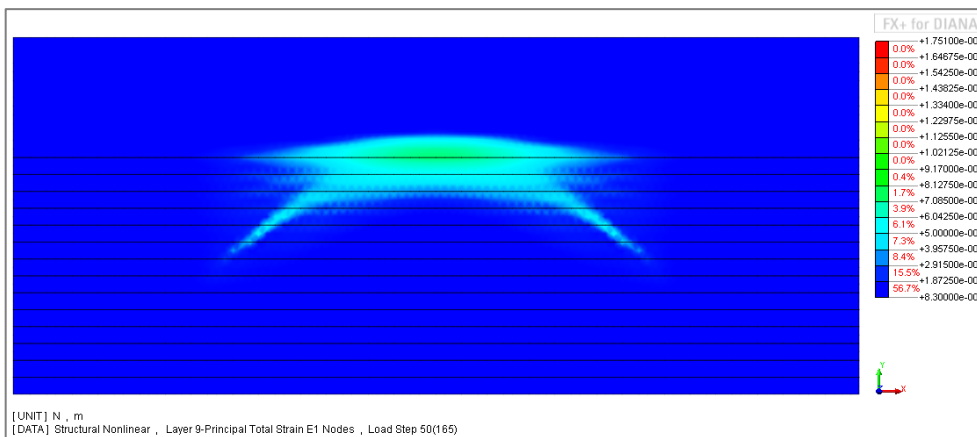*Figure 79.   Top tensile strains at step 10 for model 8 nodes, 2x2x9, v = 0.*

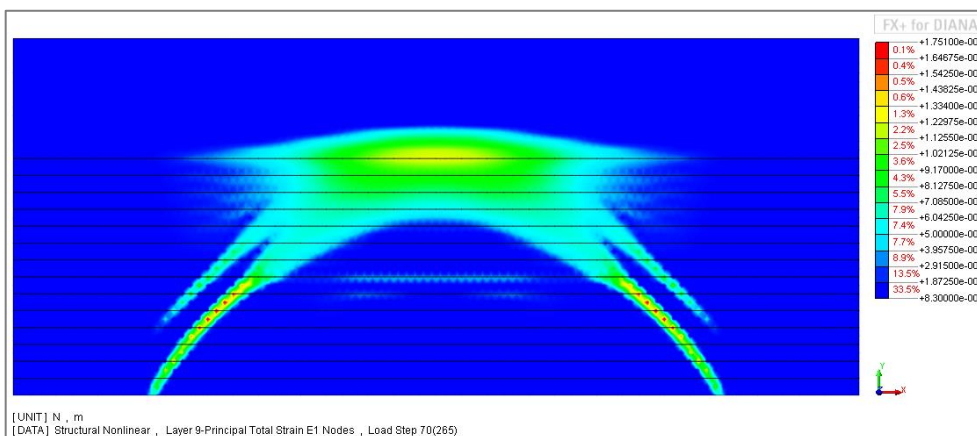*Figure 80.   Top tensile strains at step 50 for model 8 nodes, 2x2x9, v = 0.*

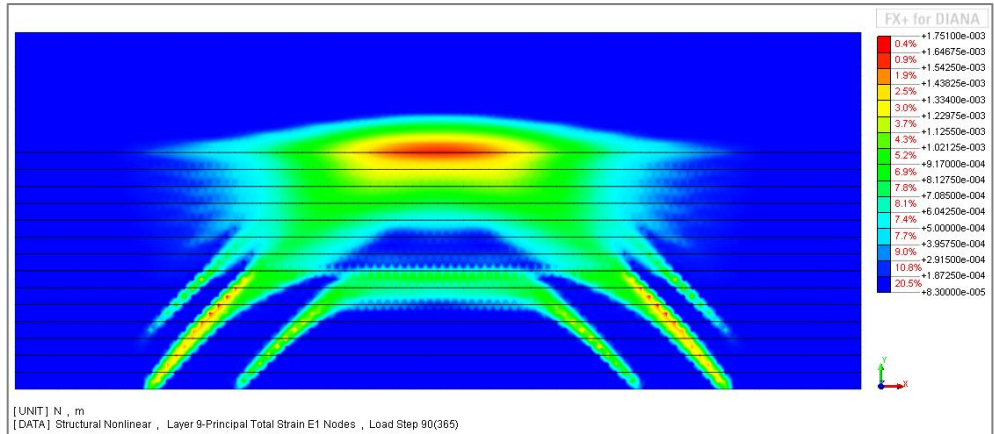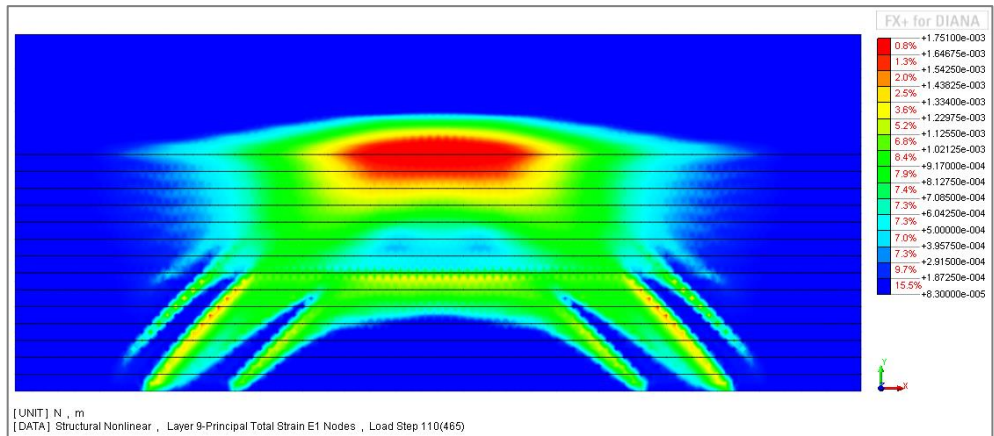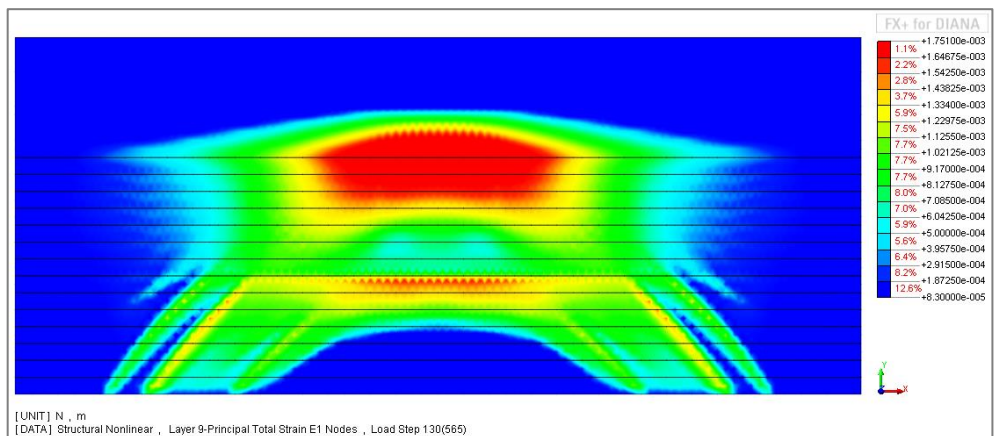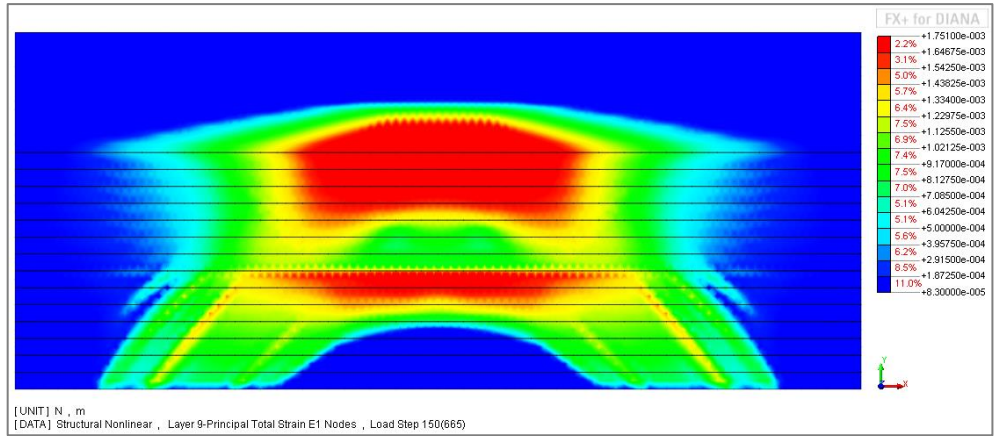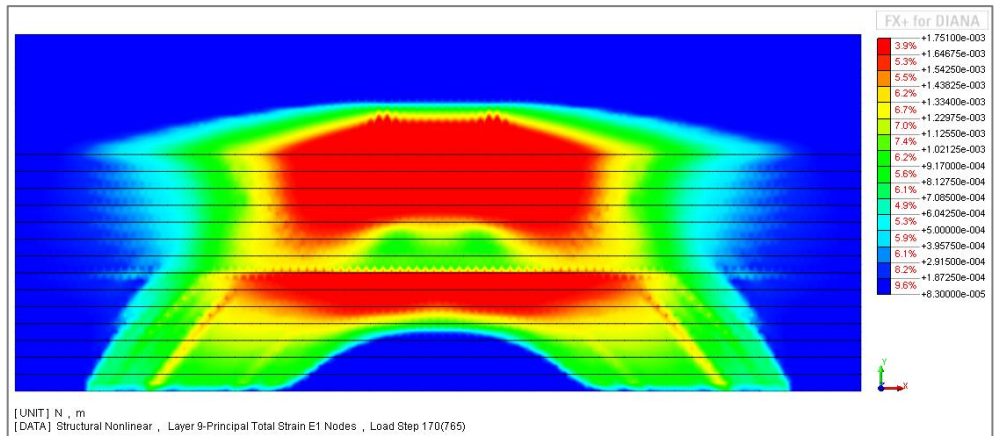*Figure 81.   Top tensile strains at step 70 for model 8 nodes, 2x2x9, v = 0.*

CHALMERS, *Civil and Environmental Engineering*, *Master's Thesis 2013:127*

Figure 82. *Top tensile strains at step 90 for model 8 nodes, 2x2x9, v = 0.*

Figure 83. *Top tensile strains at step 110 for model 8 nodes, 2x2x9, v = 0.*

Figure 84. *Top tensile strains at step 130 for model 8 nodes, 2x2x9, v = 0.*

Figure 85. *Top tensile strains at step 150 for model 8 nodes, 2x2x9, v = 0.*

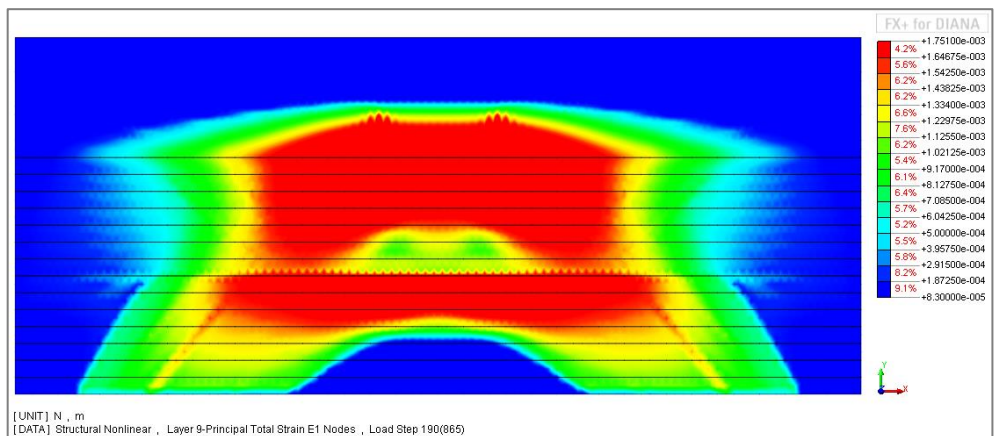*Figure 86.* *Top tensile strains at step 170 for model 8 nodes, 2x2x9, v = 0.*

Figure 87. *Top tensile strains at step 196 for model 8 nodes, 2x2x9, v = 0.*

5.3.2.2 Bottom surface

From *Figure 88* to *Figure 96*, concentration of principal tensile stresses can be seen right under the load pair closest to the cantilever edge, indicating cracked regions. When increasing the load, these regions continued to spread towards the support in a V-shape.
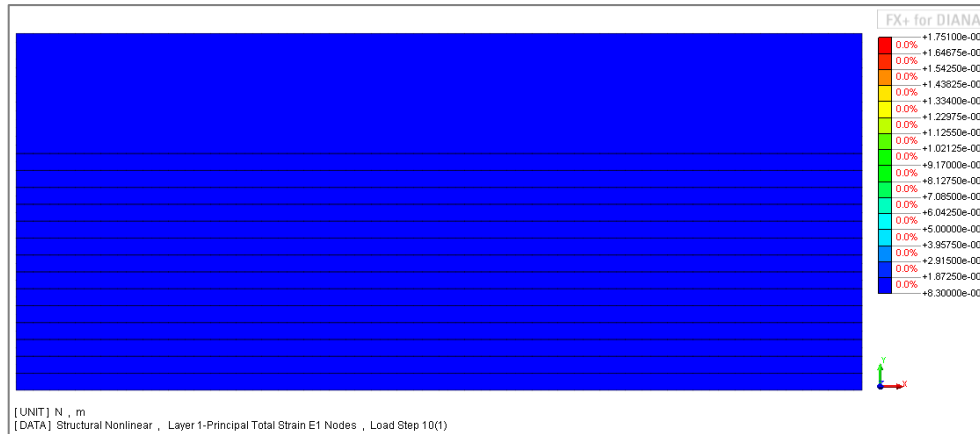

Figure 88.   Bottom tensile strains at step 10 for model 8 nodes, 2x2x9, v = 0.
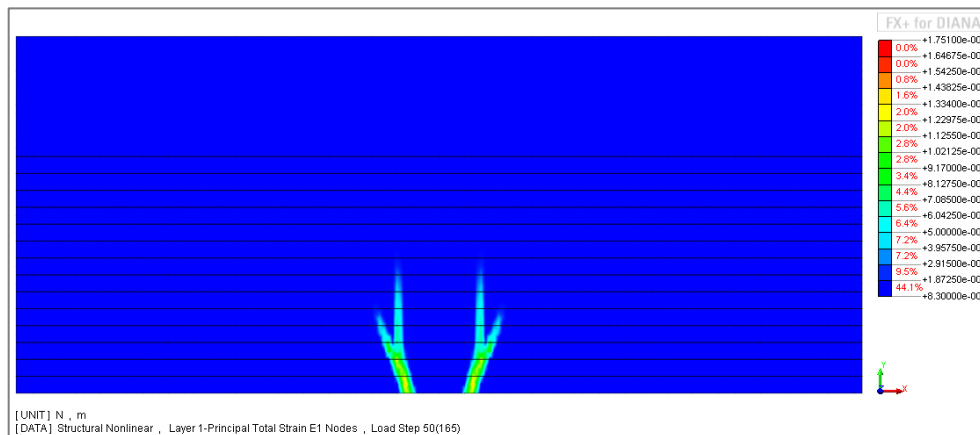

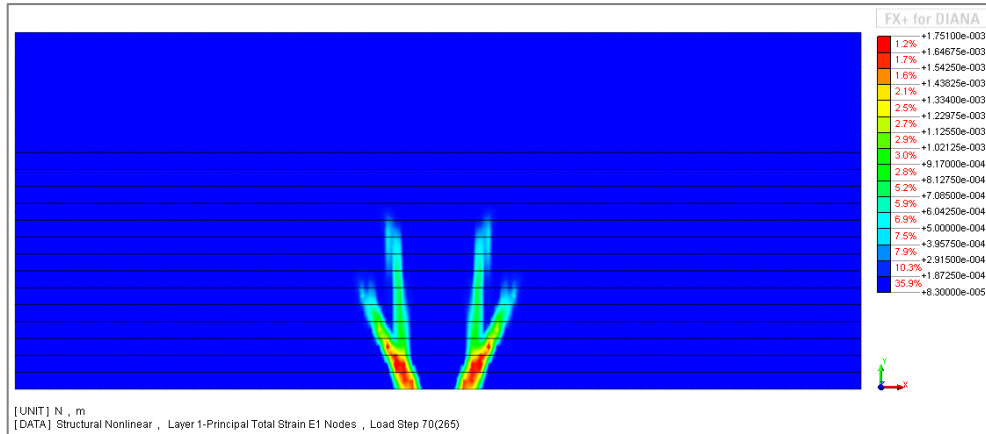*Figure 89.   Bottom tensile strains at step 50 for model 8 nodes, 2x2x9, v = 0.*

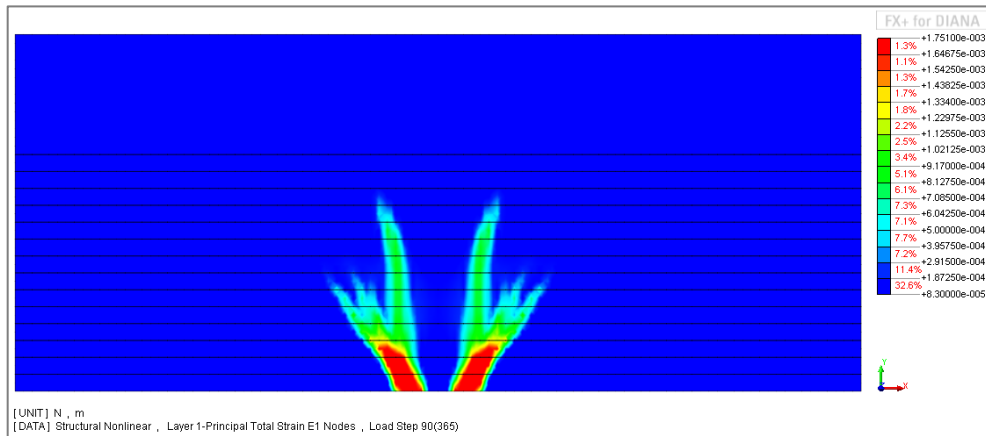*Figure 90.   Bottom tensile strains at step 70 for model 8 nodes, 2x2x9, v = 0.*

Figure 91.   Bottom tensile strains at step 90 for model 8 nodes, 2x2x9, v = 0.

Figure 92.   Bottom tensile strains at step 110 for model 8 nodes, 2x2x9, v = 0.

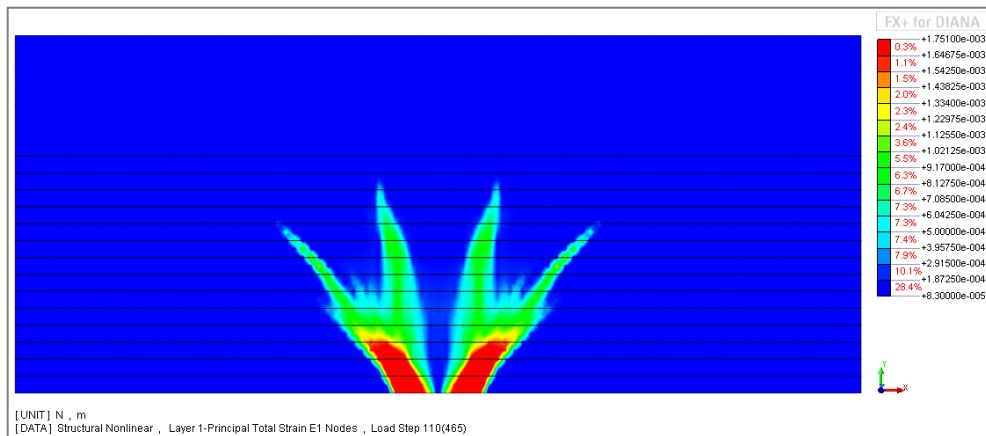**CHALMERS**, *Civil and Environmental Engineering*, *Master's Thesis 2013:127*
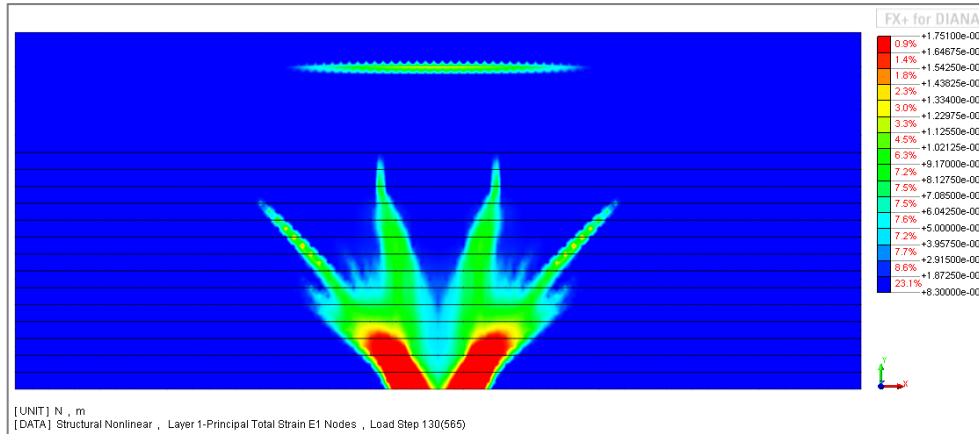
Figure 93.   Bottom tensile strains at step 130 for model 8 nodes, 2x2x9, v = 0.
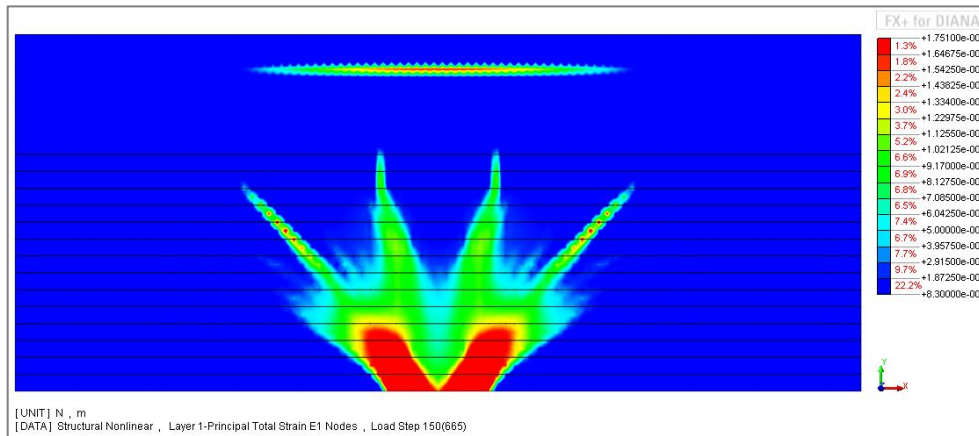

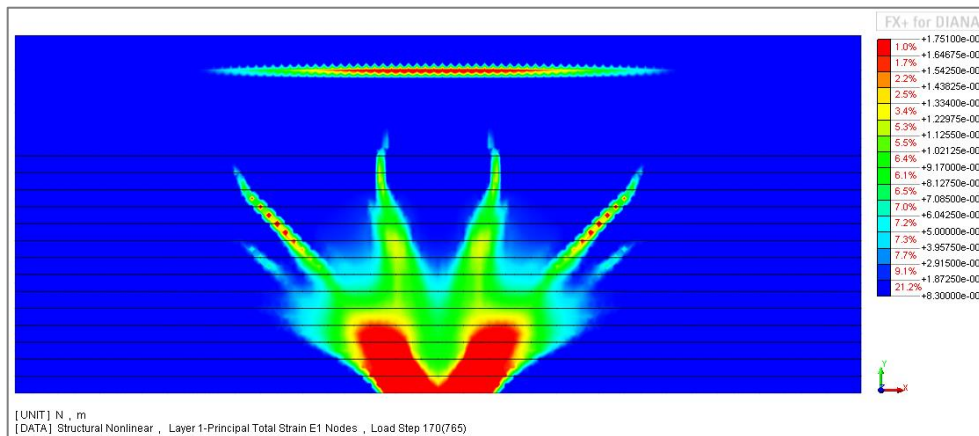*Figure 94.   Bottom tensile strains at step 150 for model 8 nodes, 2x2x9, v = 0.*

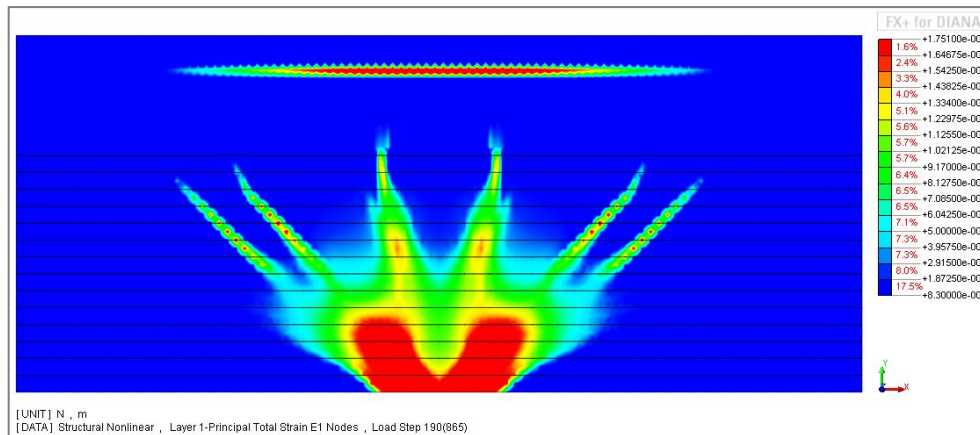*Figure 95.   Bottom tensile strains at step 170 for model 8 nodes, 2x2x9, v = 0.*

CHALMERS, *Civil and Environmental Engineering, Master's Thesis 2013:127*

Figure 96. Bottom tensile strains at step 196 for model 8 nodes, 2x2x9, v = 0.

5.3.3 Yielding of reinforcement

In section 4, it was mentioned that only for the test with four concentrated loads (DR1a), reinforcement in the top transversal direction and the bottom longitudinal direction started to yield before failure. The results shows that plastic strains were present both in the top transversal reinforcement at the fixed end and in the bottom longitudinal reinforcement underneath the edge loads, see *Figure 97* and *Figure 98*. It is possible to consider that the non-linear analysis correctly reproduces the expected results from the tested.
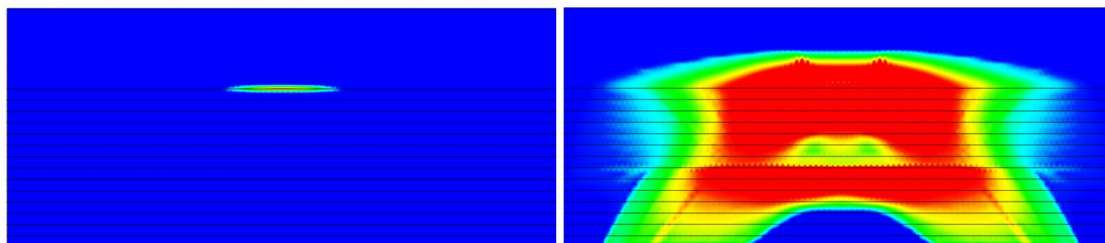

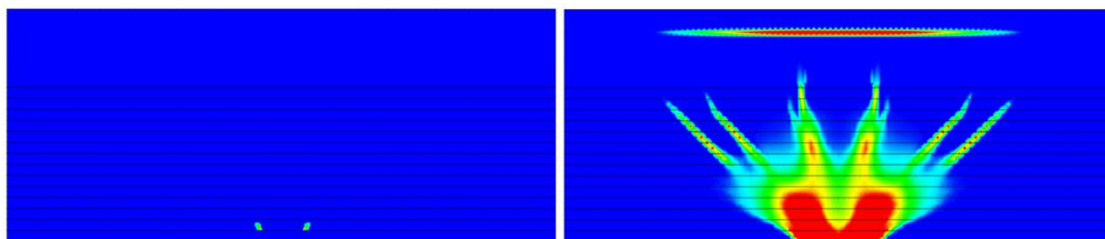*Figure 97.* Strains in the top transversal reinforcement and top tensile strains of concrete at step 196.

Figure 98. Strains in the bottom longitudinal reinforcement bottom tensile strains of concrete at step 196.

CHALMERS, *Civil and Environmental Engineering*, Master's Thesis 2013:127

5.3.4 Shear – strain relation

After investigation of crack pattern, shear distribution in the slab and yielding of the reinforcement, a relation between unusual peaks in the shear force and the crack development was found. In *Figure 99* it can be seen that the regions with large bottom principle tensile strains, indicating cracking, influenced the shear force distribution along the control line; when the crack lines approached the support, the peaks appeared.

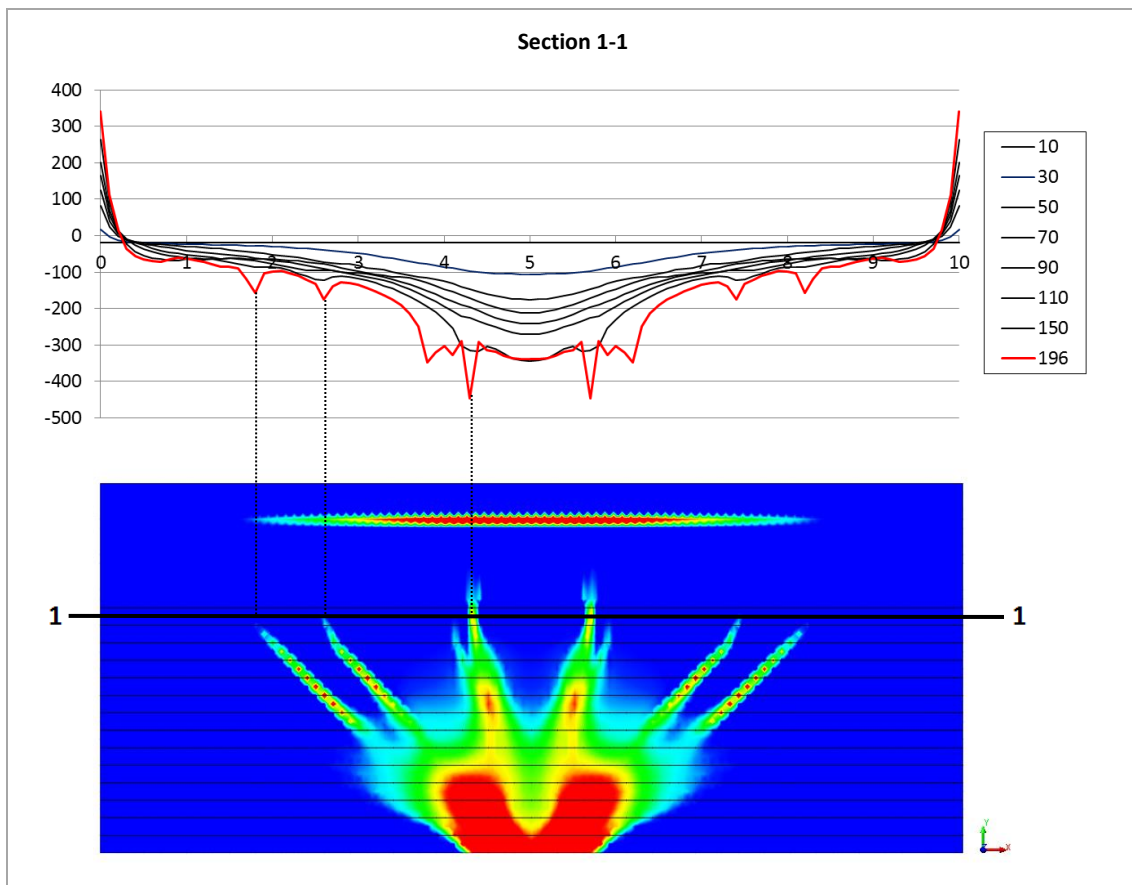*Figure 99.*   *Shear force in y-direction and bottom tensile strains at failure load for model 8 nodes, 2x2x9, v = 0.*

5.3.5 Verification of the results

As was mentioned in *section 4.5*, the way of modelling the support conditions resulted in a similar behaviour to the real slabs response. The layout of the un-deformed model with support and boundary conditions can be seen in *Figure 100*.
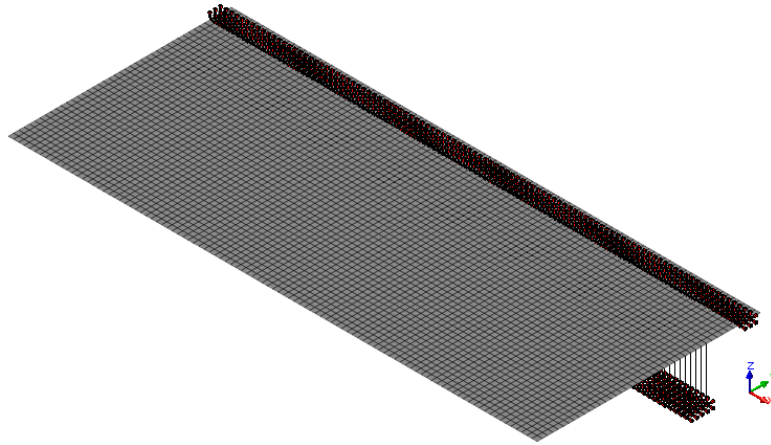
Figure 100.   The layout of the un-deformed model with support and boundary conditions indicated.

5.3.5.1 Displacement

The deformed shape after application of full self-weight is illustrated in *Figure 101*.
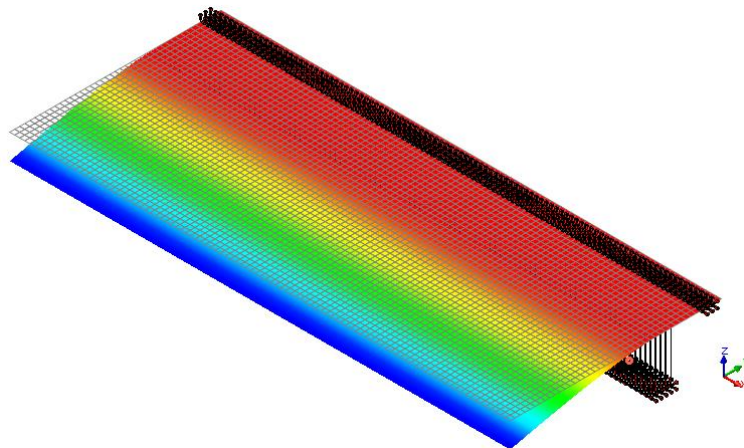
Figure 101.   Deformation due to self-weight, in perspective view.

The maximum deflection of the slab was 5.3 mm, see *Figure 102*. In order to check if the results were reasonable, hand calculations were made for a 1m wide cantilever loaded with self-weight, see appendix 1, and compared with the analysis results. The deflection value from the analysis was in between the calculated values.
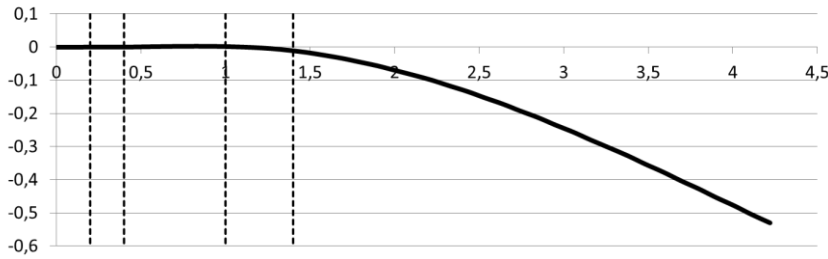
Figure 102.   Deformation due to self-weight, cross-section view.

The positions of the wheel loads were mentioned in *section 4.6.2*. The deformations caused by application of the wheel loads can be seen in *Figure 103*.
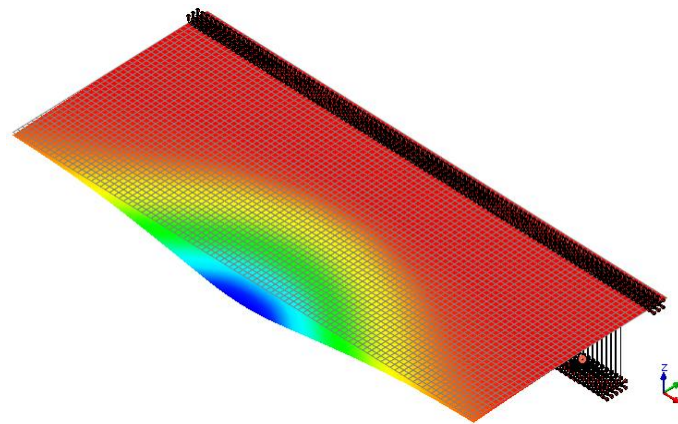

Figure 103.   Deformation due to application of wheel loads, in perspective view.

5.3.5.2   General behaviour

In *Figure 104* and *Figure 105* the shear and moment diagrams in transversal direction are illustrated for the slab cross-section. The control line was set in the middle of the slab. The general behaviour of reinforced concrete slab was investigated by observation of changes along its axis. It can be observed that the highest moment is concentrated over the supports. Moreover, at the point where shear force value equals to zero, the moment reaches its maximum value.
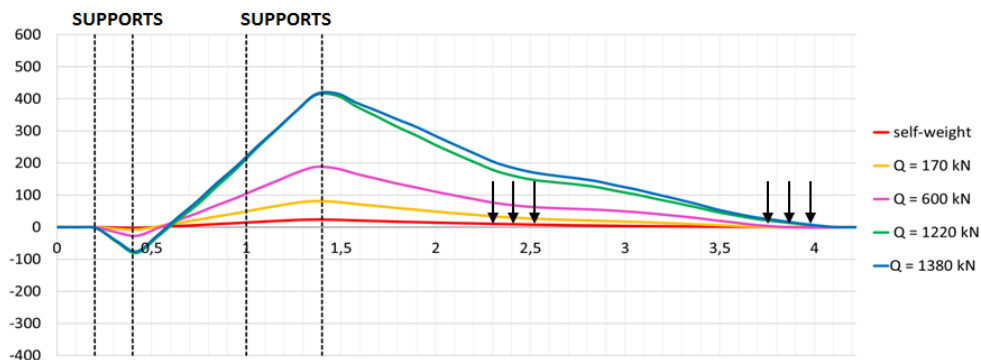
Figure 104.   Moment distribution for cross-section for different loads.
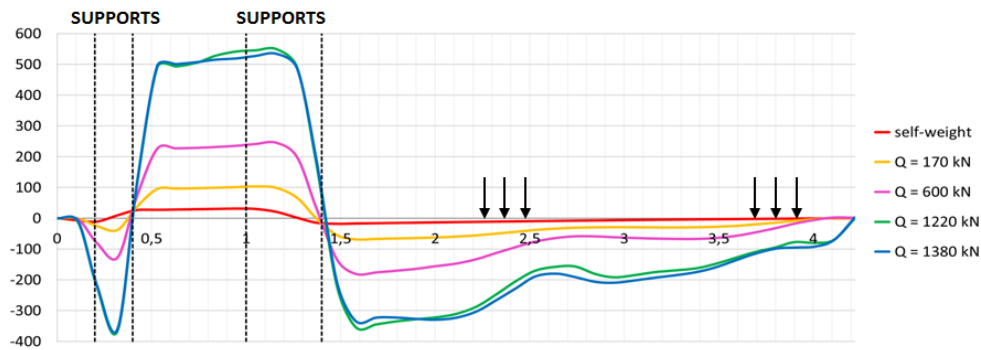
Figure 105.   Shear distribution for cross-section for different loads.

5.3.5.3   Comparison to linear analysis

To understand the difference between the linear analysis and the non-linear analysis, the shear in transversal direction for a failure load (Q = 1380 kN) was compared with a linear elastic case, see *Figure 106*. During design process, only the results with maximum shear were considered since concrete slab is designed for the maximum values that occur due to the moving point loads. However, in *Figure 106* it is shown that linear analysis is not economical with respect to dimensioning. If the peaks mentioned in *section 5.3.1* are neglected by using the trend line, it can be observed that the values obtain by linear analysis could be reduced to approximately 80% to meet the non-linear results.

Figure 106.   Shear force in y-direction at failure load compared to a linear elastic case.

6   Discussion

As a continuation of a previous master's thesis, the current study tried to answer questions formulated beforehand. The assumption, that shear force fluctuations are merely a local effect rather than an event concerning the global response, was to a great extend confirmed. One could observe that, no matter the differences in the 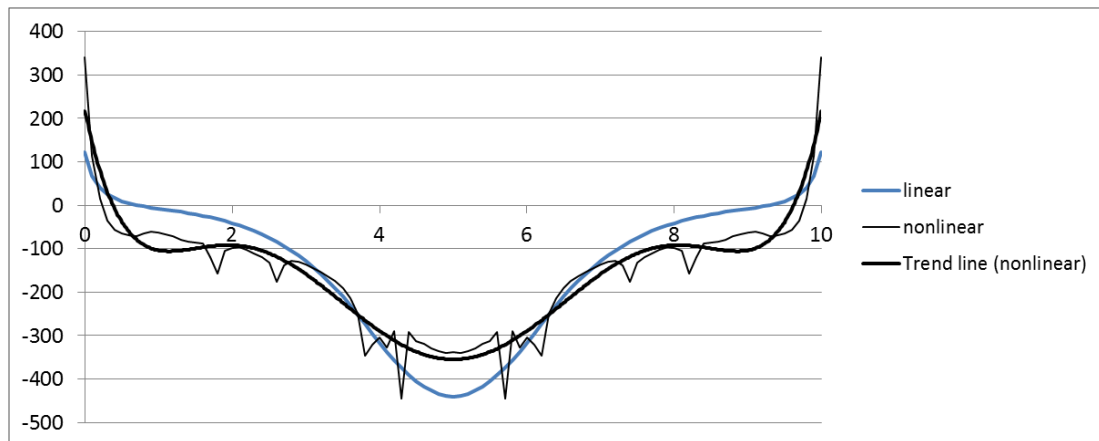models, the overall flow of shear forces remained the same with negligible variations. One possible explanation to the shear force fluctuations may lay in how the Poisson's effect is included in the analyses. Although the software can evaluate the nonlinearity of the materials with respect to redistribution of stresses it seems it cannot do the same when Poisson's effect becomes too large. As Poisson ratio gives the ratio between the strains, sustained due to loading, in two perpendicular directions, the greater the value of the main strain in the concrete is, the greater the effect on the perpendicular direction will be. However, in reality, substantial strains correspond to cracked or even fully cracked areas that are capable of transmitting only limited amount or no stresses. Therefore, the strain perpendicular to these stresses should be tiny or none.

Another fact that has to be pointed out is that the order of elements must agree with the type of analysis. A higher order elements have to be used for non-linear analyses while a lower order are good enough for linear.

Despite the reasonable results for shear, models with reduced Poisson coefficient ($v = 0$) exhibit unexpectedly stiffer behaviour when compared to the full scale tests. Therefore one must be cautious when uses this approach for modelling if Service Limit State (SLS) design is to be based on the results of that analysis. For loads up to 850 kN the reduced stiffness in the specimen is due to microcracks caused by shrinkage and other factors. At range 850÷1100 kN the stiffness of the model corresponds to the stiffness of the specimen. For loads higher than 1100 kN one possible explanation for the deviation could be the initiation of the first shear cracks in the slab, which would reduce the stiffness of the tested specimen but will not be observed in the model since the shell elements cannot describe shear cracks. Having in mind this disadvantage of this type of elements the curve for $v = 0$ in *Figure 77* is reasonable and the curve for $v = 0.2$ is unexpectedly close the test curve, which makes it misleading. It would be interesting if one could verify the proposed explanation using solid element model and find the load at which the initiation of the shear cracks start.

The choice of integration scheme did not show significant influence on the results. However, that is probably due to in-built stabilizing matrices in TNO Diana that overcome the effect of shear locking. Nevertheless not following the recommended integration schemes is highly undesirable and might be misleading if the software producer does not explicitly state that the product is able of self-managing the issue.

Although the results from the analysis is satisfactory, the reader should keep in mind that full comparison between the model and the tested slab is not possible as the shell type of elements do not allow inclined cracks to be observed; what can be studied is

merely the shear force redistribution with respect to bending cracks. To simulate the test, analysis using solid elements would be required to be capable of looking deeper into the shear type failure.

The relation between crack openings and peaks in the shear force diagram is worth further investigating. Although such extremely localized effects are very difficult to be followed during laboratory testing, gathering theoretical knowledge could help evaluating the phenomenon and consequently lead to an appropriate laboratory set-up.

7 Conclusions

The major conclusion in this thesis is that the more accurate prediction of the response and capacity of concrete bridge deck slabs under loading with respect to shear are obtained using the non-linear finite element analysis. Such an analysis describes the real behaviour of the slab since occurrence of cracking in concrete leads to stress redistributions. However, establishing an appropriate method involves many choices in order to obtain a realistic behaviour of the modelled structure. It is also crucial that the designer is well aware of the limitations of the used methods. This thesis allows giving some recommendations that may help the design to become more accurate:

- In order to get reliable results without unrealistic fluctuations of the shear force, it is recommended to use Poisson's ratio $v = 0$. This corresponds better to the Poisson's effect in concrete after tension cracking.

- With respect to the shear forces 8 nodes with reduced integration scheme 2x2 integration point in the plane of the element is recommended in order to get reliable results without unrealistic fluctuations.

- An expected response of the slab was acquired as long as the response was given by bending, and when the shear failure started to dominate the response was also as expected, not reflected in the analysis.

- Linear analysis is preferred in design. It can be used with respect to shear in cantilever slabs subjected to moving point loads since the linear results are conservative. In order not to be over-conservative, the design with respect to shear can be made with an averaged linear shear force over a certain width of the cantilever slab. For the studied case, the design could be made for a shear force approximately 0.8 times the maximum linear shear force.

- In the analysis, local peaks in the shear force appeared where the major bending cracks occur. It is hard to judge if this corresponds to a real response. It would be interesting to study this more in detail.

8   References

Bathe K. (1996): *Finite Element Procedures*, Prentice-Hall, Inc., New Jersey, USA, 1996.

Blaauwendraad J.,(2010): *Plates and FEM – Surprises and Pitfalls,* Springer, The Netherlands, 2010.

Broo H., Lundgren K., Plos M. (2008): *A guide to non-linear finite element modelling of shear and torsion in concrete bridges*, Chalmers University Of Technology, Göteborg, Sweden 2008.

Cook R.D., Malkus D. S., Plesha M.E., Witt R.J. (2004): *Concept And Applications Of Finite Element Analysis fourth addition,* John Wiley & Sons (Asia) Pte. Ltd., Singapore, 1994.

Crisfield M.A. (1994): *Non-linear Finite Element Analysis of Solid and Structures Vol.1*, John Wiley & Sons Ltd., West Sussex, England, 1994.

Engström B. (2011): *Design and analysis of continuous beams and columns*, Chalmers University of Technology, Göteborg, Sweden, 2011.

Eurocode 1 (2003*): Actions on structures - Part 2: Traffic loads on bridges.* European Committee for Standardization (2003), Brussels, 2003.

Eurocode 2 (2001*): Design of concrete structures - Part 1: General rules and rules for buildings,* European Committee for Standardization (2001), Brussels, 2001.

Guandalini S.(2005): *Poinçonnementsymétrique des dalles en bétonarmé*, PhD dissertation, (2005), Lausanne, Switzerland, 2005.

Hordijk D.A. (1991): *Local Approach to Fatigue of Concrete*, PhD thesis, Delft University of Technology, 1991.

Maekawa K., Pinmanmas A. and Okmura H. (2003): *Nonlinear mechanics of reinforced concrete*, Spon Press, London, 2003.

Mörsch E. (1908): *Reinforced concrete construction, theory and application* (in German, *"Der Eisenbetonbau, seine Theorie undAndwendung"*), 3rd Edition, Verlag von Konrad Wittwer.

Muttoni A., Schwartz J. (1991): *Behaviour of Beams and Punching in Slabs without Shear Reinforcement*, IABSE Colloquium Stuttgart, Vol. 62, Zürich: International Association for Bridge and Structural Engineering, 1991.

Muttoni A. (2003): *Shear and Punching Strength of Slabs without Shear Reinforcement*, Beton und Stahlbetonbau, V. 98, 2003.

Larsson F. (2010): *Non-linear finite analysis VSM014 – A short introduction*, Chalmers University of Technology, Göteborg, Sweden 2010

Pacoste C., Plos M., Johansson M. (2013): *Recommendations for finite element analysis for the design of reinforced concrete slabs*, Brobyggnad, Stockholm, Sweden, 2013.

Plos M. (2000): *Finite element analyses of reinforced concrete structures,* Chalmers University of Technology, Göteborg, Sweden, 2000.

Ritter W. (1899): *The Hennebique construction method* (in German, "*Die Bauweise Hennebique")*, Schweizerische Bauzeitung.

Shams Hakimi P. (2012): *Distribution of Shear Force in Concrete Slabs,* Department of Civil and Environmental Engineering, Division of Structural Engineering, Concrete Structures, Chalmers University Of Technology, Göteborg, Sweden, 2012.

TNO Diana Manual (2012): *Diana – Finite element analysis – User's Manual – Analysis Procedures – Release 9.4.4 TNO DIANA BV,* Delft, The Netherlands.

Vaz Rodrigues R. (2007): *Shear Strength of Reinforced Concrete Bridge Deck Slabs (2007)*, EPFL, Lausanne 2007.

9   Appendix - Deflection of concrete slab

(Assuming only self-weight)

Material properties - concrete C40/50

$$f_{ck} := 40\,MPa$$

$$E_c := 36\,GPa$$

$$\gamma_c := 25\,\frac{kN}{m^3}$$

Calculation for 1m of cantilver slab:

$$b := 100\,cm$$

$$l := 278\,cm$$

$$t_1 := 38\,cm$$

$$t_2 := 19\,cm$$

Deflection calculated for average thickness

Average thickness:

$$t_m := \frac{t_1 + t_2}{2} = 28.5\,cm$$

Weight of concrete:

$$g := \gamma_c \cdot t_m \cdot b = 7.125\,\frac{kN}{m}$$

Moment of interia:

$$I_m := \frac{b \cdot t_m^3}{12} = 1.929 \times 10^5\,cm^4$$

Deflection:

$$\delta_{max} := \frac{g \cdot l^4}{8 \cdot E_c \cdot I_m} = 0.766\,mm$$

Deflection calculated for the thickness at the end of cantilever

Moment of interia:

$$I_{max} := \frac{b \cdot t_1^3}{12} = 4.573 \times 10^5\,cm^4$$

Weight of concrete:

$$g_1 := \gamma_c \cdot t_2 \cdot b = 4.75\,\frac{kN}{m}$$

Deflection:

$$\delta_{max1} := \frac{g_1 \cdot l^4}{8 \cdot E_c \cdot I_{max}} + \frac{g_1 \cdot l^4}{30 \cdot E_c \cdot I_{max}} = 0.273\,mm$$